A Journey towards QCD Radiative Corrections in the SM and Beyond at the LHC

By

Satyajit Seth

[Enrolment No.: PHYS05200804004]

Saha Institute of Nuclear Physics, Kolkata

A thesis submitted to the

Board of Studies in Physical Sciences

In partial fulfillment of the requirements

For the degree of

DOCTOR OF PHILOSOPHY

of

HOMI BHABHA NATIONAL INSTITUTE

April, 2014

Homi Bhabha National Institute

Recommendations of the Viva Voce Committee

As members of the Viva Voce Committee, we certify that we have read the dissertation prepared by *Satyajit Seth* entitled "A Journey towards QCD Radiative Corrections in the SM and Beyond at the LHC" and recommend that it may be accepted as fulfilling the thesis requirement for the award of Degree of Doctor of Philosophy.

Chairman - Prof. Parthasarathi Mitra **Date:**

Guide/Convener - Prof. Prakash Mathews **Date:**

Member 1 - Prof. Avaroth Harindranath **Date:**

Member 2 - Prof. Munshi Golam Mustafa **Date:**

External Examiner - Prof. Poulose Poulose **Date:**

Final approval and acceptance of this thesis is contingent upon the candidates submission of the final copies of the thesis to HBNI.

I hereby certify that I have read this thesis prepared under my direction and recommend that it may be accepted as fulfilling the thesis requirement.

Date:

Place: (Prof. Prakash Mathews)

Guide

STATEMENT BY AUTHOR

This dissertation has been submitted in partial fulfillment of requirements for an advanced degree at Homi Bhabha National Institute (HBNI) and is deposited in the Library to be made available to borrowers under rules of the HBNI.

Brief quotations from this dissertation are allowable without special permission, provided that accurate acknowledgement of source is made. Requests for permission for extended quotation from or reproduction of this manuscript in whole or in part may be granted by the Competent Authority of HBNI when in his or her judgment the proposed use of the material is in the interests of scholarship. In all other instances, however, permission must be obtained from the author.

(Satyajit Seth)

DECLARATION

I, hereby declare that the investigation presented in the thesis has been carried out by me. The work is original and has not been submitted earlier as a whole or in part for a degree / diploma at this or any other Institution / University.

(Satyajit Seth)

List of Publications arising from the thesis

Journal

[1] "Vector boson production in association with KK modes of the ADD model to NLO in QCD at LHC", M. C. Kumar, P. Mathews, V. Ravindran, and S. Seth, *Journal of Physics*, **2011**, *G38*, 055001, [`arXiv:1004.5519`].

[2] "Graviton plus vector boson production to NLO in QCD at the LHC", M. C. Kumar, P. Mathews, V. Ravindran, and S. Seth, *Nuclear Physics*, **2011**, *B847*, 54–92, [`arXiv:1011.6199`].

[3] "Neutral triple electroweak gauge boson production in the large extra-dimension model at the LHC", M. C. Kumar, P. Mathews, V. Ravindran, and S. Seth, *Physical Review*, **2012**, *D85*, 094507, [`arXiv:1111.7063`].

[4] "Diphoton production in the ADD model to NLO+parton shower accuracy at the LHC", R. Frederix, M. K. Mandal, P. Mathews, V. Ravindran, S. Seth, P. Torrielli, and M. Zaro, *Journal of High Energy Physics*, **2012**, *1212*, 102, [`arXiv:1209.6527`].

Conferences

[1] "Associated Production of Vector Gauge Boson & Graviton to NLO QCD", M. C. Kumar, P. Mathews, V. Ravindran, and S. Seth, *Proceedings of Science*, **2011**, *RADCOR2011*, 047.

[2] "Diphoton production in the ADD model to NLO+parton shower accuracy at the LHC", M. K. Mandal, P. Mathews, V. Ravindran, and S. Seth, *Proceedings of Science*, **2013**, *RADCOR2013*, 030.

(Satyajit Seth)

In memory of my Mother -

the first and the most benevolent teacher of my life.

ACKNOWLEDGEMENTS

First of all, I would like to express my heartiest gratitude and sincere thanks to my thesis advisor Prof. Prakash Mathews for his invaluable guidance, persistent encouragement and continuous support. He made me learn how to deal with a research problem, helped me to proceed towards the right direction, assisted me to improve my line of thinking (together with my 'english' !). Apart from the academic part, he always extended his helping hand whenever I needed it, irrespective of whether the matter was personal or general and I have no word to articulate my thankfulness towards him for that.

I owe a very special gratitude to Prof. V. Ravindran who helped me all through the last five years in understanding comprehensive details of the subjects involved in my research work. Working with him was not only an enjoyable experience, but also a great achievement. I learned a lot from him during the period of my research and I am thankful to him for his imperative guidance and valuable suggestions.

My heartfelt thanks goes to all my collaborators for their crucial opinions and fruitful propositions in every stage of the work. I enjoyed working with them. I specially thank Dr. M. C. Kumar and Dr. Rikkert Frederix from whom I acruired knowledge on various numerical techniques.

The courses provided during one year Post M. Sc. associateship at SINP were very useful. I take this opportunity to thank all those teachers who gave lessons on different aspects of theoretical physics and by which I was largely benefited. I am grateful to Prof. Munshi Golam Mustafa for his continual support and assistance in many respects throughout these years of my research work. I would also like to acknowledge the cluster computing facility of Theory Division, SINP which I used extensively to carry out computational work associated with my research.

I am thankful to all my friends, seniors and juniors who made my surroundings congenial. I spent a cheerful time with Arindam, Najmul, Somdeb, Pratyay, Lab da, Santanu Da, Baishali, Shreemoyee, Niladri, Goutam and many others. Discussing physics issues with Pritibhajan da, Srijit da and Swapan da was highly effective.

This thesis would not have been possible without the ceaseless encouragement and moral support of my family members. My dearest father and my beloved (late) mother have continuously inspired me to continue my study and single-handedly got through tough times when I should have stayed with them. I remain indebted to them forever for their unconditional love and support. I express my deep sense of gratitude to my sister, grandmother, aunt, father-in-law, mother-in-law and all other members of my family for their affection and care. I have been blessed to have Banabithi as my wife and I am profoundly thankful to her for her boundless love, immense inspiration, intense support and trustful patience.

Contents

SYNOPSIS

The Standard Model (SM) of particle physics has been very successful in explaining the fundamental interactions of the elementary particles and its predictions have been verified experimentally to a very good accuracy. Also, the recent discovery of a SM scalar like particle has created vigorous excitement. In spite of its merits, there are many open questions, *e.g.* the hierarchy problem, the existence of dark matter etc., that are not addressed within its domain and plenty of room is left open for beyond standard model (BSM) physics scenarios such as extra dimensions, supersymmetry, technicolor etc. All these models are subject to experimental verification. With its unprecedented energy and luminosity, the Large Hadron Collider (LHC) at CERN is expected to unearth many interesting phenomena which are not (well-)known so far, thereby enriching the field of fundamental particle physics. The ATLAS and CMS experiments at the LHC are simultaneously hunting for new physics signals and putting stronger and stronger limits on BSM scenarios.

In order to address the hierarchy between the electroweak scale and the Planck scale, a theoretically well motivated model with large extra dimensions (LED) is proposed by Arkani-Hamed, Dimopoulos and Dvali and it has also gained a lot of interests in the field of collider phenomenology. In this model, gravity is allowed to propagate in full $(4 + d)$ dimensional space-time, where as, all SM particles are confined to the usual 3-brane in order to conceal the effect of those extra spatial dimensions (d). The extra dimensions are assumed to be compactified on a torus of common circumference and they are flat and of equal size which could be of macroscopic size. As a consequence of these assumptions, it follows from Gauss Law that the effective Planck scale (M_P) in 4-dimensions is related to the $(4 + d)$ dimensional fundamental scale (M_S) through the volume of the compactified extra dimensions. The large volume of the compactified extra spatial dimensions would account for the dilution of gravity in 4-dimensions and hence the hierarchy. Current experimental limits on deviation from inverse square law constraint the number of possible extra spatial dimensions as $d \geq 2$. The space-time is factorisable and the 4-dimensional spectrum consists of the SM confined to 4-dimensions and a tower of Kaluza-Klein (KK) modes of the graviton propagating in the full $(4 + d)$ dimensional space-time. In the context of collider physics, the study of processes with virtual graviton exchange (leading to enhanced cross section in comparison with the SM) or real graviton emission (leading to missing energy signal) would help the experimentalists to put stringent bounds on the model parameters.

In this thesis, production of neutral electroweak triple gauge bosons via virtual graviton exchange in LED are studied thoroughly along with their SM signatures. The triple gauge boson production processes in the SM are the precise predictions of the electroweak gauge theory and gauge self-couplings. They are also potential background to many new physics models like supersymmetry and technicolor. For example, $Z\gamma\gamma$ in SM is a background to signals with diphotons and missing transverse energy in gauge mediated super symmetric theories and $\gamma\gamma\gamma$ production in SM is a background to one photon plus techni-pion. Processes with three gauge bosons can also come from the large extra dimension model as gravitons couple directly to gauge bosons of the SM. While mono-jet or di-lepton production is more sensitive to the parameters of models with extra-dimensions compared to the triple gauge boson production, all these processes involve same universal coupling of gravity with the SM particles and hence can provide equally important information about the model. Moreover, in discriminating physics beyond the SM namely supersymmetry or technicolor models using triple gauge boson production, one can not ignore the potential contributions resulting from models with extra dimensions. Processes *viz.*

$\gamma\gamma\gamma, \gamma\gamma Z, \gamma ZZ, ZZZ$ are studied and results for various kinematic distributions at the LHC are presented.

At hadron colliders, observations of the BSM signals are very difficult due to the enormous QCD radiative background and the leading order (LO) prediction of a process of interest is not trustworthy to describe experimental observables solely on the basis of that approximation. It suffers from large factorisation as well as renormalisation scale uncertainties which for some processes could be as large as a factor of two. These issues go beyond normalisation of a cross section as the shapes of distributions may not be modeled correctly. Therefore, to provide quantitatively reliable theoretical predictions, higher order QCD corrections on such processes are unavoidable at the LHC. It provides a more credible prediction rate and it reduces the renormalisation as well as factorisation scale uncertainties.

This thesis aims to provide a complete study of the next-to-leading order (NLO) QCD corrections to the associated production of the vector gauge boson ($Z/W^{\pm}$) and the graviton in the large extra dimension model at the LHC. The study of graviton (G) plus gauge boson production will be very useful to probe the new physics at the LHC. It is important to note that there is a Standard Model background which gives signals similar to those of associated production of Z and G. This SM background receives a dominant contribution coming from the ZZ production process, where one of the Z bosons in the final state decays into a pair of neutrinos ($Z \to \nu\bar{\nu}$) leading to Z boson plus missing energy signals. The other Z boson can be identified via its decays to leptons, mostly electrons & muons and then constraining the lepton invariant mass close to the mass of the Z boson to consider only on-shell Z bosons. Any deviation from this SM prediction will be an indication to some beyond SM scenario and hence a study of this process would be useful in searching new physics.

At the LHC, fixed order calculation truncated to NLO at best yields results for sufficiently inclusive observable. Combining fixed order NLO and parton shower (PS) Monte Carlo would extend the coverage of the kinematical region to consistently include resummation in the collinear limit and also make a more exclusive description of the final state, that would be as realistic as possible to the experimental situation. The flexibility to incorporate hadronisation models and capability to simulate realistic final state configurations that can undergo detector simulations are the main advantages for the experimental collaborations.

This thesis focuses on the diphoton production to NLO+PS accuracy in both SM and LED at the LHC. The diphoton final state is an important signal for extra dimension searches, as the branching ratio of a KK mode decay to diphoton is twice than that of a decay to individual charged lepton pair. Both ATLAS and CMS have analysed the diphoton invariant mass spectrum using a constant K-factor for the full range of the invariant mass distribution to put lower bounds on extra dimension scale to NLO accuracy. However, this choice is not sensitive to possible distortions of distributions that can arise at NLO. That is why, diphoton final state is studied extensively in the LED model to NLO in QCD and matching to HERWIG parton shower is implemented using the MC@NLO formalism. Based on this work, the event files for various number of extra dimensions ($d = 2$ to 6) together with the complete code are uploaded on the website http://amcatnlo.cern.ch so that the experimentalists can download and use them to shower with specific cuts according to their requirement. This is the first time MC@NLO formalism has been used for a process in the LED model and it will significantly help extra dimension searches at the LHC to constrain the LED model parameters.

List of Figures

Chapter 1

Prelude

1.1 Introduction

Advancement of collider experiments has drawn an utmost attention of all of us since last few years. Recent discovery of the new resonance at ATLAS (*A Toroidal LHC ApparatuS*) and CMS (*Compact Muon Solenoid*) experiments of the *Large Hadron Collider* (LHC) indicating the existence of Higgs boson, has created a lot of delight and excitement in the high energy and particle physics community. The *Standard Model* (SM) of particle physics has been very successful in explaining the fundamental interactions of the elementary particles and its predictions have been verified experimentally to a very good accuracy. However, no signature of the one and only elementary scalar particle, named Higgs boson, which is the outcome of the famous Brout-Englert-Higgs mechanism [1, 2, 3, 4, 5, 6], had been found until recently [7, 8]. Suffice it to say, with this discovery, the SM which describes the electromagnetic, weak and strong interactions in a methodical and systematic way, is rife with all its constituent particles, though it is true that more data is needed to be sure whether the new particle is a SM Higgs boson or something else predicted by some other theories.

Quantum Chromo Dynamics (QCD) is an impartible portion of the SM. It deals with the strong interaction between the quark and the gluon which are known to be the most elementary particles of any hadron, namely proton, neutron *etc.* QCD is a *Quantum Field Theory* (QFT) which describes the non-abelian nature of the colour field. It is basically SU(3) Yang-Mills theory of the coloured fermions which are called quarks. In QCD, gluon acts as mediator of the strong force similar to the photon mediating electromagnetic interactions in *Quantum Electro Dynamics* (QED). However, there is a major difference between the characteristics of photon and gluon and that makes QCD a bit special. Though photon does not carry any electric charge, gluon carries a special kind of charge, which is known as colour charge and due to this reason, self interactions among the gluons are quite obvious unlike photons. Confinement and asymptotic freedom are two special properties of the QCD. Running of strong coupling is of opposite nature compared to the running of electromagnetic or weak coupling. At some low energy of about 200 MeV, the strong coupling diverges leading to confinement of the quarks and gluons. Whereas, at very high energies, the interaction between the quarks and gluons becomes very weak which in fact allows one to do perturbative calculation in this region, as they are considered to be asymptotically free there.

There are many standard books and interesting lecture notes (*viz.*, [9, 10, 11, 12, 13] to name a few) available in the literature describing all aspects of the SM and QCD in great detail. We prefer not to write them down again in this thesis which will nothing but a mere repetition of those things resulting into unnecessary large volume of the thesis. Rather, after presenting a brief overview on the method of higher order corrections in section 1.2, we would like to briefly introduce, in section 1.3, some beyond standard model scenarios, as we shall be going to use one of them extensively in the subsequent chapters.

1.2 Higher Order Corrections

Involvement of initial state partons in a hadron collider turns it into a QCD machine, as these partons having non-zero colour charge naturally take part in strong interactions. A hadron collider produces lots of QCD background due to the abundance of partons both in the initial and final states of a given process and therefore consideration of mere *Leading Order* (LO) approximation becomes very much unreliable. Note that, although the smallness of the strong coupling value makes the perturbation theory to work, it is not too small to take a handful of subsequent higher order terms into account. As a consequence, QCD radiative corrections become very significant for they can enhance the LO predictions as well as diminish the arbitrary scale uncertainties in theoretical predictions. *Next-to-Leading Order* (NLO) correction provides a better estimation of the total rate and reduces the renormalisation scale (μ_R) and the factorisation scale (μ_F) uncertainties to a reasonable extent. Further, the presence of hard jets in the final state, due to these radiative corrections has the potential to modify the shapes of several kinematical distributions of the particles that are under study at LO. Obtaining such a modification to the shapes of the distributions is beyond the scope of normalization of the corresponding LO distributions by a constant K-factor. Hence, it requires an explicit computation of the cross sections or distributions to NLO in QCD. Owing to this importance of the radiative corrections, they have been computed for several important processes in the SM as well as in many *Beyond Standard Model* (BSM) scenarios. Sometimes, it becomes also necessary to have the results with *Next-to-Next-to-Leading Order* (NNLO) accuracy depending on the process of interest and the exactitude achieved at NLO. However, this thesis deals with calculations up to NLO.

1.2.1 Fixed Order Calculation

Let us consider an example of a SM process at the LHC, say $PP \to e^+e^-$ (Drell-Yan production process) to describe higher order QCD corrections up to a fixed order ($\mathcal{O}(\alpha_s)$) in a vivid way. The partonic contribution at LO comes from the subprocess $q\bar{q} \to e^+e^-$ as depicted in Fig. 1.1. One can easily find the LO partonic cross section of this process following the standard method of matrix element calculation and the 2-body phase space integration. Now, as we are interested in doing NLO QCD correction of it, first of all, we have to find all those Feynman diagrams, which will participate in calculating $\mathcal{O}(\alpha_s)$ contribution, where α_s is the strong coupling strength. NLO partonic cross section can be written as the sum of three individual contributions in the following way,

$$\sigma_{\rm NLO} \simeq \int d^4\Phi_2 \; B + \int d^4\Phi_2 \int_{loop} d^n l \; V + \int d^n\Phi_3 \; R \qquad , \tag{1.1}$$

where B is the LO or Born contribution, V is the virtual contribution and R is the contribution coming from the real emission processes. All of them are related to the calculation of matrix element square ($|M^2|$) in each sub-category. Φ_2 and Φ_3 denote the 2-body and 3-body phase spaces respectively. In the second and last terms of eq. (1.1), the loop integration (with loop momenta l) and the 3-body phase space integration have to be carried out in n space-time dimensions where we can consider $n = (4 + \epsilon)$, ϵ being an infinitesimally small quantity ($\epsilon \to 0$), in order to regularise the *Ultra-Violet* (UV) and *Infra-Red* (IR) divergences appearing as poles in ϵ. This procedure is known as dimensional regularisation [14]. In this present example, LO contribution, which comes from the partonic subprocess $q\bar{q} \to e^+e^-$,

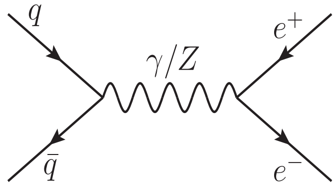

Figure 1.1: Leading order Feynman diagram of the process $q\bar{q} \to e^+e^-$.

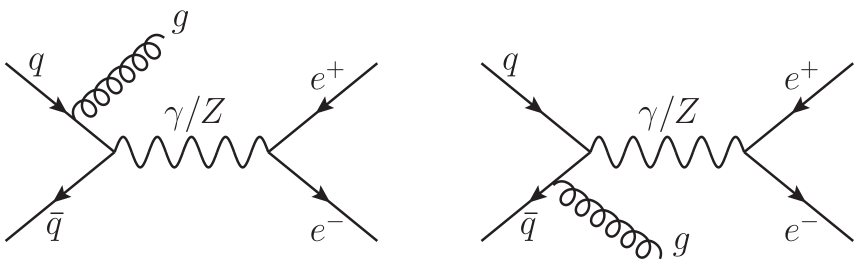

Figure 1.2: $q\bar{q}$ initiated real emission Feynman diagrams originating from the process $q\bar{q} \to e^+e^-$.

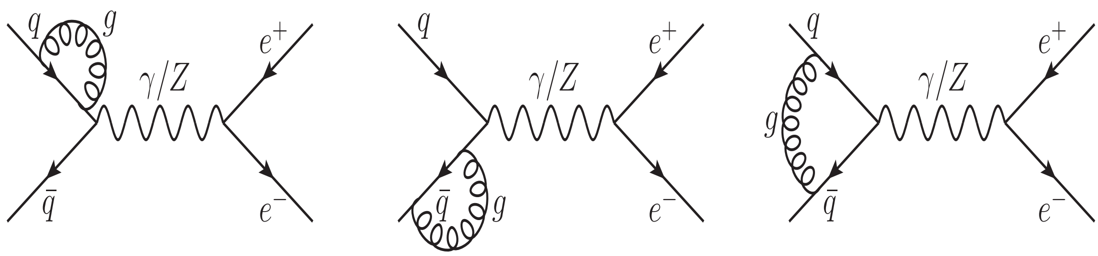

Figure 1.3: Feynman diagrams appearing in virtual correction of the process $q\bar{q} \to e^+e^-$.

is actually $\mathcal{O}(\alpha_s^0)$. Apart from the $q\bar{q}$ initiated real emission diagrams presented in Fig. 1.2, $\mathcal{O}(\alpha_s)$ contributions also come from the squared matrix elements of the following real emission subprocesses: (i) $qg \to e^+e^-q$, (ii) $\bar{q}g \to e^+e^-\bar{q}$. In addition, another $\mathcal{O}(\alpha_s)$ contribution comes from the interference of the LO diagrams with the diagrams appearing due to the virtual correction (see Fig. 1.3). Together with all these contributions, one finally gets the complete partonic cross section at NLO which indeed needs to be convoluted with the *Parton Distribution Functions* (PDF) of the initial state quarks or gluons that are coming from the two colliding protons at the LHC, in order to get the final cross section of the actual process (*i.e.*, $PP \to e^+e^-$) we started with. There are many implicit non-trivial analytic techniques and latent semi-analytical and numerical methodologies that one has to face at the time of doing NLO correction of a process of interest. All the ins and outs of a complete fixed order NLO calculation of a process (real graviton emission process in association with a vector boson) at the LHC are presented in chapter 3 in great detail.

1.2.2 Parton Shower

When we are dealing with a hard subprocess (for example, $\gamma^* \to q\bar{q}$), the external particles are by definition hard and they can eventually emit additional partons which carry on emitting other ones persistently, as we know that accelerated particles radiate. At this point, it is practically impossible to calculate the matrix

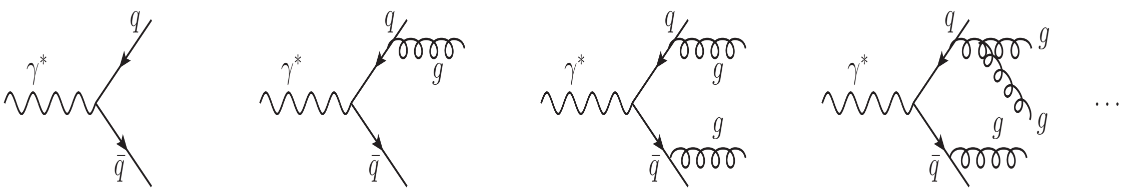

Figure 1.4: Feynman diagrams resulting from parton shower effect on the process $\gamma^* \to q\bar{q}$.

element square of all of these diagrams (see Fig. 1.4) and study their complete contribution, as we can see that the particle multiplicity is gradually increasing which will in practice make the calculation more tedious and cumbersome. Besides, it is clear from Fig. 1.4 that, as we go from left to right in those diagrams, four momenta of the additional partons become lesser due to the energy-momentum conservation. Therefore, it would be significant enough, if we can at least take into account all these effects in the collinear limit. This phenomena is known as *Parton Shower*

(PS) which, in principle, resums large logarithmic contributions coming from such collinear effects and continues until the hard process evolves down to the hadronisation scale. In case of initial state showering, incoming partons are evolved backward starting from the hard subprocess scale determined by the PDF up to the scale of the constituents in the incoming hadrons.

In this context, let us recall the universal relation of a splitted matrix element square, as depicted in Fig. 1.5, in case of collinear factorisation:

$$|M_{n+1}|^2 \; d\Phi_{n+1} \simeq |M_n|^2 \; d\Phi_n \; \frac{dq^2}{q^2} \; dz \; \frac{d\phi}{2\pi} \; \frac{\alpha_s}{2\pi} \; P_{a\to bc}(z) \qquad , \tag{1.2}$$

where M_{n+1} is the matrix element of any $2 \to n+1$ process, while M_n is the matrix

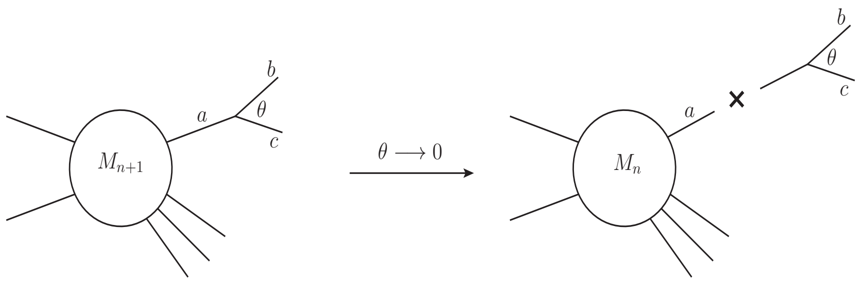

Figure 1.5: Schematic diagram of collinear factorisation.

element of the process when the splitting of the parton 'a' is aborted. The $(n+1)$-body and n-body phase spaces are denoted by Φ_{n+1} and Φ_n respectively. α_s is the usual strong coupling; $z = E_b/E_a$, is the relative energy of the daughter parton 'b' with respect to the energy of the parent parton 'a'; ϕ is the azimuthal angle between the polarisation of 'a' with the plane of branching and $P_{a\to bc}(z)$ denotes the famous Altarelli-Parisi splitting kernel. The variable q is known as the evolution variable which can be set in a variety of ways such as the transverse momentum (P_T) of 'a', the angle (θ) between the two daughter particles *etc.*

With the help of the Poisson statistics, we can say that, if a branching is expected to occur obeying the pattern p, the probability of observing such splitting n times is,

$$\mathcal{P}(n;p) = \frac{e^{-p}\ p^n}{n!} \qquad . \tag{1.3}$$

Using this, we can now readily find that the probability of observing no such splitting is,

$$\mathcal{P}(0;p) = e^{-p} \qquad . \tag{1.4}$$

Likewise, using eq. (1.2), we can define the following Sudakov factor,

$$\Delta(Q_1, Q_2) \quad = \quad \exp\left[-\frac{\alpha_s}{2\pi}\int_{Q_1}^{Q_2}\frac{dq^2}{q^2}\int_{z_{min}}^{z_{max}} dz\ P(z)\right] \qquad , \tag{1.5}$$

which in practice provides the non-splitting probability of parton 'a', when the evolution parameter varies from Q_1 to Q_2. A Monte Carlo routine can be written based on the application of Sudakov factor to describe a chain of parton splitting. Besides, simultaneous study of soft emissions helps in settling up the right evolution parameter to be used in the *Parton Shower Monte Carlo* (PSMC), thereby ensuring angular ordering and/or colour ordering. For example, HERWIG [15, 16, 17, 18, 19] is an angular ordered PSMC program, where as, multiple options of evolution parameters are available in PYTHIA [20, 21, 22, 23, 24].

Nevertheless, it is obvious that the parton shower, which stands solely on the basis of collinear and/or soft approximation, can not describe the hard radiation correctly. Therefore, it is necessary to use the matrix elements in order to describe hard radiations together with the PSMC, which is valid only in the soft/collinear region. In a sense, they are complementary to each other and we need to merge them together avoiding double counting and ensuring regular distributions. In one hand, it is customary to use the high multiplicity matrix elements for describing hard radiations and merge them with parton shower following the CKKW [25, 26, 27, 28, 29] or MLM [30, 31] algorithm, whereas on the other hand, one can start with the NLO corrected results to describe the hard radiations and match them with parton shower using the MC@NLO [32] or POWHEG [33, 34, 35] formalism. Note that the later approach possesses several advantages over the first one such as, consistent inclusion of K-factor information in detector simulation, estimation of theoretical scale dependencies in a meaningful way, impact of NLO corrected observable shapes on acceptance studies and so on. We shall describe a complete NLO result matched with parton shower using the MC@NLO formalism in chapter 4 for the diphoton production process both in the SM and in a particular BSM at the LHC.

1.3 Beyond Standard Model

In spite of its merits, the SM has many open questions that are not addressed within its domain and a plenty of room is left open for some beyond SM physics scenarios to address them. *SUperSYmmetry* (SUSY), extra dimensions, technicolor models are a few to name such BSM scenarios. With the advent of the high energetic hadron colliders, it is quite feasible to probe these new scenarios in the laboratory experiments. The LHC with its unprecedented center mass energy of 14 TeV and with luminosities as high as 10^{34} cm^{-2} s^{-1}, offers the best possibility of discovering the possible new physics that is hidden so far at lower energies.

1.3.1 Large Extra Dimension

One of such BSM scenarios that has gained a lot of interest and has been studied well in the context of collider phenomenology is the *Large Extra Dimension* (LED) model proposed by Arkani-Hamed, Dimopoulos and Dvali [36, 37, 38]. This model, which is also known as the ADD model, is theoretically well motivated and it addresses the hierarchy problem with the concept of extra spatial dimensions. A viable mechanism to hide these extra spatial dimensions (d) from the SM particles is to confine the latter to a 3-brane and allow only the gravity to propagate in the full $(4 + d)$ dimensional space-time. For simplicity, the extra dimensions can be assumed to be flat, of the same size and compactified on a d-dimensional torus of radius $R/(2\pi)$. After the compactification, the scale M_s of the extra dimensional theory is related to the Planck scale M_p as,

$$M_p^2 = C_d \; M_s^{2+d} \; R^d \qquad , \tag{1.6}$$

where $C_d = 2 \; (4\pi)^{-\frac{d}{2}}/\Gamma(d/2)$ and R is the size of the extra dimensions. This compactification implies that a massless graviton propagating in $(4 + d)$ dimensions manifests itself as a tower of massive graviton modes in 4-dimensions, with mass

$$m_{\vec{n}}^2 = 4\pi^2 \vec{n}^2/R^2 \qquad , \tag{1.7}$$

where $\vec{n} = \{n_1, n_2, ..., n_d\}$ and $n_i = \{0, 1, 2, ...\}$. Here, the zero mode corresponds to the 4-dimensional massless graviton. As the inverse square law of gravity has been tested down to only few μm so far [39], the size of the extra spatial dimensions in this model can be taken as large as this limit. The hierarchy between the electroweak scale and the Planck scale can then be accounted for by this large volume of the extra dimensions, as can be seen from eq. (1.6). For $M_s \sim \mathcal{O}(\text{TeV})$, the above limit on R constrains the number of extra dimensions to $d \geq 2$.

In the effective theory valid below the scale M_s, these gravitons couple to the SM fields through energy momentum tensor $T^{\mu\nu}$ of the latter with the coupling $\kappa = \sqrt{16\pi}/M_p$, as given by [40, 41],

$$\mathcal{L}_{int} \quad = \quad -\frac{\kappa}{2} \sum_{\vec{n}=0}^{\infty} T^{\mu\nu}(x) \; h_{\mu\nu}^{(\vec{n})}(x) \qquad , \tag{1.8}$$

where $h_{\mu\nu}^{(\vec{n})}$ contains one spin-2 state, $(n-1)$ spin-1 states and $n(n-1)/2$ spin-0 states and the zero mode of the KK tower corresponds to the massless graviton in the 4 space-time dimensions.

Since the coupling is through the energy momentum tensor, gravitons can couple to all the SM fields with the same coupling strength κ irrespective of their charge, colour and flavor. The Feynman rules for the above interaction Lagrangian are given in [40, 41]. To order κ^2, the above Lagrangian allows processes involving SM fields and virtual gravitons in the intermediate state or real gravitons in the final state. In the context of collider phenomenology, this gives rise to a very rich and interesting signals that can be explored at the present LHC. The virtual exchange of the gravitons can lead to the deviation from the SM predictions whereas the real emission of the gravitons can lead to the missing energy signal. Though the coupling of each graviton mode to the SM fields is M_p suppressed, the large multiplicity of the available graviton modes can give rise to observable effects. Hence, there will be a summation over the graviton modes at the amplitude level for the virtual graviton exchanges and at the cross section level for the real graviton emissions. As the size of the extra dimensions could be large in this model, the mass splitting *i.e.*, $(2\pi/R)$ is very small and hence this summation over the graviton modes can be approximated to be an integral in the continuum limit, with the density of the graviton modes given by [40],

$$\rho(m_{\vec{n}}) = \frac{R^d \; m_{\vec{n}}^{d-2}}{(4\pi)^{d/2} \; \Gamma(d/2)} \qquad . \tag{1.9}$$

In case of virtual graviton exchange process, the effective graviton propagator, after summing over all KK states can be expressed as,

$$\begin{aligned} \mathcal{D}_{ij}(s_{ij}) &= \sum_{\vec{n}} \frac{1}{s_{ij} - m_{\vec{n}}^2 + i\varepsilon} \\ &= \int_0^\infty dm_{\vec{n}}^2 \; \rho(m_{\vec{n}}) \; \frac{1}{s_{ij} - m_{\vec{n}}^2 + i\varepsilon} \\ &= \frac{1}{\kappa^2} \frac{8\pi}{M_S^4} \left(\frac{\sqrt{s_{ij}}}{M_S} \right)^{(d-2)} \left[\pi + 2iI(\Lambda/\sqrt{s_{ij}}) \right] \quad , \end{aligned} \tag{1.10}$$

where $s_{ij} = (p_i + p_j)^2$ is the invariant mass of the final state particles (with 4-momenta p_i and p_j), directly attached to the KK mode at the parton level and the function $I(\Lambda/\sqrt{s_{ij}})$ is described in [40], which depends on the UV cutoff Λ. As stated earlier, although the interaction of KK modes with the SM particles is suppressed by the coupling κ (eq. (1.8)), the cumulative effect of summing over large number of accessible KK modes (eq. (1.10)) compensates the suppression, making the effective coupling significant enough to have observable effects. It is usual practice to set the UV cutoff $\Lambda = M_S$ and simplify the summation of virtual KK modes [40, 41] to do the phenomenology. In this thesis, we follow the approach of [40] all the way through any analysis which retains the details of the number of extra dimensions. The numerator of the spin-2 KK graviton propagator [40] in n-dimensions can be expressed as,

$$B_{\mu\nu,\rho\sigma}(k) \;=\; \zeta_{\mu\rho}\zeta_{\nu\sigma} + \zeta_{\mu\sigma}\zeta_{\nu\rho} - \frac{2}{(n-1)}\zeta_{\mu\nu}\zeta_{\rho\sigma} \qquad , \tag{1.11}$$

where $\zeta_{\mu\nu} = (g_{\mu\nu} - k_\mu k_\nu / m^2_{\vec{n}})$. Here, k is the momentum flowing through the propagator.

For the real graviton production process at the collider experiment, the inclusive cross section is given by the following convolution,

$$d\sigma = \int_0^\infty dm^2_{\vec{n}}\ \rho(m_{\vec{n}})\ d\sigma_{m_{\vec{n}}} \qquad , \tag{1.12}$$

where $d\sigma_{m_{\vec{n}}}$ is the cross section for the production of a single graviton of mass $m_{\vec{n}}$. This collective contribution of the graviton modes results in their non-negligible interaction with the SM fields and offers the best possibility of probing the low scale quantum gravity effects at the colliders experiments.

1.3.2 Warped Extra Dimension

In the warped extra dimension scenario, we briefly describe the extra dimensional model proposed by Randall and Sundrum, in which there is only one extra spatial dimension and this model is also known as RS model [42, 43]. In RS model, the fifth dimension is compactified on $\mathbf{S}^1/\mathbf{Z}^2$ orbifold with radius R_c, which is of the order of Planck length. The Planck 3-brane with positive tension is situated at the orbifold fixed point $y = 0$, while the TeV 3-brane with negative tension is located at another orbifold fixed point $y = \pi R_c$. The geometry of this 5-dimensional space-time, which is warped, can be defined with the following metric,

$$ds^2 = e^{-2\mathcal{K}y}\ \eta_{\mu\nu} dx^\mu dx^\nu + dy^2 \qquad , \tag{1.13}$$

where $0 < y < \pi R_c$; $\eta_{\mu\nu}$ is the usual 4-dimensional flat Minkowski metric and $\mathcal{K}$ denotes the constant negative curvature of the non-factorisable AdS_5 space-time. Gravity can propagate on the bulk, while the SM fields are localised on the TeV brane. While gravity originates on the Planck brane, a TeV scale can be generated on the TeV brane for $\mathcal{K}R_c \sim 10$, thus solving the hierarchy between the electroweak scale and the Planck scale. Further, it has been shown in [44, 45, 46, 47], that the value of $\mathcal{K}R_c$ can be stabilised against quantum fluctuations by minimising the potential of the modulus field, which has to be introduced in the bulk for this purpose.

The tower of KK excitations ($h^{(n)}_{\mu\nu}$) of the graviton couples to the SM energy momentum tensor ($T^{\mu\nu}$) through the following interaction Lagrangian,

$$\mathcal{L}_{int} \;=\; -\frac{1}{\overline{M_p}} T^{\mu\nu}(x) h^{(0)}_{\mu\nu}(x) - \frac{e^{\pi\mathcal{K}R_c}}{\overline{M_p}} \sum_{n=1}^{\infty} T^{\mu\nu}(x) h^{(n)}_{\mu\nu}(x) \qquad , \tag{1.14}$$

where $\overline{M_p}$ is the reduced Planck scale. The first term in the above Lagrangian denotes the contribution of the zero mode graviton which is M_p suppressed. However, contributions coming from the massive KK modes get enhanced due to the presence of the exponential factor $e^{\pi\mathcal{K}R_c}$ in the last term of the above mentioned Lagrangian and they produce interactions comparable to the electroweak strength. For this reason, we can only consider the interaction of the massive KK gravitons with the SM fields without any loss of generality and the interaction Lagrangian can be written as follows,

$$\mathcal{L}_{int} \simeq -\frac{\overline{c_0}}{m_0}\sum_n^{\infty} T^{\mu\nu}(x) h^{(n)}_{\mu\nu}(x) \quad , \tag{1.15}$$

where $\overline{c_0} = \mathcal{K}/\overline{M_p}$ is an effective coupling and $m_0 = \mathcal{K}e^{-\pi\mathcal{K}R_c}$ sets a mass scale for the massive KK mode gravitons. The masses of $h^{(n)}_{\mu\nu}$ are given by,

$$M_n = x_n \, \mathcal{K} \, e^{-\pi\mathcal{K}R_c} \quad , \tag{1.16}$$

where x_ns' are the zeros of the Bessel function $J_1(x)$. Since $\mathcal{K}$ is related to the curvature of the fifth dimension, we cannot consider large values of $\mathcal{K}$ in order to get rid of the large curvature effects. Moreover, $\mathcal{K}$ cannot be too small compared to the value of $\overline{M_p}$, as it will in turn reintroduce hierarchy. These considerations constrain the value of $\overline{c_0}$ within the limit $0.01 < \overline{c_0} < 0.1$. Except for the overall warp factor, Feynman rules [40, 41] for the RS model is exactly similar to the ADD model. However, the mass gap between the KK modes of graviton in RS case is quite distinct from ADD scenario and the summation over such KK modes leads to the effective graviton propagator [48] defined as,

$$\begin{aligned} \mathcal{D}_{eff}(s_{ij}) &= \sum_{n=1}^{\infty} \frac{1}{s_{ij} - M_n^2 + iM_n\Gamma_n} \\ &= \frac{1}{m_0^2}\sum_{n=1}^{\infty} \frac{X_s^2 - X_n^2 - i\frac{\Gamma_n}{m_0}X_n}{(X_s^2 - X_n^2)^2 + \frac{\Gamma_n^2}{m_0^2}X_n^2} \quad , \end{aligned} \tag{1.17}$$

where $X_s = \sqrt{s_{ij}}/m_0$, $X_n = M_n/m_0$ and Γ_n corresponds to the width of the n-th KK mode. The summation over n is kinematically bounded and can be calculated numerically.

1.4 Conclusion

In this chapter, we have presented the essence of higher order QCD corrections in the context of hadron collider, namely LHC. We have described the importance of doing NLO correction and outlined the available standard techniques to perform it. Necessity of incorporating parton shower effects with the fixed order results has also been illustrated. Besides, we have briefly described some of the BSM scenarios, namely ADD and RS model. Equipped with all these notions, we are now ready to study the phenomenology of a process in a BSM scenario at the LHC. In the next chapter, we will discuss the prospects of probing large extra dimension model at the LHC through neutral triple gauge boson production processes in LO.

Chapter 2

Triple Gauge Boson Production

2.1 Introduction

The di-lepton [49, 50, 51, 52, 53, 54], di-gauge boson [53, 54, 55, 56, 57, 58, 59, 60] and di-jet [61, 62] final states have been extensively studied in the context of extra dimension models. The triple gauge boson final state is also an interesting new physics signal in some of the beyond SM scenarios [63]. In this chapter, we consider the neutral triple gauge boson production at the LHC and study how the ADD model would alter the SM expectation. In the SM, the triple gauge boson final state is an important signal as it depends on the 3-point and 4-point couplings among the gauge bosons which is a test of the electroweak theory. This process in the SM has been studied to LO [64, 65] and its extension to the NLO was on the Les Houches wishlist [63, 66] and has been finally achieved in [67, 68, 69, 70]. The triple gauge boson production processes in the SM are the precise predictions of the electroweak gauge theory and gauge self-couplings. They are also potential backgrounds to many new physics models like SUSY and technicolor. For example, $Z\gamma\gamma$ in SM is a background to signals with di-photons and missing transverse energy in gauge mediated supersymmetric theories [71] and $\gamma\gamma\gamma$ production in SM is a background to one photon plus techni-pion [72]. Processes with three gauge bosons can also come from the ADD model as gravitons couple directly to gauge bosons of the SM. While mono-jet or di-lepton production is more sensitive to parameters of the model with extra dimensions compared to the triple gauge boson production, all these processes involve same universal coupling of gravity with the SM particles and hence can provide equally important information about the model. Moreover, in discriminating physics beyond the SM namely SUSY or technicolor models using triple gauge boson production, one can not ignore the potential contributions resulting from models with extra dimensions.

In this analysis, we consider the process $PP \to VVV\ X$, where we restrict to the neutral gauge bosons $V = \gamma, Z$ and X is some hadronic final state. The following four final states are the subject of this analysis: (*i*) $\gamma\gamma\gamma$ (*ii*) $\gamma\gamma Z$ (*iii*) γZZ and (*iv*) ZZZ.

2.2 Neutral Triple Gauge Boson Production

The neutral gauge boson final state at the hadron collider $PP \to VVV\ X$ at LO comes from the following subprocess,

$$q(p_1) + \bar{q}(p_2) \longrightarrow V(p_3) + V(p_4) + V(p_5) \qquad , \tag{2.1}$$

where $V = \gamma, Z$ and X is any final state hadron. The SM diagram for the above process is shown in Fig. 2.1 with all possible permutations of final states. For the final state with at least two ZZs, Higgs boson could contribute by coupling to the quarks, but this is negligible in the vanishing quark mass limit. In the case of ZZZ final state, there are additional Higgs strahlung diagrams, but their contribution is also quite small and becomes faded in the present Higgs mass limit. Hence, we have not included the processes with the Higgs boson. Moreover, $gg \to VVV$ subprocess, though it is formally NNLO in QCD, could substantially contribute at $\mathcal{O}(\alpha_s^0)$ in the low invariant mass region of the final state vector bosons due to large gluon densities at small x. However, this effect starts diminishing as the invariant mass grows up to higher values wherein the ADD model begins to dominate over the SM contribution and therefore such effect has not been taken care of in our present study. In the ADD

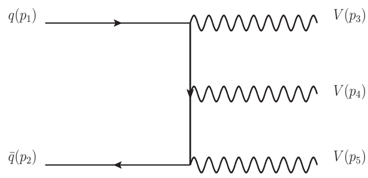

Figure 2.1: Typical Feynman diagram for triple gauge boson production in SM.

model, the KK modes of the graviton (G) couple to V bosons, quarks, anti-quarks as well as to quark-antiquark-V boson vertex [40]. Four categories of Feynman diagrams that give a VVV final state in ADD model are shown in Fig. 2.2. We have

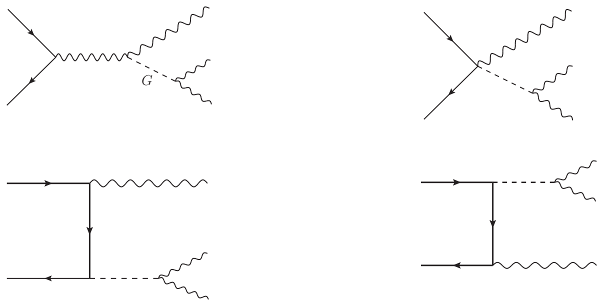

Figure 2.2: Typical Feynman diagrams for triple gauge boson production in ADD model. Dashed line represents the KK graviton (G) and the other particle lines are same as they are in Fig. 2.1.

used unitary gauge ($\xi \to \infty$) for the Z boson and the Feynman gauge ($\xi = 1$) for the photon.

In the SM, the LO process for the production of $\gamma\gamma\gamma$ at hadron colliders results from the annihilation of a quark and an anti-quark. In the ADD model, the production mechanism is again from the same initial states, but one of the three photons remains attached to either of the $q\bar{q}\gamma$, $\gamma\gamma G$, $q\bar{q}\gamma G$ vertices and the other two photons come from the decay of KK graviton. The typical Feynman diagrams that contribute in the SM and in the ADD model are shown in Fig. 2.1 and 2.2. The Feynman rules for the processes with KK graviton can be found in [40, 41]. All the expressions for the matrix element squared with proper spin, color sums and averages are obtained using a symbolic program based on FORM [73]. The KK graviton propagator $\mathcal{D}_{ij}$ and the numerator of the spin-2 propagator [40] of the KK graviton are illustrated in eq. (1.10) and (1.11) respectively. Terms proportional to negative powers of mass of KK mode in $\zeta_{\mu\nu}$ do not contribute as they are proportional to $k_\mu k_\nu$. This provides a useful check on our calculation. The matrix elements have been checked for gauge invariance. We performed similar computation for evaluating the parton level subprocesses for $\gamma\gamma Z$, γZZ and ZZZ productions. In the following we list few of the important observations.

For the $\gamma\gamma Z$ production, in the limit $m_Z \to 0$ (m_Z being the mass of Z boson), we reproduce the matrix elements for $\gamma\gamma\gamma$ process with the changes: $(C_V^2 + C_A^2)/4 \longrightarrow Q_f^2$, $T_Z \longrightarrow e$, where C_V, C_A are the vector and axial vector couplings of the weak gauge boson respectively, $T_Z = e/(\sin\theta_w \cos\theta_w)$ and Q_f is the electric charge of the quark flavors. In the case of γZZ production, we find that the parton level subprocesses in SM and ADD model are similar to those of the $\gamma\gamma Z$ production with the changes $\gamma \leftrightarrow Z$. The squared matrix element for γZZ production that comes from ADD model alone is not related to the one coming from $\gamma\gamma\gamma$ production. The reason is that some of the terms proportional to m_Z^2, that appear in the GZZ vertex, cancel all the inverse power of m_Z^2 present in the Z boson polarisation sum, giving contributions that have no analogous ones in the $\gamma\gamma\gamma$ process. However, the expression for the SM squared matrix element of γZZ is related to that of $\gamma\gamma\gamma$ process in the SM if we take $m_Z \to 0$, $(C_V^4 + 6C_V^2 C_A^2 + C_A^4)/16 \longrightarrow Q_f^4$ and $T_Z \longrightarrow e$. For ZZZ production, squared matrix elements involving ADD vertices do not have any relation with those of $\gamma\gamma\gamma$ production for the same reason as described in γZZ production case. The SM squared matrix element of this process is related to the one for the $\gamma\gamma\gamma$ process in SM with the following replacement in the limit $m_Z \to 0$, $(C_V^6 + 15C_V^4 C_A^2 + 15C_V^2 C_A^4 + C_A^6)/64 \longrightarrow Q_f^6$, $T_Z \longrightarrow e$. In fact, we empirically find that the most general formula for the replacement of n number of Z boson(s) with photon(s) in the SM squared matrix element is,

$$\frac{(C_V^2 + C_A^2)^n + 2n(n-1)(C_V^2 C_A^2 (C_V^2 + C_A^2)^{n-2})}{4^n} \longrightarrow Q_f^{2n} \qquad , \tag{2.2}$$

which works for all the above three processes with $n = 1, 2, 3$. We have provided the expressions of the squared matrix elements for the $\gamma\gamma\gamma$ production process in Appendix A. For the rest of the processes discussed above, such expressions of the squared matrix elements are too large to be presented in this thesis. Rather, they could be made available upon request.

2.3 Numerical Results

In this section, we present different kinematical distributions for the production of neutral triple gauge bosons. The predictions are for the LHC at center of mass energy $\sqrt{S} = 14$ TeV. We have used CTEQ6L parton densities [74]. For the strong coupling constant that appears in CTEQ6L, we use $\Lambda_{QCD} = 0.226$ GeV and $n_f = 5$ flavors. We set the factorisation scale $\mu_F = P_T^V$ for the transverse momentum distribution of V and $\mu_F = Q$ for the invariant mass (Q) distribution of the di-boson pair. In addition we apply the following cuts on P_T^V and the rapidity y^V,

$$P_T^{\gamma,Z} \geq 25 \text{ GeV} \qquad \text{and} \qquad y^{\gamma,Z} < 2.7 \quad . \tag{2.3}$$

We also ensure that in general the invariant mass of the di-boson (*i.e.*, any two identical bosons among the three Vs) is less than M_S. We use $m_Z = 91.1876$ GeV and $\sin^2\theta_w = 0.2312$. The fine structure constant is taken as $\alpha = 1/128$.

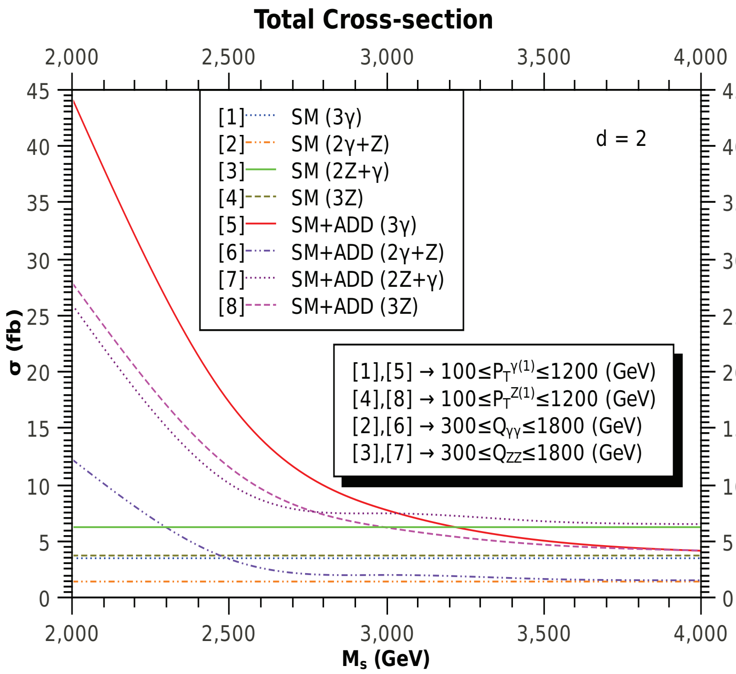

Figure 2.3: Total cross sections for all triple neutral gauge boson production processes, shown as a function of M_S for $d = 2$. Horizontal lines correspond to various SM contributions.

CMS [75] and ATLAS [76] have already reported searches for signatures of extra dimensions in the diphoton mass spectrum at the LHC for 7 TeV p p collisions. The 95 % lower bound on M_S vary between $2.27 - 3.53$ TeV depending on the number of extra dimensions $d = 3 - 7$ for ATLAS and M_S vary between $2.3 - 3.8$ TeV depending on the number of extra dimensions $d = 2 - 7$ for CMS, both using a fixed K-factor of about 1.6 [56, 57]. We have used the phenomenologically viable ADD

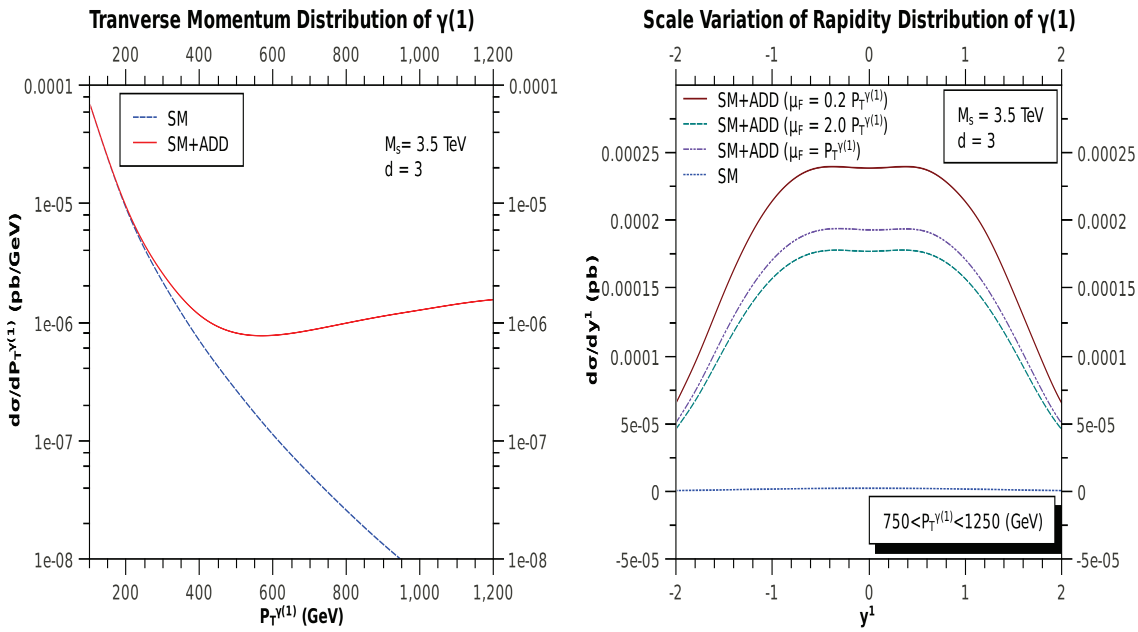

Figure 2.4: Transverse momentum distribution of γ_1 (left panel) for $M_S = 3.5$ TeV and $d = 3$. Rapidity distribution of γ_1 (right panel) for $M_S = 3.5$ TeV and $d = 3$ in the region where $P_T^{\gamma_1} \in (750, 1250)$ GeV and its dependence on the factorisation scale in the range $\mu_F = 0.2 P_T^{\gamma_1}$ and $\mu_F = 2 P_T^{\gamma_1}$.

model parameters for our present study.

For the processes involving more than one photon, it is important to isolate photons from each other *i.e.*, they need to be well separated in phase space so that they can be identified as separate objects in the detector. To do this, we consider a cone of radius $R = \sqrt{(\Delta y)^2 + (\Delta\phi)^2}$ in the rapidity-azimuthal angle plane (y, ϕ) and ensure that the minimum separation between any two photons is taken to be $R_{\gamma\gamma} = 0.4$. In the following, we describe our findings for the various triple gauge boson production processes.

The total cross sections for various processes involving neutral triple gauge boson final states as a function of M_S for a fixed value of $d = 2$ are given in Fig. 2.3. We set $d = 2$ to make the effect of varying M_S on the SM+ADD cross sections visible for all the processes considered in the present chapter. The SM contributions that

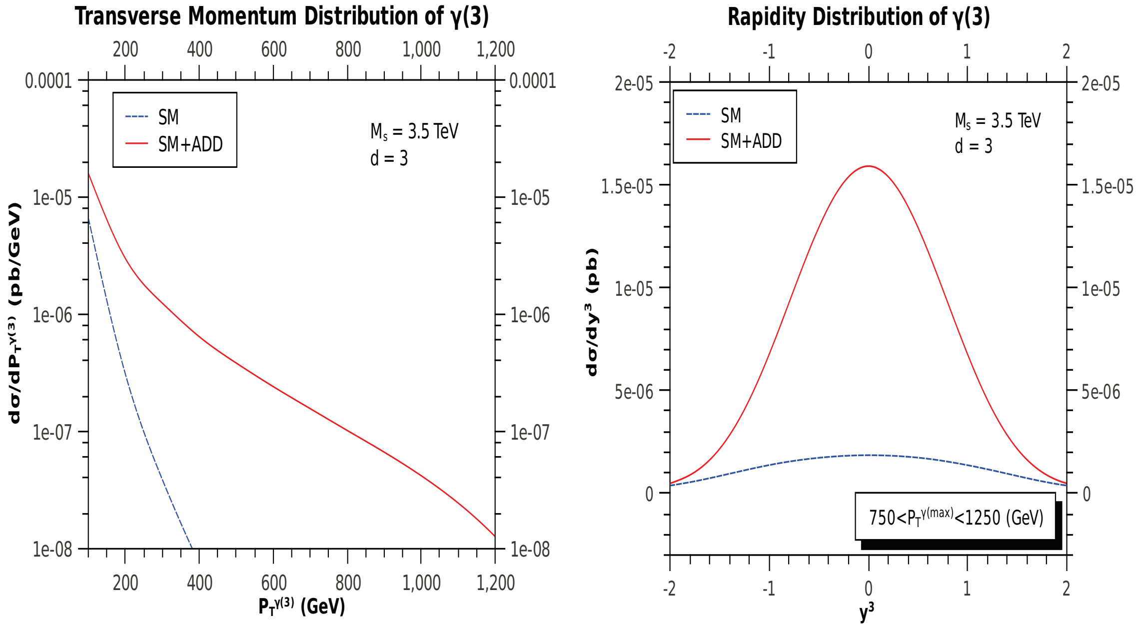

Figure 2.5: Transverse momentum distribution of γ_3 (left panel) for $M_S = 3.5$ TeV and $d = 3$. Rapidity distribution of γ_3 (right panel) for $M_S = 3.5$ TeV and $d = 3$ in the region where $P_T^{\gamma_3} \in (750, 1250)$ GeV.

do not depend on ADD model parameter M_S appear as horizontal lines.

2.3.1 $\gamma\gamma\gamma$ Production

In this case, the three photons in the final state are classified in such a way that $P_T^{\gamma_1} > P_T^{\gamma_2} > P_T^{\gamma_3}$. We have compared our predictions for $P_T^{\gamma_1}$ distribution in the SM against those given in [70] and found a very good agreement confirming the correct implementation of our analytical results in our numerical code. In the left panel of Fig. 2.4, we present the transverse momentum distribution of γ_1 in SM as well as in SM+ADD (*i.e.*, SM, ADD and the interference between them). We have chosen $M_S = 3.5$ TeV and $d = 3$ as representative parameters of the ADD model. In the high $P_T^{\gamma_1}$ region, the distribution of SM+ADD is fully controlled by processes coming from ADD model and is enhanced due to the dominant contributions of the KK modes. In the right panel of Fig. 2.4, rapidity distribution of the most energetic photon γ_1 is shown for $750 < P_T^{\gamma_1} < 1250$ GeV in SM and SM+ADD. It is seen that the SM contribution is extremely small in this range.

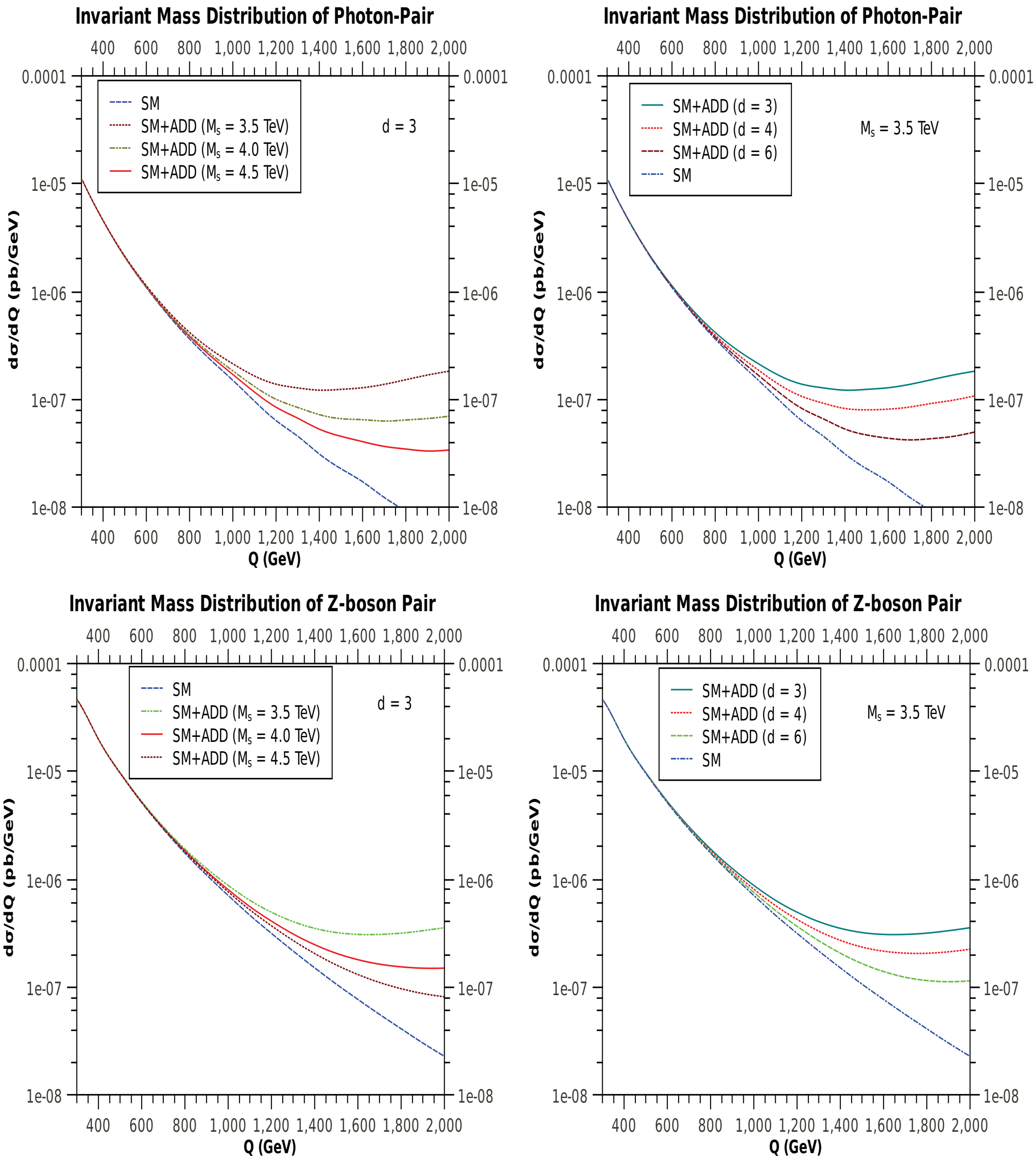

Figure 2.6: Invariant mass distribution of the photon pair in $\gamma\gamma Z$ final state (top panel) and Z boson pair in γZZ final state (bottom panel) for $d = 3$ with different values of M_S (left) and for $M_S = 3.5$ TeV with different values of d (right).

In order to estimate the factorisation scale μ_F dependence present in our LO results, in the right panel of Fig. 2.4 we have plotted rapidity distributions for three different choices of μ_F *i.e.*, $\mu_F = (0.2, 1, 2)P_T^{\gamma_1}$. In the central rapidity region, the variation of the rapidity distribution with respect to the factorisation scale is the largest. With respect to the central choice of $\mu_F = P_T^{\gamma_1}$, the variation is about 23.6 % and 8.2 % for the choice of $\mu_F = 0.2\ P_T^{\gamma_1}$ and $\mu_F = 2\ P_T^{\gamma_1}$ respectively.

The P_T distribution of γ_2 is found to be similar to that of γ_1, but it is different for γ_3 (the least energetic photon among the three) as shown in Fig. 2.5 (left panel). Similarly its rapidity distribution, which is shown in Fig. 2.5 (right panel), is also different from the most energetic photon.

2.3.2 $\gamma\gamma Z$ Production

Here, the invariant mass distribution of the photon pair is a useful observable because in the ADD model, the photon pair is one of the clean decay modes of the KK graviton and in the region of interest, this could give an enhancement of the tail of the distribution. In Fig. 2.6 (top left panel) we have presented the invariant mass distributions of the photon pair for different choices of $M_S = (3.5, 4, 4.5)$ TeV fixing $d = 3$, while in the top right panel the same distribution is plotted for different choices of $d = 3, 4, 6$, but for a fixed value of $M_S = 3.5$ TeV. We find that the KK modes dominate over the SM contribution for larger values of invariant masses (around 400 GeV or above, for a given set of M_S and d values) of photon pairs leading to a significant enhancement of the signal over the background. We plot the factorisation scale dependence of invariant mass distributions of photon pairs in Fig. 2.7 (left panel) for different choices of μ_F, *i.e.*, $\mu_F = (0.2, 2)Q$.

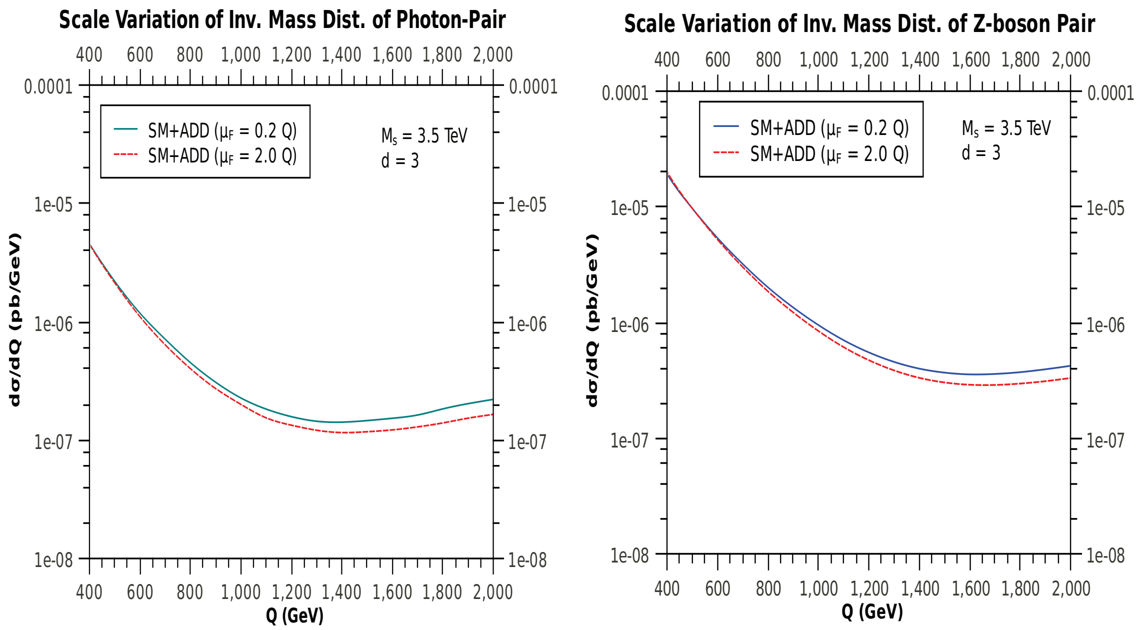

Figure 2.7: Dependence of invariant mass distribution of the photon pair in $\gamma\gamma Z$ final state (left panel) and Z boson pair in γZZ final state (right panel) on the factorisation scale for $d = 3$ and $M_S = 3.5$ TeV.

2.3.3 γZZ Production

Invariant mass of Z boson pair is again a useful observable. We have done a similar analysis as we did for $\gamma\gamma Z$ and use the same choice of factorisation scale and ADD model parameters. The invariant mass distributions are shown in the lower panels of Fig. 2.6 for different choices of M_S and d. We find that the invariant mass distributions of photon pairs in $\gamma\gamma Z$ production and Z boson pairs here have similar qualitative behavior. In order to investigate the uncertainty resulting from the factorisation scale μ_F, in Fig. 2.7 (right panel), we have plotted the invariant mass distributions of the Z boson pair for different choices of μ_F, *i.e.*, $\mu_F = (0.2, 2)Q$.

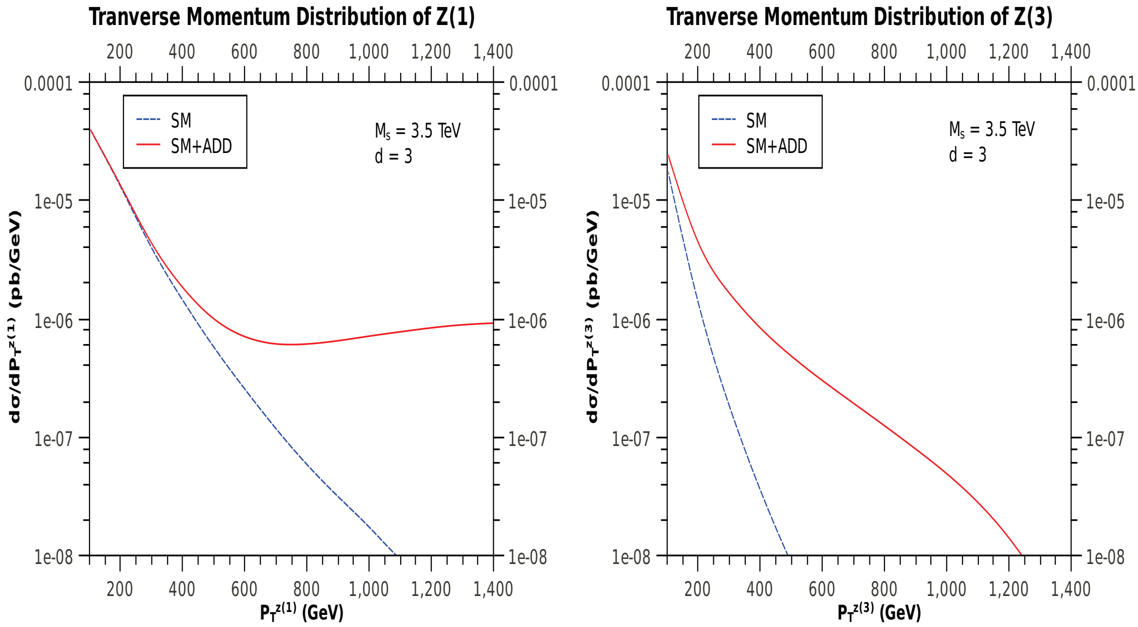

Figure 2.8: Transverse momentum distribution of Z_1 (left panel) and Z_3 (right panel) for $M_S = 3.5$ TeV and $d = 3$.

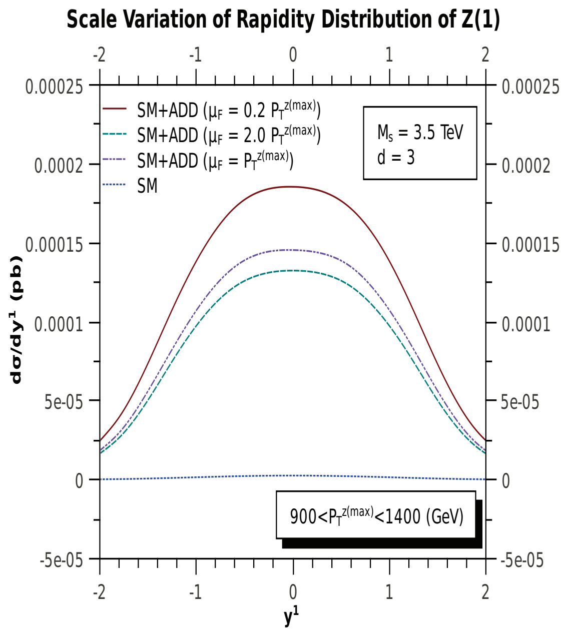

Figure 2.9: Rapidity distribution of Z_1 for $M_S = 3.5$ TeV and $d = 3$ in the region where $P_T^{Z_1} \in (900, 1400)$ GeV.

2.3.4 ZZZ Production

We have classified triple Z bosons in such a way that $P_T^{Z_1} > P_T^{Z_2} > P_T^{Z_3}$ and for the $P_T^{Z_i}$ distribution, we make the choice of factorisation scale as $\mu_F = P_T^{Z_i}$, where $i = 1, 2, 3$. In Fig. 2.8, we have presented the transverse momentum distributions of Z_1 (left panel) and Z_3 (right panel) for SM and SM+ADD with $M_S = 3.5$ TeV and $d = 3$. Also, rapidity distribution of Z_1 for SM and SM+ADD with the same model parameters is shown in Fig. 2.9. For the rapidity distribution, we have put the constrain: $900 < P_T^{Z_1} < 1400$ GeV. As in the case of $\gamma\gamma\gamma$, the $P_T^{Z_2}$ distribution is similar to that of $P_T^{Z_1}$ distribution. We have also shown the sensitivity of rapidity distribution to the factorisation scale μ_F by varying it between $\mu_F = 0.2 P_T^{Z_1}$ and $\mu_F = 2 P_T^{Z_1}$. In the central rapidity region, we estimate the variation of the rapidity distribution with the factorisation scale and find that for $\mu_F = 0.2 P_T^{Z_1}$ and $\mu_F = 2 P_T^{Z_1}$, such variations are about 27.5 % and 8.9 % respectively with respect to those at $\mu_F = P_T^{Z_1}$. The rapidity distribution for Z_2 is similar to that of Z_1 while Z_3 is different.

So far, in our numerical analysis, we have put the UV cutoff $\Lambda = M_S$ which is the conventional choice to do the phenomenology as mentioned earlier. The sensitivity of the choice of UV cutoff is presented in Fig. 2.10 for $P_T^{\gamma_1}$ distribution of $\gamma\gamma\gamma$ final state and also for the invariant mass distribution of $\gamma\gamma$ pair of $\gamma\gamma Z$ process by varying $\Lambda = (0.9,\ 0.95,\ 1) M_S$. The cross section at $P_T^{\gamma_1} = 1200$ GeV varies between 10 - 24 % as we vary $\Lambda = (0.9,\ 0.95) M_S$ as compared to $\Lambda = M_S$ for the $\gamma\gamma\gamma$ process. Similarly, for the cross section of $\gamma\gamma Z$ process at $Q = 2000$ GeV, the variation stands between 7 - 15 % in the same range of Λ.

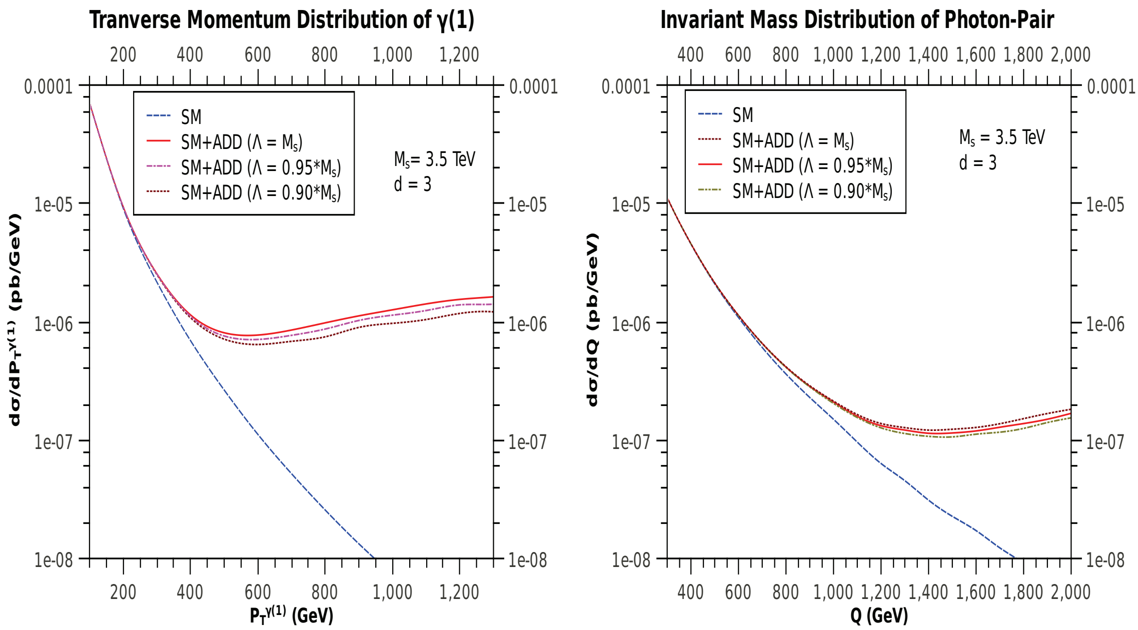

Figure 2.10: $P_T^{\gamma_1}$ distribution of $\gamma\gamma\gamma$ final state (left) and invariant mass distribution of the photon pair in $\gamma\gamma Z$ final state (right) using the cutoff scale $\Lambda = (0.9,\ 0.95,\ 1)M_S$ for $M_S = 3.5$ TeV and $d = 3$.

2.4 Pentagon Reduction

To make the pavement towards NLO corrections of these processes involving tensor couplings, reduction of 5-point tensor integrals will inevitably be required. Therefore, in this section, we deal with the way of reducing the one loop 5-point tensor integrals (up to rank-4) using the Passarino-Veltman reduction technique [77, 78, 79]. In fact, numerous activities have been performed in reducing one loop tensor integrals and calculating the scalar ones (see for example [80, 81, 82, 83, 84]). The following work is basically an extension of what was done in [85], where reduction of 4-point tensor integrals (up to rank-3) was taken care of. Here, we describe the usage of projective momenta technique and define new projective momenta to perform a complete study of reducing 4-rank 4-point and the full 5-point tensor integrals up to rank-4. All the analytical results are given in detail so that they can easily be coded in any analytical or numerical programme.

2.4.1 Notation & Convention

We define up to 5-point integrals in the following way,

$$A_0(M_1) = (2\pi\mu)^{4-n} \int \frac{d^n l}{i\pi^2} \frac{1}{D_1} \qquad ,$$

$$B_{\{0,\mu,\mu\nu\}}(p_1, M_1, M_2) = (2\pi\mu)^{4-n} \int \frac{d^n l}{i\pi^2} \frac{\{1, l_\mu, l_\mu l_\nu\}}{D_1 D_2} \qquad ,$$

$$C_{\{0,\mu,\mu\nu,\mu\nu\rho\}}(p_1, p_2, M_1, M_2, M_3) = (2\pi\mu)^{4-n} \int \frac{d^n l}{i\pi^2} \frac{\{1, l_\mu, l_\mu l_\nu, l_\mu l_\nu l_\rho\}}{D_1 D_2 D_3} \qquad ,$$

$$\begin{aligned} &D_{\{0,\mu,\mu\nu,\mu\nu\rho,\mu\nu\rho\lambda\}}(p_1, p_2, p_3, M_1, M_2, M_3, M_4) \\ &\qquad = (2\pi\mu)^{4-n} \int \frac{d^n l}{i\pi^2} \frac{\{1, l_\mu, l_\mu l_\nu, l_\mu l_\nu l_\rho, l_\mu l_\nu l_\rho l_\lambda\}}{D_1 D_2 D_3 D_4} \qquad , \end{aligned}$$

$$\begin{aligned} &E_{\{0,\mu,\mu\nu,\mu\nu\rho,\mu\nu\rho\lambda\}}(p_1, p_2, p_3, p_4, M_1, M_2, M_3, M_4, M_5) \\ &\qquad = (2\pi\mu)^{4-n} \int \frac{d^n l}{i\pi^2} \frac{\{1, l_\mu, l_\mu l_\nu, l_\mu l_\nu l_\rho, l_\mu l_\nu l_\rho l_\lambda\}}{D_1 D_2 D_3 D_4 D_5} \qquad . \end{aligned} \tag{2.4}$$

where M_is are the masses of off-shell internal lines and p_is are the on-shell 4-momentum of external particles and D_is are given here under:

$$D_1 = l^2 - M_1^2 + i\epsilon \qquad ,$$

$$D_2 = (l + p_1)^2 - M_2^2 + i\epsilon \qquad ,$$

$$D_3 = (l + p_1 + p_2)^2 - M_3^2 + i\epsilon \qquad ,$$

$$D_4 = (l + p_1 + p_2 + p_3)^2 - M_4^2 + i\epsilon \qquad ,$$

$$D_5 = (l + p_1 + p_2 + p_3 + p_4)^2 - M_5^2 + i\epsilon \qquad . \tag{2.5}$$

Note that, for the sake of simplicity, we keep ourselves confined to present analytical results involving massless internal lines in the loop. However, it is straight forward to extend such calculation for massive internal lines with nominal changes in few selective variables. It is evident that the above integrals listed in eq. (2.4) are symmetric in their Lorentz indices and they can be easily demonstrated in Lorentz covariant way as follows,

$$\begin{aligned} B_\mu &= p_{1\mu} B_1 \qquad , \\ B_{\mu\nu} &= p_{1\mu} p_{1\nu} B_{21} + g_{\mu\nu} B_{22} \qquad , \end{aligned} \tag{2.6}$$

$$\begin{aligned} C_\mu &= p_{1\mu} C_{11} + p_{2\mu} C_{12} \qquad , \\ C_{\mu\nu} &= p_{1\mu} p_{1\nu} C_{21} + p_{2\mu} p_{2\nu} C_{22} + \{p_1 p_2\}_{\mu\nu} C_{23} + g_{\mu\nu} C_{24} \qquad , \\ C_{\mu\nu\rho} &= p_{1\mu} p_{1\nu} p_{1\rho} C_{31} + p_{2\mu} p_{2\nu} p_{2\rho} C_{32} + \{p_1 p_1 p_2\}_{\mu\nu\rho} C_{33} + \{p_1 p_2 p_2\}_{\mu\nu\rho} C_{34} \end{aligned}$$

$$+\ \{p_1 g\}_{\mu\nu\rho} C_{35} + \{p_2 g\}_{\mu\nu\rho} C_{36} \qquad , \tag{2.7}$$

$$\begin{aligned}
D_\mu &= p_{1\mu} D_{11} + p_{2\mu} D_{12} + p_{3\mu} D_{13} \qquad , \\
D_{\mu\nu} &= p_{1\mu} p_{1\nu} D_{21} + p_{2\mu} p_{2\nu} D_{22} + p_{3\mu} p_{3\nu} D_{23} \\
&\quad + \{p_1 p_2\}_{\mu\nu} D_{24} + \{p_1 p_3\}_{\mu\nu} D_{25} + \{p_2 p_3\}_{\mu\nu} D_{26} + g_{\mu\nu} D_{27} \qquad , \\
D_{\mu\nu\rho} &= p_{1\mu} p_{1\nu} p_{1\rho} D_{31} + p_{2\mu} p_{2\nu} p_{2\rho} D_{32} + p_{3\mu} p_{3\nu} p_{3\rho} D_{33} \\
&\quad + \{p_1 p_1 p_2\}_{\mu\nu\rho} D_{34} + \{p_1 p_1 p_3\}_{\mu\nu\rho} D_{35} + \{p_1 p_2 p_2\}_{\mu\nu\rho} D_{36} \\
&\quad + \{p_1 p_3 p_3\}_{\mu\nu\rho} D_{37} + \{p_2 p_2 p_3\}_{\mu\nu\rho} D_{38} + \{p_2 p_3 p_3\}_{\mu\nu\rho} D_{39} \\
&\quad + \{p_1 p_2 p_3\}_{\mu\nu\rho} D_{310} + \{p_1 g\}_{\mu\nu\rho} D_{311} + \{p_2 g\}_{\mu\nu\rho} D_{312} + \{p_3 g\}_{\mu\nu\rho} D_{313} \qquad , \\
D_{\mu\nu\rho\lambda} &= p_{1\mu} p_{1\nu} p_{1\rho} p_{1\lambda} D_{41} + p_{2\mu} p_{2\nu} p_{2\rho} p_{2\lambda} D_{42} + p_{3\mu} p_{3\nu} p_{3\rho} p_{3\lambda} D_{43} \\
&\quad + \{p_1 p_1 p_1 p_2\}_{\mu\nu\rho\lambda} D_{44} + \{p_1 p_1 p_1 p_3\}_{\mu\nu\rho\lambda} D_{45} + \{p_1 p_1 p_2 p_2\}_{\mu\nu\rho\lambda} D_{46} \\
&\quad + \{p_1 p_1 p_2 p_3\}_{\mu\nu\rho\lambda} D_{47} + \{p_1 p_1 p_3 p_3\}_{\mu\nu\rho\lambda} D_{48} + \{p_1 p_2 p_2 p_2\}_{\mu\nu\rho\lambda} D_{49} \\
&\quad + \{p_1 p_2 p_2 p_3\}_{\mu\nu\rho\lambda} D_{410} + \{p_1 p_2 p_3 p_3\}_{\mu\nu\rho\lambda} D_{411} + \{p_1 p_3 p_3 p_3\}_{\mu\nu\rho\lambda} D_{412} \\
&\quad + \{p_2 p_2 p_2 p_3\}_{\mu\nu\rho\lambda} D_{413} + \{p_2 p_2 p_3 p_3\}_{\mu\nu\rho\lambda} D_{414} + \{p_2 p_3 p_3 p_3\}_{\mu\nu\rho\lambda} D_{415} \\
&\quad + \{p_1 p_1 g\}_{\mu\nu\rho\lambda} D_{416} + \{p_2 p_2 g\}_{\mu\nu\rho\lambda} D_{417} + \{p_3 p_3 g\}_{\mu\nu\rho\lambda} D_{418} \\
&\quad + \{p_1 p_2 g\}_{\mu\nu\rho\lambda} D_{419} + \{p_1 p_3 g\}_{\mu\nu\rho\lambda} D_{420} + \{p_2 p_3 g\}_{\mu\nu\rho\lambda} D_{421} + \{g g\}_{\mu\nu\rho\lambda} D_{422} \quad ,
\end{aligned} \tag{2.8}$$

$$\begin{aligned}
E_\mu &= p_{1\mu} E_{11} + p_{2\mu} E_{12} + p_{3\mu} E_{13} + p_{4\mu} E_{14} \qquad , \\
E_{\mu\nu} &= p_{1\mu} p_{1\nu} E_{21} + p_{2\mu} p_{2\nu} E_{22} + p_{3\mu} p_{3\nu} E_{23} + p_{4\mu} p_{4\nu} E_{24} \\
&\quad + \{p_1 p_2\}_{\mu\nu} E_{25} + \{p_1 p_3\}_{\mu\nu} E_{26} + \{p_1 p_4\}_{\mu\nu} E_{27} \\
&\quad + \{p_2 p_3\}_{\mu\nu} E_{28} + \{p_2 p_4\}_{\mu\nu} E_{29} + \{p_3 p_4\}_{\mu\nu} E_{210} + g_{\mu\nu} E_{211} \qquad ,
\end{aligned}$$

$$
\begin{aligned}
E_{\mu\nu\rho} &= p_{1\mu}p_{1\nu}p_{1\rho}E_{31} + p_{2\mu}p_{2\nu}p_{2\rho}E_{32} + p_{3\mu}p_{3\nu}p_{3\rho}E_{33} + p_{4\mu}p_{4\nu}p_{4\rho}E_{34} \\
&+ \{p_1p_1p_2\}_{\mu\nu\rho}E_{35} + \{p_1p_1p_3\}_{\mu\nu\rho}E_{36} + \{p_1p_1p_4\}_{\mu\nu\rho}E_{37} \\
&+ \{p_1p_2p_2\}_{\mu\nu\rho}E_{38} + \{p_1p_3p_3\}_{\mu\nu\rho}E_{39} + \{p_1p_4p_4\}_{\mu\nu\rho}E_{310} \\
&+ \{p_1p_2p_3\}_{\mu\nu\rho}E_{311} + \{p_1p_2p_4\}_{\mu\nu\rho}E_{312} + \{p_1p_3p_4\}_{\mu\nu\rho}E_{313} \\
&+ \{p_2p_2p_3\}_{\mu\nu\rho}E_{314} + \{p_2p_2p_4\}_{\mu\nu\rho}E_{315} + \{p_2p_3p_3\}_{\mu\nu\rho}E_{316} \\
&+ \{p_2p_4p_4\}_{\mu\nu\rho}E_{317} + \{p_2p_3p_4\}_{\mu\nu\rho}E_{318} + \{p_3p_3p_4\}_{\mu\nu\rho}E_{319} \\
&+ \{p_3p_4p_4\}_{\mu\nu\rho}E_{320} + \{p_1g\}_{\mu\nu\rho}E_{321} + \{p_2g\}_{\mu\nu\rho}E_{322} \\
&+ \{p_3g\}_{\mu\nu\rho}E_{323} + \{p_4g\}_{\mu\nu\rho}E_{324} \qquad , \\
E_{\mu\nu\rho\lambda} &= p_{1\mu}p_{1\nu}p_{1\rho}p_{1\lambda}E_{41} + p_{2\mu}p_{2\nu}p_{2\rho}p_{2\lambda}E_{42} + p_{3\mu}p_{3\nu}p_{3\rho}p_{3\lambda}E_{43} + p_{4\mu}p_{4\nu}p_{4\rho}p_{4\lambda}E_{44} \\
&+ \{p_1p_1p_1p_2\}_{\mu\nu\rho\lambda}E_{45} + \{p_1p_1p_1p_3\}_{\mu\nu\rho\lambda}E_{46} + \{p_1p_1p_1p_4\}_{\mu\nu\rho\lambda}E_{47} \\
&+ \{p_1p_1p_2p_2\}_{\mu\nu\rho\lambda}E_{48} + \{p_1p_1p_3p_3\}_{\mu\nu\rho\lambda}E_{49} + \{p_1p_1p_4p_4\}_{\mu\nu\rho\lambda}E_{410} \\
&+ \{p_1p_1p_2p_3\}_{\mu\nu\rho\lambda}E_{411} + \{p_1p_1p_2p_4\}_{\mu\nu\rho\lambda}E_{412} + \{p_1p_1p_3p_4\}_{\mu\nu\rho\lambda}E_{413} \\
&+ \{p_1p_2p_2p_2\}_{\mu\nu\rho\lambda}E_{414} + \{p_1p_2p_2p_3\}_{\mu\nu\rho\lambda}E_{415} + \{p_1p_2p_2p_4\}_{\mu\nu\rho\lambda}E_{416} \\
&+ \{p_1p_2p_3p_3\}_{\mu\nu\rho\lambda}E_{417} + \{p_1p_2p_3p_4\}_{\mu\nu\rho\lambda}E_{418} + \{p_1p_2p_4p_4\}_{\mu\nu\rho\lambda}E_{419} \\
&+ \{p_1p_3p_3p_3\}_{\mu\nu\rho\lambda}E_{420} + \{p_1p_3p_3p_4\}_{\mu\nu\rho\lambda}E_{421} + \{p_1p_3p_4p_4\}_{\mu\nu\rho\lambda}E_{422} \\
&+ \{p_1p_4p_4p_4\}_{\mu\nu\rho\lambda}E_{423} + \{p_2p_2p_2p_3\}_{\mu\nu\rho\lambda}E_{424} + \{p_2p_2p_2p_4\}_{\mu\nu\rho\lambda}E_{425} \\
&+ \{p_2p_2p_3p_3\}_{\mu\nu\rho\lambda}E_{426} + \{p_2p_2p_3p_4\}_{\mu\nu\rho\lambda}E_{427} + \{p_2p_2p_4p_4\}_{\mu\nu\rho\lambda}E_{428} \\
&+ \{p_2p_3p_3p_3\}_{\mu\nu\rho\lambda}E_{429} + \{p_2p_3p_3p_4\}_{\mu\nu\rho\lambda}E_{430} + \{p_2p_3p_4p_4\}_{\mu\nu\rho\lambda}E_{431} \\
&+ \{p_2p_4p_4p_4\}_{\mu\nu\rho\lambda}E_{432} + \{p_3p_3p_3p_4\}_{\mu\nu\rho\lambda}E_{433} + \{p_3p_3p_4p_4\}_{\mu\nu\rho\lambda}E_{434} \\
&+ \{p_3p_4p_4p_4\}_{\mu\nu\rho\lambda}E_{435} + \{p_1p_1g\}_{\mu\nu\rho\lambda}E_{436} + \{p_1p_2g\}_{\mu\nu\rho\lambda}E_{437} \\
&+ \{p_1p_3g\}_{\mu\nu\rho\lambda}E_{438} + \{p_1p_4g\}_{\mu\nu\rho\lambda}E_{439} + \{p_2p_2g\}_{\mu\nu\rho\lambda}E_{440} \\
&+ \{p_2p_3g\}_{\mu\nu\rho\lambda}E_{441} + \{p_2p_4g\}_{\mu\nu\rho\lambda}E_{442} + \{p_3p_3g\}_{\mu\nu\rho\lambda}E_{443} \\
&+ \{p_3p_4g\}_{\mu\nu\rho\lambda}E_{444} + \{p_4p_4g\}_{\mu\nu\rho\lambda}E_{445} + \{gg\}_{\mu\nu\rho\lambda}E_{446} \qquad . \qquad (2.9)
\end{aligned}
$$

In the above equations (eq. (2.6)-(2.9)), we have adopted some short-hand notations which are given here under:

$$\{p_i p_j p_k p_l\}_{\mu\nu\rho\lambda} = \sum_{\sigma(i,j,k,l)} p_{\sigma(i)_\mu} p_{\sigma(j)_\nu} p_{\sigma(k)_\rho} p_{\sigma(l)_\lambda} \qquad , \tag{2.10}$$

with $\sigma(i,j,k,l)$ denoting all different permutations of (i,j,k,l). Similar is the case for $\{p_i p_j p_k\}_{\mu\nu\rho}$ and $\{p_i p_j\}_{\mu\nu}$ expansions.

$$\begin{aligned} \{p_i p_j g\}_{\mu\nu\rho\lambda} &= \{p_i p_j\}_{\mu\nu} g_{\rho\lambda} + \{p_i p_j\}_{\mu\rho} g_{\nu\lambda} + \{p_i p_j\}_{\mu\lambda} g_{\nu\rho} \\ &+ \{p_i p_j\}_{\nu\rho} g_{\mu\lambda} + \{p_i p_j\}_{\nu\lambda} g_{\mu\rho} + \{p_i p_j\}_{\rho\lambda} g_{\mu\nu} \qquad , \end{aligned} \tag{2.11}$$

$$\{p_i g\}_{\mu\nu\rho} = p_{i_\mu} g_{\nu\rho} + p_{i_\nu} g_{\mu\rho} + p_{i_\rho} g_{\mu\nu} \qquad , \tag{2.12}$$

$$\{gg\}_{\mu\nu\rho\lambda} = g_{\mu\nu} g_{\rho\lambda} + g_{\mu\rho} g_{\nu\lambda} + g_{\mu\lambda} g_{\nu\rho} \qquad . \tag{2.13}$$

At this stage, our aim is to find all the co-efficients of $D_{\mu\nu\rho\lambda}$ (in eq. (2.8)) and for all others represented in eq. (2.9). Rest of the co-efficients of eq. (2.6),(2.7),(2.8) have already been calculated and they are listed in [85].

2.4.2 Reduction of 4-point 4-rank Tensor

Apparently, it seems that, if we want to find out the co-efficients of $D_{\mu\nu\rho\lambda}$, we have to deal with a 22×22 matrix. But, this can be reduced to a 3×3 matrix problem by introducing three projective momenta P_is' which would have the following properties:

$$P_i^\mu p_{j\mu} = \delta_{ij} \qquad \forall \qquad i,j = 1,2,3 \qquad . \tag{2.14}$$

The existence of such projective momenta is directly related to the existence of X^{-1} matrix, where the X matrix is defined as follows,

$$X(p_1, p_2, p_3) \equiv X_{[1,2,3]} = \begin{pmatrix} p_1^2 & p_1.p_2 & p_1.p_3 \\ p_1.p_2 & p_2^2 & p_2.p_3 \\ p_1.p_3 & p_2.p_3 & p_3^2 \end{pmatrix} \quad . \tag{2.15}$$

In other words, if these three 4-momenta p_1, p_2, p_3 form an independent set resulting $det[X] \neq 0$, then only construction of such P_is would be possible. Construction of an another projective tensor $P^{\mu\nu}$ is inevitable in order to find out the co-efficients of $D_{\mu\nu}$ (eq. (2.8)) and its form and properties are given below:

$$P^{\mu\nu} = \frac{1}{(n-3)} \left\{ g^{\mu\nu} - \sum_{i=1}^{3} P_i^\mu p_i^\nu \right\} \quad , \tag{2.16}$$

$$p_{i\mu} P^{\mu\nu} = 0 \quad \text{and} \quad g_{\mu\nu} P^{\mu\nu} = 1 \quad . \tag{2.17}$$

With the correct combination of these two types of projective tensors mentioned above, we can now define a new projective tensor which is essential to be able to find some of the co-efficients of $D_{\mu\nu\rho\lambda}$ and it is of the following form,

$$P^{\mu\nu\rho}_{i,j,k} = P_i^\mu P_j^\nu P_k^\rho - (P_i.P_j) P^{\mu\nu} P_k^\rho - (P_j.P_k) P^{\mu\nu} P_i^\rho - (P_k.P_i) P^{\mu\nu} P_j^\rho \quad . \tag{2.18}$$

For example, by applying $P^{\mu\nu\rho}_{1,1,1}$ on $D_{\mu\nu\rho\lambda}$, we get the following matrix identity which is indeed a 3×3 matrix relation:

$$P^{\mu\nu\rho}_{1,1,1} D_{\mu\nu\rho\lambda} \begin{pmatrix} p_1^\lambda \\ p_2^\lambda \\ p_3^\lambda \end{pmatrix} = X_{[1,2,3]} \begin{pmatrix} D_{41} \\ D_{44} \\ D_{45} \end{pmatrix} + \begin{pmatrix} 3D_{416} \\ 0 \\ 0 \end{pmatrix} = \begin{pmatrix} R_{441} \\ R_{442} \\ R_{443} \end{pmatrix} \quad . \tag{2.19}$$

In a like manner, we can easily get similar kind of matrix equations (see Appendix B.1), which in fact provide the solution for the co-efficients ranging from D_{41} to D_{415} with the proper choice of $P_{i,j,k}$, provided we need to know the exact solution for the rest of the unknown variables (*e.g.* D_{416} and $R_{441-443}$ in eq. (2.19)) beforehand. In order to find such relations involving the co-efficients D_{416} to D_{421}, we need to operate $P^{\mu\nu} P_i^{\rho}$ on $D_{\mu\nu\rho\lambda}$ where $i = 1, 2, 3$. Following is just one of these relations:

$$P^{\mu\nu} P_1^{\rho} D_{\mu\nu\rho\lambda} \begin{pmatrix} p_1^{\lambda} \\ p_2^{\lambda} \\ p_3^{\lambda} \end{pmatrix} = X_{[1,2,3]} \begin{pmatrix} D_{416} \\ D_{419} \\ D_{420} \end{pmatrix} + \begin{pmatrix} D_{422} \\ 0 \\ 0 \end{pmatrix} = \begin{pmatrix} R_{4422} \\ R_{4423} \\ R_{4424} \end{pmatrix} \quad . \tag{2.20}$$

Rest of them are listed in Appendix B.1. Now, the only co-efficient left to evaluate is D_{422}, which demands invocation of another new projection operator ($P^{\mu\nu\rho\lambda}$), that obeys the following relation:

$$P^{\mu\nu\rho\lambda} = \left(\frac{n-3}{n-1}\right) P^{\mu\nu} P^{\rho\lambda} \qquad , \tag{2.21}$$

and applying this projective tensor on $D_{\mu\nu\rho\lambda}$, we finally get,

$$P^{\mu\nu\rho\lambda} D_{\mu\nu\rho\lambda} = D_{422} \qquad . \tag{2.22}$$

At this point, complete solutions for these co-efficients are one step away, as we are to derive the solutions for the R-functions right away. The calculation is straight forward and it will be more vivid with the following explicit derivation of R_{441} given here under:

$$R_{441} \;=\; P_{1,1,1}^{\mu\nu\rho} D_{\mu\nu\rho\lambda} p_1^{\lambda}$$

$$
\begin{aligned}
&= (2\pi\mu)^{4-n}\int \frac{d^n l}{i\pi^2} P^{\mu\nu\rho}_{1,1,1}\frac{l_\mu l_\nu l_\rho l_\lambda}{D_1 D_2 D_3 D_4} p_1^\lambda \\
&= (2\pi\mu)^{4-n}\int \frac{d^n l}{i\pi^2}[P_1^\mu P_1^\nu P_1^\rho - 3(P_1.P_1)P^{\mu\nu}P_1^\rho]\frac{l_\mu l_\nu l_\rho}{D_1 D_2 D_3 D_4}(l.p_1) \\
&= (2\pi\mu)^{4-n}\int \frac{d^n l}{i\pi^2}[P_1^\mu P_1^\nu P_1^\rho - 3(P_1.P_1)P^{\mu\nu}P_1^\rho]\frac{l_\mu l_\nu l_\rho}{D_1 D_2 D_3 D_4} \\
&\quad \times \frac{1}{2}[(l+p_1)^2 - l^2 - p_1^2] \\
&= \frac{1}{2}\left\{(2\pi\mu)^{4-n}\int \frac{d^n l}{i\pi^2}[P_1^\mu P_1^\nu P_1^\rho - 3(P_1.P_1)P^{\mu\nu}P_1^\rho]\frac{l_\mu l_\nu l_\rho}{D_1 D_3 D_4}\right. \\
&\quad - (2\pi\mu)^{4-n}\int \frac{d^n l}{i\pi^2}[P_1^\mu P_1^\nu P_1^\rho - 3(P_1.P_1)P^{\mu\nu}P_1^\rho] \\
&\qquad\qquad \times \frac{(l-p_1)_\mu (l-p_1)_\nu (l-p_1)_\rho}{l^2(l+p_2)^2(l+p_2+p_3)^2} \\
&\quad \left. - (2\pi\mu)^{4-n}\int \frac{d^n l}{i\pi^2}[P_1^\mu P_1^\nu P_1^\rho - 3(P_1.P_1)P^{\mu\nu}P_1^\rho]\frac{l_\mu l_\nu l_\rho\, p_1^2}{D_1 D_2 D_3 D_4}\right\} \\
&= \frac{1}{2}[P_1^\mu P_1^\nu P_1^\rho - 3(P_1.P_1)P^{\mu\nu}P_1^\rho][C_{\mu\nu\rho}(p_1+p_2,p_3) - C_{\mu\nu\rho}(p_2,p_3) \\
&\quad +(\{llp_1\}_{\mu\nu\rho} - \{lp_1p_1\}_{\mu\nu\rho} + p_1^\mu p_1^\nu p_1^\rho)C_0(p_2,p_3) - p_1^2 D_{\mu\nu\rho}(p_1,p_2,p_3)] \\
&= \frac{1}{2}[C_{31}(p_1+p_2,p_3) + C_0(p_2,p_3) - p_1^2 D_{31}(p_1,p_2,p_3)] \qquad . \qquad (2.23)
\end{aligned}
$$

Rest of the R-functions can be derived in the similar way and all of them are listed in Appendix B.1.

2.4.3 Reduction of 5-point Tensor

The main thing to remember at the time of reducing 5-point tensor integrals is that, here the number of independent external 4-momenta is four (*i.e.*, p_1, p_2, p_3, p_4) and one has to define all the projective momenta and projective tensors consistently. So, to keep pace with the above statement, it is obvious that we would require four projective momenta with the following properties,

$$
P_i^\mu p_{j\mu} = \delta_{ij} \qquad \forall \qquad i,j = 1,2,3,4 \qquad . \qquad (2.24)
$$

In this case, X-matrix has to be redefined and the projective tensor $P^{\mu\nu}$ has to be modified maintaining the same properties as described in eq. (2.17), in the following way,

$$X(p_1, p_2, p_3, p_4) \equiv X_{[1,2,3,4]} = \begin{pmatrix} p_1^2 & p_1.p_2 & p_1.p_3 & p_1.p_4 \\ p_1.p_2 & p_2^2 & p_2.p_3 & p_2.p_4 \\ p_1.p_3 & p_2.p_3 & p_3^2 & p_3.p_4 \\ p_1.p_4 & p_2.p_4 & p_3.p_4 & p_4^2 \end{pmatrix} \quad , \tag{2.25}$$

$$P^{\mu\nu} = \frac{1}{(n-4)} \left\{ g^{\mu\nu} - \sum_{i=1}^{4} P_i^{\mu} p_i^{\nu} \right\} \quad . \tag{2.26}$$

With the help of the above two projection operators, we can easily reduce E_μ and $E_{\mu\nu}$ and their expressions are provided in detail in Appendix B.2. In order to reduce $E_{\mu\nu\rho}$ and $E_{\mu\nu\rho\lambda}$, projective tensors similar to $P_{i,j}^{\mu\nu}$ and $P_{i,j,k}^{\mu\nu\rho}$ would work with the only modification therein that the latin indices will now run from 1 to 4, unlike the 4-point reduction case, where they are running from 1 to 3, *i.e.*,

$$P_{i,j}^{\mu\nu} = P_i^{\mu} P_j^{\nu} - (P_i.P_j) P^{\mu\nu} \quad , \tag{2.27}$$

$$P_{i,j,k}^{\mu\nu\rho} = P_i^{\mu} P_j^{\nu} P_k^{\rho} - (P_i.P_j) P^{\mu\nu} P_k^{\rho} - (P_j.P_k) P^{\mu\nu} P_i^{\rho} - (P_k.P_i) P^{\mu\nu} P_j^{\rho} \quad , \tag{2.28}$$

where $i, j, k = 1, 2, 3, 4$. In addition, to find out the solution for the co-efficient E_{446} in eq. (2.9), one has to consider the following relation,

$$\mathcal{P}^{\mu\nu\rho\lambda} E_{\mu\nu\rho\lambda} = E_{446} \quad , \tag{2.29}$$

where

$$\mathcal{P}^{\mu\nu\rho\lambda} = \left(\frac{1}{2n-7} \right) P^{\mu\nu} P^{\rho\lambda} \quad . \tag{2.30}$$

All the (4×4) matrix relations along with the R-functions for all reduced 5-point integrals are systematically jotted down in Appendix B.2.

2.5 Conclusion

In this chapter, we have studied the neutral triple gauge boson production processes at the LHC in theories with large extra dimensions which are produced via the exchange of a tower of KK graviton, taking into account the SM contributions altogether. All the final state photons and Z bosons are taken to be real. We have performed various checks on our analytical results and the numerical predictions are obtained using a Monte Carlo code which allows us to implement various experimental cuts. For the case in which the gauge bosons in the final state are identical we have presented the transverse momentum distribution by ordering the transverse momentum as $P_T^{V_1} > P_T^{V_2} > P_T^{V_3}$. We find that $P_T^{V_1}$ and $P_T^{V_2}$ distributions are similar but the one for $P_T^{V_3}$ is different. The rapidity distributions are also presented. For the case where one of the gauge bosons in the final state is different, we choose to use the invariant mass distribution of the identical di-bosons, as it would be a better discriminator in the region of interest. We have also studied their dependencies on the ADD model parameter M_S and the number of extra dimensions d, keeping the UV scale $\Lambda = M_S$. In addition, we have reported the sensitivity of the choice of Λ by varying it from $\Lambda = 0.9M_S$ to $0.95M_S$. We have also studied the dependence of our LO predictions on the factorisation scale. Nevertheless, a detailed calculation of 5-point tensor integral reduction using Passarino-Veltman technique has been presented in order to reveal its analytical results in a ready-to-use format. Howsoever, we have not yet dealt with complete calculation of any process to the NLO accuracy. In the next chapter, we will present NLO QCD correction to the associated production of the vector gauge boson ($Z/W^{\pm}$) and the graviton in the LED model at the LHC and discuss its effect on various kinematical observables.

Chapter 3

Real Graviton Production

3.1 Introduction

We already know that the collective contribution of the graviton modes reveals their non-negligible interaction with the SM fields and offers the best possibility of probing the low scale quantum gravity effects at the collider experiments. Consequently, a very rich and interesting collider signals of some important processes have been reported in the literature, but most of them are available only at the leading order in the perturbation theory [40, 41, 61, 62, 86, 87, 88]. The K-factors in some cases are found to be as high as a factor of two. Pair production processes are the best to exemplify the case of virtual graviton effects, where the NLO QCD corrections are computed for di-lepton [50, 51, 52, 89], diphoton [56, 57], di-Z and W^+ W^- [59, 60, 90, 91] production processes. In the context of missing energy signals in LED model, the NLO QCD corrections are presented for the processes (*i*) jet plus graviton production [92] and (*ii*) photon plus graviton production [93]. In each of these two cases, it is shown that the K-factors can be as high as 1.5 at the LHC. In this present chapter, we are going to compute the NLO QCD corrections to the associated production of vector gauge boson and the graviton at the LHC and give a quantitative estimate of the impact of these radiative corrections.

The gravitons when produced at the collider experiments escape the experimental detection due to their small couplings and negligible decays into SM particles. The production of vector bosons ($V = Z,\ W^{\pm}$) together with such an invisible gravitons (G) can give rise to a very large missing transverse momentum signals at collider experiments. Hence, the study of graviton plus gauge boson production, in general, would be a useful one in probing the new physics at the LHC. This process has been studied at LO in the context of lepton colliders [94, 95] as well as at the hadron colliders [96] and also has been implemented in Pythia8 [97]. The process is an important one and stands complementary to the more conventional ones involving the graviton production, like jet plus graviton or photon plus graviton productions, that are generally useful in the search of extra dimensions at the collider experiments.

It is important to note that there is a SM background which gives signature similar to those of associated production of Z and G. This SM background receives a dominant contribution coming from the ZZ production process, where one of the Z bosons in the final state decays into a pair of neutrinos ($Z \to \nu\bar{\nu}$) leading to Z boson plus missing energy signal. The other Z boson can be identified via its decays to leptons, mostly electrons and muons and then constraining the lepton invariant mass close to the mass of the Z boson to consider only the on-shell Z bosons. A detailed study of the event selection and the minimization of other SM contributions to this process $ZZ \to l\bar{l}\nu\bar{\nu}$, using MC@NLO [32] and Pythia [24], is taken up in the context of ATLAS detector simulation and is presented in [98]. Any deviation from this SM prediction will hint some beyond SM scenario and hence a study of this process will be useful in searching the new physics.

In the context of extra dimensions, a study of the Z plus graviton production at

LO at the LHC is discussed in [96], where the Z boson identification is done with the leptonic decay modes and using the cuts on the leptons as specified in [98]. It is worth noting here that a signal of Z boson plus missing energy can also come from the production of Z plus unparticle $\mathcal{U}$, where the unparticle leads to missing energy signal. A study of such process based on ATLAS detector simulation [96] shows that the vector unparticles are difficult to be probed using this channel, whereas the tensor unparticles can give signals identical to that of the graviton. In view of the above, it is worth studying gauge boson plus missing energy signals, in particular ZG production, which could be useful to confirm the extra dimensional signals once they are seen in the main channels like jet or photon plus missing energy.

In what follows, we describe the computation of NLO cross sections for the processes under study. Since our focus is on the QCD part in this work, we will confine our calculation to the production of on-shell Z and $W^{\pm}$ bosons. A more detailed study involving their decays into leptons requires a full detector level simulation with the appropriate cuts at NLO and is beyond the scope of this thesis.

3.2 Analytical Details

3.2.1 Leading Order Calculation

At the lowest order in the perturbation theory, the associated production of the vector gauge boson and the graviton takes place via the quark anti-quark initiated subprocess given by,

$$q_{a'}(p_1) + \bar{q}_{b'}(p_2) \to V(p_3) + G(p_4) \qquad , \tag{3.1}$$

where $V = Z, W^{\pm}$ and a', b' are flavour indices. The corresponding Feynman diagrams are shown in Fig. 3.1. These diagrams are obtained by considering the tree level $q\bar{q}V$ diagram and by attaching the graviton line to all possible external legs and the $q\bar{q}V$ vertex. The Feynman rules and the summation of polarization tensor

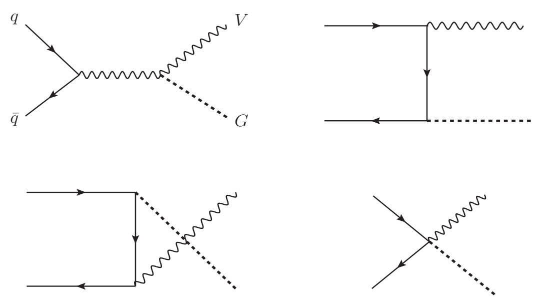

Figure 3.1: Feynman diagrams that contribute to the associate production of the vector boson and the graviton at the leading order.

of the graviton are given in [40, 41]. The couplings of the fermions to the Z and W bosons are given by,

$$- i\frac{eT_Z}{2}\ \gamma^{\mu}(C_v - C_a\gamma^5)\ , \qquad -i\frac{eT_W}{2}\ \gamma^{\mu}(1-\gamma^5) \qquad , \tag{3.2}$$

where

$$T_Z = \frac{1}{\cos\theta_W\ \sin\theta_W}\ , \qquad T_W = \frac{1}{\sqrt{2}\ \sin\ \theta_W} \qquad ,$$

and the co-efficients C_v and C_a are

$$C_v = T_3^f - 2\ \sin^2\theta_W\ Q_f\ , \qquad C_a = T_3^f \qquad . \tag{3.3}$$

Here, Q_f and T_3^f denote the electric charge and the third component of the isospin of the quarks respectively and θ_W is the weak mixing angle. For the vector gauge boson, the propagator in the unitary gauge ($\xi \to \infty$) has been used throughout. This choice of the unitary gauge in the electroweak sector has the advantage of having vanishing goldstone and ghost contributions. The leading order matrix elements for the associated production of Z boson and the graviton are computed using the algebraic manipulation program FORM [73] and the square amplitude (in n space-time dimensions) is as follows,

$$
\begin{aligned}
\sum_{spin} \overline{|M|}^2 = \frac{1}{4}\,\frac{1}{3}\,\frac{1}{96}\,(C_v^2 + C_a^2)\,\frac{\kappa^2\, T_Z^2}{(D^2\, t^2\, u^2)}\times \\
\Big[12m^{10}(n-2)tu + m^2 tu\{3(n-2)^2t^4 - 2[-68+n(104+(-31+ \\
n)n)]t^3u + 2[284+n(-264+(63-2n)n)]t^2u^2 - 2[-68+n(104+(n- \\
31)n)]tu^3 + 3(n-2)^2u^4 - 48m_Z^6(n-2)(t+u) - 4m_Z^4[3(n-9)(n- \\
2)t^2 + 2(124+3(n-21)n)tu + 3(n-9)(n-2)u^2] + 4m_Z^2(t+u)[3(n- \\
5)(n-2)t^2 - 2(-90+n(n+35))tu + 3(n-5)(n-2)u^2]\} - 3m^8\{12(n- \\
2)tu(t+u) + m_Z^2[(n-2)^2t^2 + 2(16+(n-14)n)tu + (n-2)^2u^2]\} - \\
3m^6\{4m_Z^4(18+(n-13)n)tu - 2m_Z^2(t+u)[(n-2)^2t^2 + 2(26+n(2n- \\
21))tu + (n-2)^2u^2] - tu[(n-2)(10+n)t^2 + 2(-32+3n(2+n))tu + \\
(n-2)(10+n)u^2]\} + 2t^2u^2\{32m_Z^6(n-2) - 8m_Z^4(-6+n+n^2)(t+ \\
u) + (40+(n-17)n)(t+u)[(n-2)t^2 + 2(n-4)tu + (n-2)u^2] - \\
m_Z^2[(n-2)(48+(n-25)n)t^2 + 2(-156+n(118+(n-27)n))tu + \\
(n-2)(48+(n-25)n)u^2]\} + m^4\{48m_Z^6(n-2)tu + 24m_Z^4(18+(n- \\
12)n)tu(t+u) - 6tu(t+u)[(n-2)nt^2 + 2(-12+n(3n-4))tu + (n- \\
2)nu^2] - m_Z^2[3(n-2)^2t^4 + 12(n-6)(3n-5)t^3u + 2(604+n(25n- \\
344))t^2u^2 + 12(n-6)(3n-5)tu^3 + 3(n-2)^2u^4]\}\Big] \quad ,
\end{aligned}
\tag{3.4}
$$

where $D = (s - m_Z^2)$ and s, t, u are the usual Mandelstam invariants. Here m_Z and m denote the masses of Z boson & KK graviton respectively. The over all bar in LHS of eq. (3.4) represents that the matrix elements have been averaged over the spins and the colors of the initial state particles and summed over those of the final state ones.

3.2.2 Next-to-Leading Order Calculation

At the NLO in the perturbation theory, the cross sections receive $\mathcal{O}(\alpha_s)$ contributions from real emission as well as virtual diagrams. The integration over the phase space of the real emission diagrams will give rise to IR divergences (soft and collinear) in the limit where the additional parton at NLO is either soft and/or collinear to the initial state partons. On the other hand, the integration over the loop momenta in the virtual diagrams will also give rise to IR divergences, in addition to the UV divergences. In our calculation, we regulate all these divergences using dimensional regularisation with $n = (4+\epsilon)$, n being the number of space-time dimensions. Completely anti-commuting γ_5 prescription [99] is used to handle γ_5 in n dimensions. Here, it should be noted that as the gravitons couple to the energy momentum tensor of the SM fields, which is a conserved quantity, there won't be any UV divergences coming from the loop diagrams.

There are several methods available in the literature to compute NLO QCD corrections. Standard methods based on fully analytical computation deal with the phase space and loop integrals in n-dimensions and give a finite $\mathcal{O}(\alpha_s)$ contribution to the cross sections, after the real and the virtual contributions are added together and the initial state collinear singularities are absorbed into the bare PDF. However, these methods are not useful whenever the particles in the final state are subjected to either experimental cuts or some isolation algorithms. In such cases, semi analytical methods like phase space slicing method [100] or dipole subtraction method [101] are extremely useful. In the present work, we have resorted to the former with two cutoffs to compute the radiative corrections. In this method, the IR divergences appearing in the real diagrams can be handled in a convenient way by slicing the soft and collinear divergent regions from the full three body phase space. The advantage of this method is that the integration over the remaining phase space can be carried out in 4-dimensions, rather than in n-dimensions, using standard Monte Carlo techniques. In what follows, we give some of the details about the implementation of this phase space slicing method in our NLO computation.

Real Emission Processes

There are two types of subprocesses that contribute to the associated production of the vector gauge boson and the graviton at NLO in QCD. They proceed by $q\bar{q}$ and qg initial states. At parton level, the $2 \to 3$ quark anti-quark initiated subprocess is given by,

$$q_{a'}(p_1) \ + \ \bar{q}_{b'}(p_2) \to V(p_3) \ + \ G(p_4) \ + \ g(p_5) \qquad .$$

We find that 14 diagrams contribute to this subprocess and a few of them are depicted in Fig. 3.2. These diagrams are obtained by taking the t-channel $q\bar{q} \to Vg$ diagram at tree level and by attaching the graviton line to all possible external as well as internal lines and to the vertices. The remaining diagrams are obtained by interchanging the vector boson and the graviton lines in Fig. 3.2. In general, diagrams such as those involving gluons and massless quarks are prone to be singular in the soft and collinear regions of the 3-body phase space integration. In the phase space slicing method that we have adopted here, these soft and collinear regions are separated from the full 3-body phase space using two small cutoff parameters, namely δ_s and δ_c, that define these singular regions. In the center of mass frame of the partons, the soft region is defined as: $0 \leq E_5 \leq \frac{1}{2}\delta_s\sqrt{s}$, where E_5 is the

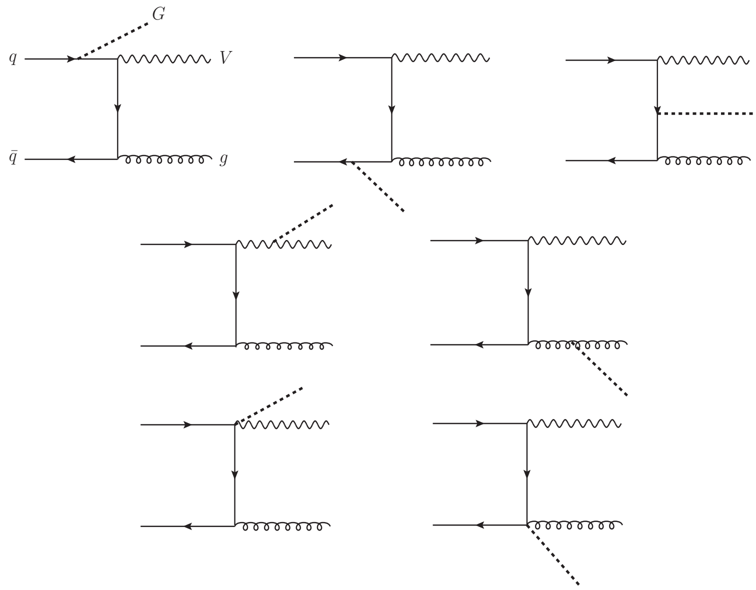

Figure 3.2: Real gluon emission diagrams.

gluon energy and $\sqrt{s}$ is the parton center of mass energy. Integration of the eikonal approximated $2 \to 3$ matrix elements over the soft region of the phase space gives the $\mathcal{O}(\alpha_s)$ 2-body contribution,

$$d\hat{\sigma}_S = a_s\ C_F\ F(\epsilon, \mu_R, s) \left(\frac{16}{\epsilon^2} + \frac{16}{\epsilon}\ \ln\ \delta_s + 8\ \ln^2\ \delta_s \right)\ d\hat{\sigma}_0 \qquad , \tag{3.5}$$

where

$$F(\epsilon, \mu_R, s) = \left[\frac{\Gamma(1+\frac{\epsilon}{2})}{\Gamma(1+\epsilon)} \left(\frac{4\pi\mu_R^2}{s} \right)^{-\frac{\epsilon}{2}} \right], \quad C_F = \frac{N^2-1}{2N} \quad \text{and} \quad a_s = \frac{\alpha_s(\mu_R)}{4\pi} \quad .$$

Here, $\alpha_s(\mu_R) = g_s^2(\mu_R)/4\pi$ with g_s being the running strong coupling constant, μ_R is the renormalisation scale and N is the number of colors. The region complementary to that of the soft region (S), *i.e.*, $E_5 > \frac{1}{2}\delta_s\sqrt{s}$, is defined as the hard region (H) of the phase space. Within this hard region "H", the emitted gluon can be collinear to the incoming massless quark or anti-quark and hence can give rise to hard collinear divergences. By introducing another small cutoff parameter (δ_c), we separate these collinear divergences from the hard region. The hard collinear region (HC) can be defined as: $0 \leq -t_{ij} \leq \delta_c s$ ($i = 1,2$ and $j = 5$), where $t_{ij} = (p_i - p_j)^2$. In the collinear limit, both the $2 \to 3$ matrix elements and the 3-body phase space get simplified to be expressed in terms of the born cross section as,

$$\begin{aligned} d\sigma_{HC}^{q\bar{q}} &= 4a_s\ d\hat{\sigma}_0\ F(\epsilon, \mu_R, s) \left(\frac{1}{\epsilon}\right)\Big\{\big[P_{qq}(z,\epsilon) f_{q/P}(x_1/z)\ f_{\bar{q}/P}(x_2) + (q \leftrightarrow \bar{q})\big] \\ &\quad +(x_1 \leftrightarrow x_2)\Big\}\frac{dz}{z}\ \left(\delta_c \frac{1-z}{z}\right)^{\frac{\epsilon}{2}} dx_1\ dx_2 \qquad , \end{aligned} \tag{3.6}$$

where $f_{a/P}(x)$ is the bare PDF and $P_{ab}(z,\epsilon)$ is the unregulated splitting functions in n-dimensions (where $a, b = q, \bar{q}, g$) and it is related to the usual Altarelli-Parisi splitting kernels as $P_{ab}(z,\epsilon) = P_{ab}(z) + \epsilon P'_{ab}(z)$ [100]. Here z denotes the fraction of the incoming parton's ('b') momentum carried by the parton 'a'. Note that for P_{qq} splitting in the hard region, since a fraction of the parton momentum *i.e.*, δ_s is already carried away by the gluon, the effective limits of the integration for z will be $0 < z < 1 - \delta_s$.

Apart from the $q\bar{q}$ initiated subprocess at NLO, there will also be a $q(\bar{q})g$ initiated subprocess given by,

$$q_{a'}(p_1)\ +\ g(p_2)\ \ \to\ \ V(p_3)\ + G(p_4)\ +\ q_{b'}(p_5) \qquad .$$

Here the emitted parton, being a quark or an anti-quark instead of a gluon, won't give rise to soft singularity. However, there will be hard collinear singularities whenever the emitted quark (anti-quark) becomes collinear to the incoming partons. These collinear singularities are separated using the cutoff δ_c in the same way as in the case of $q\bar{q}$ initiated subprocess. The cross section in this collinear region turns out to be,

$$d\sigma_{HC}^{qg,\bar{q}g} = 4a_s \; d\hat{\sigma}_0 \; F(\epsilon, \mu_R, s) \left(\frac{1}{\epsilon}\right) \Big\{ \big[P_{\bar{q}g}(z,\epsilon) \; f_{q/P}(x_1) \; f_{g/P}(x_2/z) + (q \leftrightarrow \bar{q}) \big]$$

$$+ (x_1 \leftrightarrow x_2) \Big\} \; \frac{dz}{z} \; \left(\delta_c \frac{1-z}{z}\right)^{\frac{\epsilon}{2}} dx_1 \; dx_2 \qquad . \tag{3.7}$$

These initial state collinear divergences, appearing as poles in ϵ in eq. (3.6) & (3.7), are purely due to the massless nature of the partons involved in the scattering process. These divergences can be factored out from the parton level cross sections and absorbed into the bare PDF at an arbitrary factorization scale μ_F, a process called mass factorization. In the $\overline{MS}$ scheme, the scale dependent PDF $f_{a/P}(x, \mu_F)$ can be expressed in terms of the bare PDF as follows,

$$f_{a/P}(x, \mu_F) = f_{a/P}(x) + \; 2a_s \; \sum_b \left(\frac{1}{\epsilon}\right) F(\epsilon, \mu_R, \mu_F) \int_x^1 \frac{dz}{z} \; P_{ab}(z) \; f_{b/P}(x/z) \; . \tag{3.8}$$

Substituting these parton densities in $d\hat{\sigma}_0$ produces collinear singular counter terms which when added with the hard collinear contributions results in the following $\mathcal{O}(\alpha_s)$ contribution [56, 57, 59, 60, 90, 91],

$$d\sigma_{coll} = 2a_s \; d\hat{\sigma}_0 \; F(\epsilon, \mu_R, s) \bigg(\Big\{ f_{\bar{q}/p}(x_2, \mu_F) [\widetilde{f}_{q/p}(x_1, \mu_F) + f_{q/p}(x_1, \mu_F)$$

$$\left(-\frac{2}{\epsilon} + \ln \frac{s}{\mu_F^2}\right) A_{q\to q+g}] + (q \leftrightarrow \bar{q}) \Big\} + (x_1 \leftrightarrow x_2) \bigg) \; dx_1 \; dx_2 \; , \tag{3.9}$$

where $A_{q\to q+g} = C_F \left(2 \ln \delta_s + \frac{3}{2}\right)$. The tilde parton distribution functions are given by [93, 100],

$$\widetilde{f}_{q/P}(x, \mu_F) = \sum_{b=q,g} \int_x^{1-\delta_s \delta_{qb}} \frac{dy}{y} f_{b/P}(x/y, \mu_F) \times \widetilde{P}_{qb}(y) \qquad , \tag{3.10}$$

where

$$\widetilde{P}_{ab}(y) = P_{ab}(y) \ln\Big(\delta_c \, \frac{1-y}{y} \frac{s}{\mu_F^2}\Big) - P'_{ab}(y) \qquad . \tag{3.11}$$

Note that there would be an additional factor of two, as the parton in the final state can be collinear to either of the incoming partons, which is implicit from $(q \leftrightarrow \bar{q})$ in eq. (3.9). At this stage, one can observe that the divergent pieces, that are proportional to $(\ln \delta_s)$, cancel among themselves. However, there are singularities still remaining that will get cancelled only with those coming from the loop integrals in the virtual diagrams. In what follows, we present the details of the virtual corrections to our process.

Virtual Corrections

The NLO cross sections also receive contributions coming from the virtual corrections as well as the wave function renormalisation to the $2 \to 2$ LO processes. The corresponding Feynman diagrams are obtained by considering possible one loop virtual gluonic corrections to the tree level Feynman diagram for $q\bar{q} \to Z$ and then by attaching the graviton line to all possible internal as well as external lines and to vertices, as allowed by the Feynman rules [40, 41]. This way we find 27 diagrams, out of which 8 diagrams correspond to external leg corrections and can be omitted as they vanish in the massless quark limit. Out of the remaining 19 diagrams, 11 are shown in Fig. 3.3. The rest of the diagrams can easily be obtained by inverting the charge flow direction of the quark lines in the last eight diagrams shown in Fig. 3.3. Interference of these one loop diagrams with the born diagrams gives $\mathcal{O}(\alpha_s)$ contributions. Due to tensorial interaction of gravitons with the SM fields, the loop integrals involve higher powers of loop momenta in their numerators and hence the

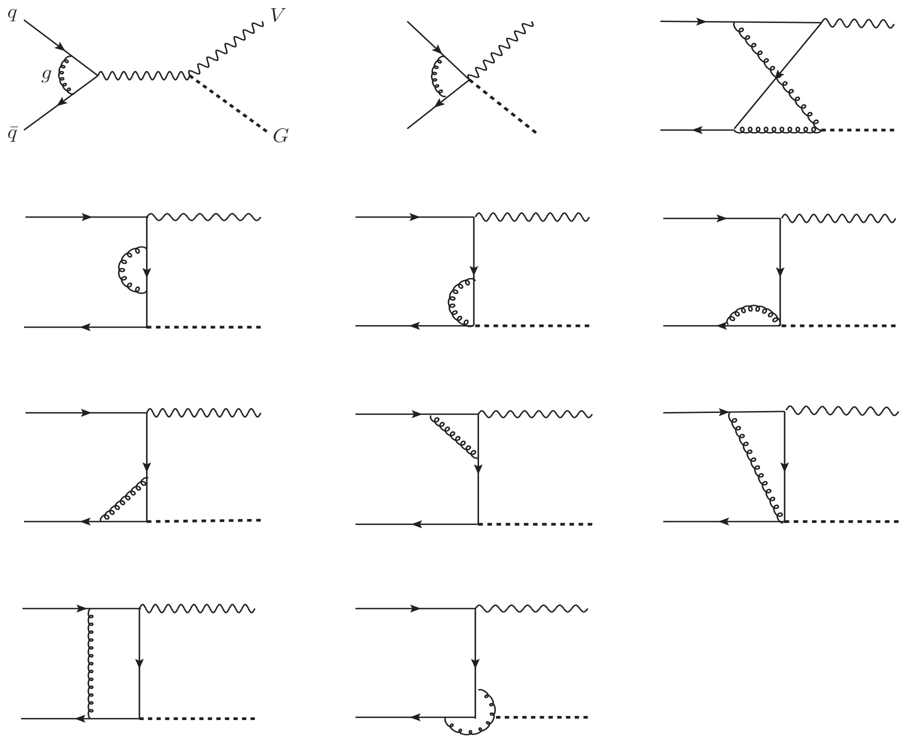

Figure 3.3: Virtual gluon emission diagrams.

reduction of tensorial integrals to scalar ones becomes complicated. We have written a symbolic program using FORM [73] to perform this reduction in n-dimensions. The resulting scalar integrals are then evaluated exactly (see [102]) and they are listed in Appendix C. Substituting these scalar integrals, we can express the $\mathcal{O}(\alpha_s)$ contribution resulting from the virtual processes as,

$$\begin{aligned} d\hat{\sigma}_V &= a_s\ d\hat{\sigma}_0\ F(\epsilon,\mu_R,s) C_F \left(-\frac{16}{\epsilon^2}+\frac{12}{\epsilon}\right) \\ &\quad +C\Bigg[V_1\ \ln^2\left(\frac{-t}{\mu^2}\right)+V_2\ D_0^{fin}(p_1,k,q)+V_3\ D_0^{fin}(p_2,k,q) \\ &\quad +V_4\ \ln^2\left(\frac{-u}{\mu^2}\right)+V_5\ \ln^2\left(\frac{-m^2}{\mu^2}\right)+V_6\ \ln^2\left(\frac{-m_Z^2}{\mu^2}\right)+V_7\ \ln^2\left(\frac{s}{\mu^2}\right) \\ &\quad +V_8\ \ln\left(\frac{-t}{\mu^2}\right)+V_9\ \ln\left(\frac{-u}{\mu^2}\right)+V_{10}\ i\ C_0(k,q)+V_{11}+V_{12}+V_{13}\ \ln\left(\frac{m_Z}{\mu^2}\right) \end{aligned}$$

$$+V_{14}\ \ln\left(\frac{m}{\mu^2}\right) + V_{15}\ \zeta_2\Bigg] \qquad , \tag{3.12}$$

where $C = a_s\,\kappa^2\,(C_v^2{+}C_a^2)\,T_Z^2\,C_F/(4N)$, $C_0^{\rm fin}$ and $D_0^{\rm fin}$ are the finite parts of the scalar integrals C_0 and D_0 respectively and they are listed in Appendix C along with V_i, where $i = 1, 2, \ldots, 15$. It is clear from the above expression that the integration over the loop momenta in $(4+\epsilon)$ dimensions leads to soft and collinear singularities which appear as poles in ϵ. We found that the UV divergences that appear in the intermediate stages cancel among various diagrams thanks to the conservation of SM energy momentum tensor to this order in perturbation theory. Now, when we add $\mathcal{O}(\alpha_s)$ contributions coming from eq. (3.5), (3.9) and (3.12), we observe that the remaining soft and collinear singularities cancel among themselves as expected, leaving a finite expression for the 2-body contribution which can be computed using Monte Carlo techniques. In other words, the 2-body contribution given by,

$$d\sigma^{2-\rm body} = d\sigma_S \ + \ d\sigma_{coll} \ + \ d\sigma_V \qquad , \tag{3.13}$$

is found to be free from both UV and IR singularities and hence suitable for further numerical evaluation.

In addition to the above contribution, we also have the hard non-collinear region $\overline{HC}$ of the phase space which does not suffer from any IR singularities by construction. The contributions from this region can be obtained by integrating the $2 \to 3$ matrix elements using standard Monte Carlo integrations. Owing to the divergence free nature of the integration, the $2 \to 3$ matrix elements computed in 4-dimensions will suffice our purpose. These matrix elements are again computed using FORM. We have made several checks to ensure the correctness of our results, namely the gauge invariances in QCD, electroweak and gravity sectors. Since contributions from hard non-collinear regions involve three body phase space integrals of final state particles having different masses, care is needed to parametrize as well as to determine the limits of various integrations. We devote our next subsection to discuss this.

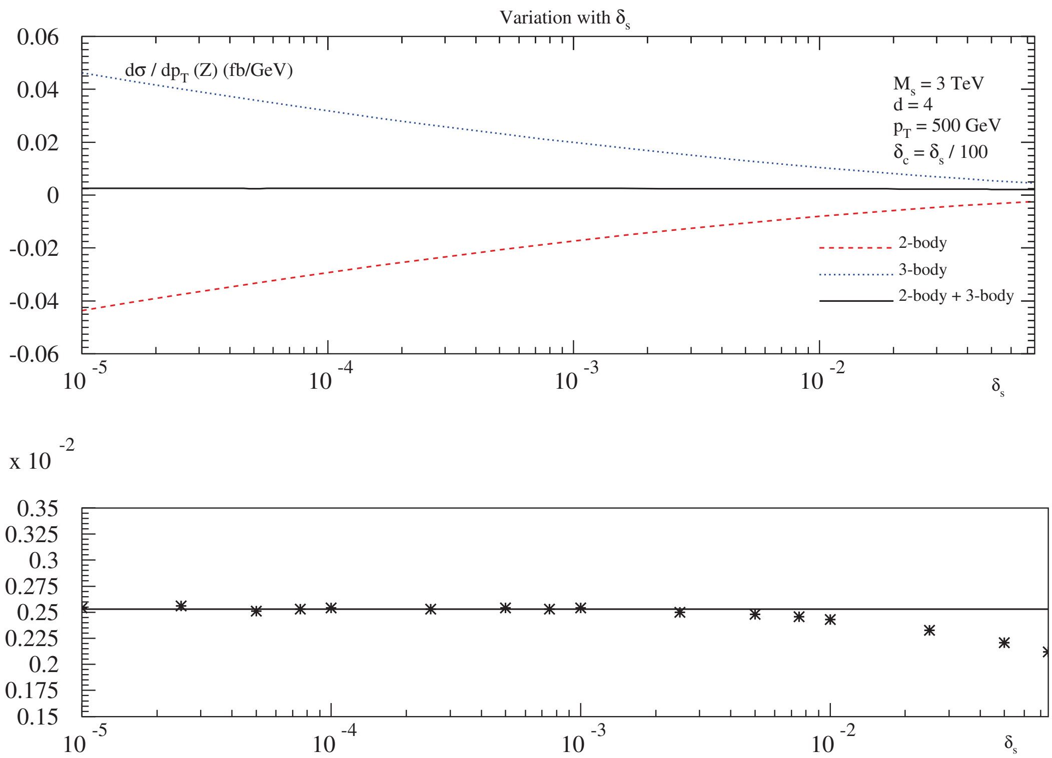

Figure 3.4: Variation of the transverse momentum distribution of Z boson with δ_s for $M_s = 3$ TeV and $d = 4$, keeping the ratio $\delta_s/\delta_c = 100$ fixed.

3.2.3 Three Body Contribution

In this section, we will present briefly how we have implemented various constraints imposed by the two cutoff phase space slicing method and cuts on the phase space

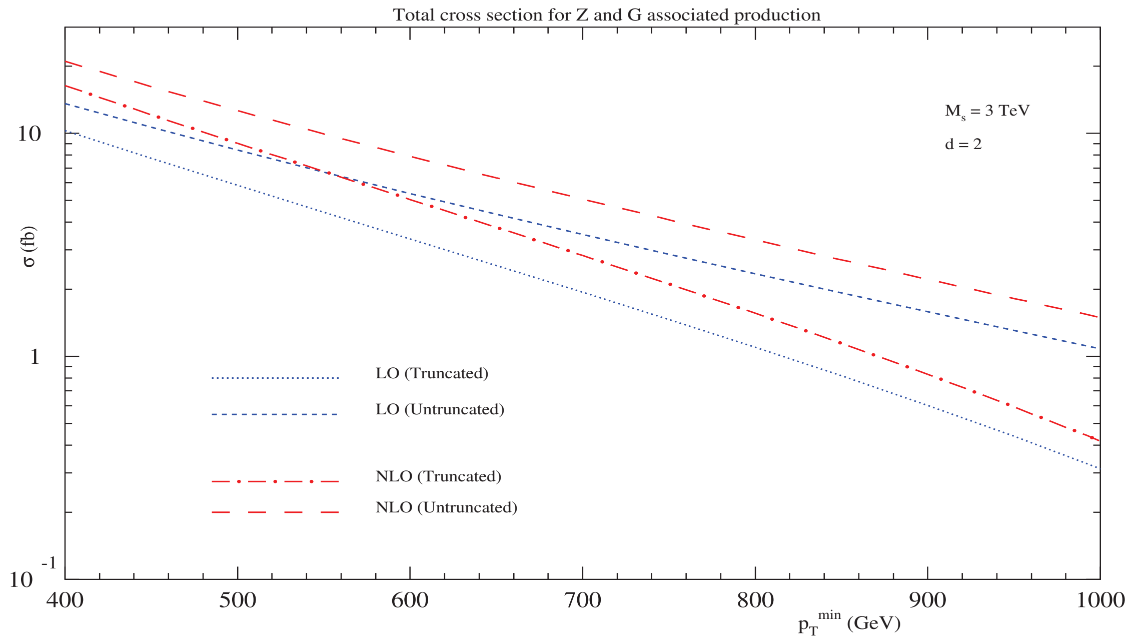

Figure 3.5: Total cross section for the associated production of Z and G as a function of p_T^{min} for $M_s = 3$ TeV and $d = 2$.

integrals for the $2 \to 3$ subprocesses. We are interested in the following cross section:

$$d\sigma^{3-\text{body}} = \int_{\overline{HC},cuts} d\Gamma_3 \, |M^{2\to 3}_{q\bar{q},qg}|^2 \qquad , \tag{3.14}$$

where the three-body phase space measure is given by,

$$d\Gamma_3 = \left(\Pi_{i=1}^{3} \frac{d^3 p_i}{(2\pi)^3 2E_i}\right)(2\pi)^4 \delta^{(4)}(p_1 + p_2 - p_3 - p_4 - p_5) \qquad . \tag{3.15}$$

It is easy to parameterize all the momenta in the center of mass frame of initial state partons and then boost them to the lab frame or the center of mass frame of the hadrons. The 4-momenta of the massless partons in the initial state, moving along

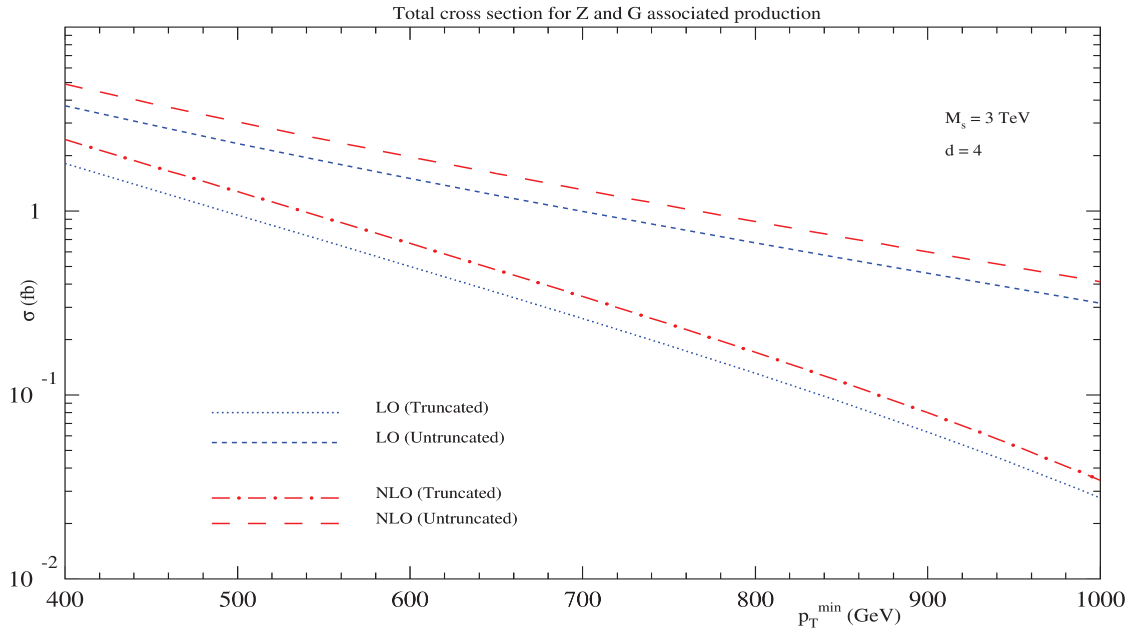

Figure 3.6: Total cross section for the associated production of Z and G as a function of p_T^{min} for $M_s = 3$ TeV and $d = 4$.

the z-axis are given by,

$$p_1 = \frac{\sqrt{s}}{2}(1,0,0,1), \quad p_2 = \frac{\sqrt{s}}{2}(1,0,0,-1) \qquad , \tag{3.16}$$

where $\sqrt{s}$ is the parton center of mass energy. The corresponding 4-momenta of the massive particles in the final state are given by $p_i = (E_i,\ \vec{p}_i)$ with masses $m_i^2 = E_i^2 - |\vec{p}_i|^2$, for $i = 3,4,5$. For the three body case, it is easy to consider the momentum direction of one of the final state particles, say $\vec{p}_5$, as the reference direction and then parameterize the other two momenta $\vec{p}_3$ and $\vec{p}_4$ with respect to this direction,

$$\vec{p}_5 \quad = \quad |\vec{p}_5|\ (\sin\theta,\ 0,\ \cos\theta) \qquad , \tag{3.17}$$

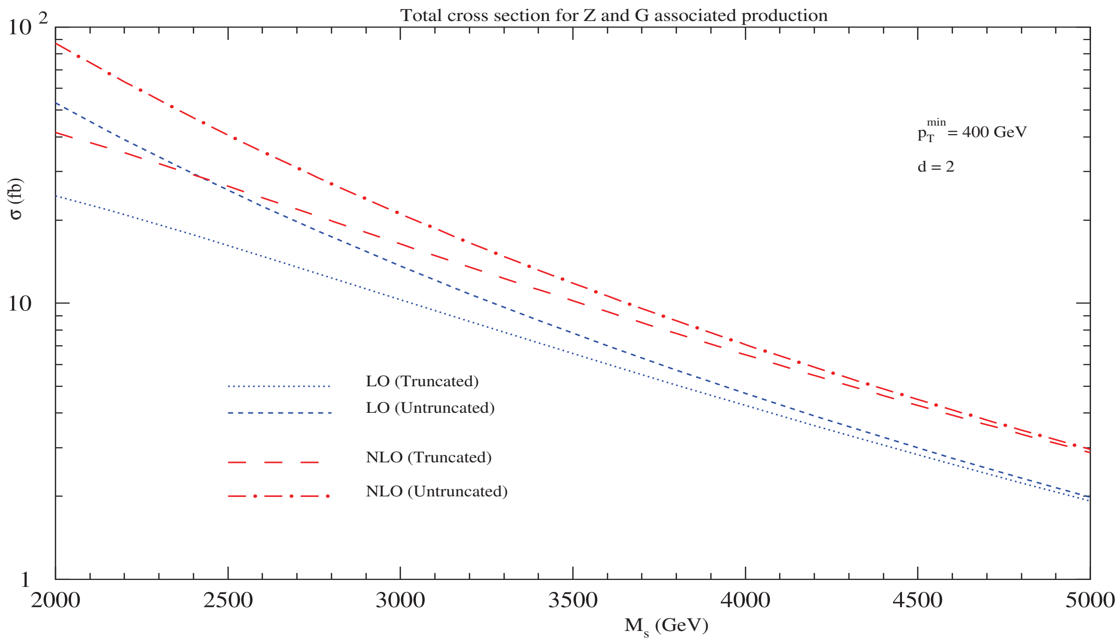

Figure 3.7: Total cross section for the associated production of Z boson and graviton, shown as a function of M_s for $d = 2$.

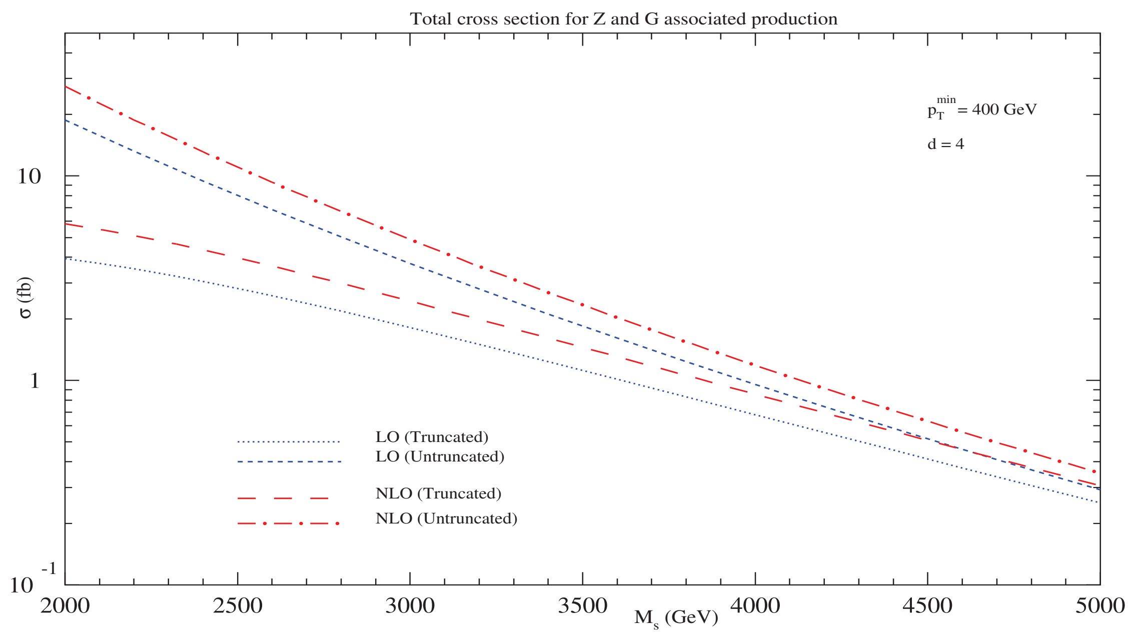

Figure 3.8: Total cross section for the associated production of Z boson and graviton, shown as a function of M_s for $d = 4$.

where θ is the angle between $\vec{p}_5$ and the z-axis. The momentum of $\vec{p}_3$ can now be parameterized with respect to the direction of $\vec{p}_5$ and then followed by a rotation in the xz-plane by an angle of θ to get $\vec{p}_3 = (p_3^x, p_3^y, p_3^z)$ in the center of mass frame of the partons as given by,

$$
\begin{aligned}
p_3^x &= |\vec{p}_3| \left(\cos\theta \, \cos\alpha \, \sin\beta + \sin\theta \, \cos\beta\right) \qquad , \\
p_3^y &= |\vec{p}_3| \, \sin\alpha \, \sin\beta \qquad , \\
p_3^z &= |\vec{p}_3| \left(\cos\theta \, \cos\beta - \sin\theta \, \cos\alpha \, \sin\beta\right) \qquad ,
\end{aligned}
\tag{3.18}
$$

where α and β are the azimuthal and polar angles of $\vec{p}_3$ with respect to $\vec{p}_5$. The 4-momentum of p_4 simply follows from the energy momentum conservation. The three body phase space in eq. (3.15) can now be expressed in terms of the angular variables using,

$$
\frac{d^3 p_i}{2E_i} = d^4 p_i \; \delta(p_i^2 - m_i^2) = \frac{|\vec{p}_i|}{2} \; dE_i \; d\Omega_i \qquad , \tag{3.19}
$$

to get

$$
d\Gamma_3 = \frac{|\vec{p}_3||\vec{p}_5|}{4(2\pi)^5} \; dE_3 \; d\Omega_3 \; dE_5 \; d\Omega_5 \; \delta(p_4^2 - m_4^2) \qquad , \tag{3.20}
$$

where $d\Omega_3 = d\cos\beta \; d\alpha$ and $d\Omega_5 = d\cos\theta \; d\phi$. Further, the angle β can be eliminated using,

$$
2 \; |\vec{p}_3| \; |\vec{p}_5| \; \cos\beta = |\vec{p}_4|^2 - |\vec{p}_3|^2 - |\vec{p}_5|^2 \qquad . \tag{3.21}
$$

Finally, out of the nine integration variables of the three body phase space, in eq. (3.15), we are left with four independent variables *viz.*, E_3, E_5, θ and α, due to the presence of 4-momentum conserving delta function and the rotational invariance over the reference momentum direction $\vec{p}_5$. The three body phase space can then be written in terms of these four independent variables as,

$$d\Gamma_3 = \frac{1}{8(2\pi)^4}\ dE_3\ dE_5\ d\cos\theta\ d\eta \qquad . \tag{3.22}$$

The limits of integration of E_3 and E_5 can be obtained from the constraint $|\cos\beta| \leq 1$ and they are given here under [103],

$$E_5^{min} = m_5, \qquad E_5^{max} = \frac{1}{2\sqrt{s}}[s + m_5^2 - (m_3 + m_4)^2] \qquad , \tag{3.23}$$

and

$$E_3^{max,min} = \frac{1}{2B}\left[A(B + m_+ m_-) \pm |\vec{p}_5|\sqrt{(B - m_+^2)(B - m_-^2)}\right] \qquad , \tag{3.24}$$

where

$$A = \sqrt{s} - E_5, \quad B = A^2 - |\vec{p}_5|^2 \quad \text{and} \quad m_\pm = m_3 \pm m_4 \qquad . \tag{3.25}$$

Finally, all the parton momenta can be boosted back to the lab frame or to the center of mass frame of the hadrons by a boost factor in the limit of the zero rest mass of the hadrons given by,

$$\beta = \frac{P_{cm}}{E_{cm}} = \frac{(x_1 - x_2)}{(x_1 + x_2)} \qquad , \tag{3.26}$$

where x_1 and x_2 are the fractions of the incoming hadron momenta carried by the partons in the center of mass frame of the hadrons.

We have implemented this phase space parameterization in our numerical code written in Fortran language. We set $m_3 = m_V$ (m_V being the mass of vector boson), $m_4 = m$ and $p_3 = k$, $p_4 = q$ in our code and p_5 is derived using the conservation of 4-momenta. The phase space integrations as well as various convolutions in the two and three body contributions are done using VEGAS multi dimensional integration package. In what follows, we present the impact of our NLO corrections on various observables.

3.3 Numerical Results

In this section, we present various kinematic distributions for the associated production of the graviton and the vector gauge boson to NLO in QCD at the LHC. The results are presented for proton-proton collision energy of $\sqrt{S} = 14$ TeV. As discussed before, the inclusive cross section for the graviton production involves the summation of all possible graviton modes. This summation in the continuum limit leads to an integral over the graviton mass. The limits of this integral are set by the kinematics from 0 to $(\sqrt{s} - m_V)$, where $\sqrt{s}$ is the parton center of mass energy and $m_V = m_Z, m_W$. The masses of the gauge bosons and the weak mixing angle are given by [104],

$$m_Z = 91.1876 \text{ GeV}, \quad m_W = 80.398 \text{ GeV}, \quad \sin^2\theta_w = 0.2312 \quad . \tag{3.27}$$

The fine structure constant is taken to be $\alpha = 1/128$. Throughout our study, we have used CTEQ6L1 and CTEQ6.6M parton density sets [105] for LO and NLO cross sections respectively. The strong coupling constant is calculated at two loop order in the $\overline{MS}$ scheme with $\alpha_s(m_Z) = 0.118$ ($\Lambda_{\text{QCD}} = 0.226$ GeV). We have also set the number of light flavours $n_f = 5$. The following cuts are used for our numerical study,

$$p_T^{Z,W} > p_T^{min}, \quad p_T^{miss} > p_T^{min}, \quad |y^{Z,W}| \leq 2.5 \qquad . \tag{3.28}$$

For the 2-body process, the missing transverse momentum is same as that of the gauge boson. On the other hand for the 3-body process, it does not need to be so due to the presence of an observable jet in the final state and hence it amounts purely to the graviton transverse momentum. The observable jet is defined as the one that satisfies the following conditions,

$$p_T^{jet} > 20 \text{ GeV} \quad \text{and} \quad |\eta^{jet}| \leq 2.5 \qquad . \tag{3.29}$$

Whenever the jet does not satisfy the above conditions, the missing transverse momentum is approximated to be that of the gauge boson.

The LED model is an effective field theory valid below the UV cutoff scale M_s, which is expected to be of the order of a few TeV . At the LHC energy $\sqrt{S} = 14$ TeV, it is very well possible that the partonic center of mass energies can exceed this scale M_s and lead to the signals that do not correspond to the compactified extra dimensions of the LED model. This necessitates the need to quantify the UV sensitivity of the theory and this issue was already addressed in [41], according to which the cross sections can be computed in two different ways, one with 'truncation', where the cross sections are set to zero whenever the hard scale Q involved in the problem exceeds M_s and the other with 'untruncation', where there is no such constraint imposed on the cross sections. As pointed out in [41], if these two results converge then the predictions are valid and the model is viable, otherwise the untruncated cross sections can dominate the truncated ones, implying the calculations are not under control. In our calculation, we choose the hard scale to be the invariant mass (Q) of the gauge boson and the graviton, which at LO is the same as the center of mass energy of the partons $\sqrt{s}$. We have considered both truncated as well as untruncated cases at the time of presenting few selective kinematical observables. However, most of our distributions are obtained with our default choice of truncation scheme.

3.3.1 Neutral Gauge Boson

Before proceeding towards kinematic distributions, we would do some consistency checks on the calculation. First, we check for the stability of the cross sections against the variation of the slicing parameters δ_s and δ_c. The sum of the 2-body and the 3-body contributions given in eq. (3.13) and (3.14) is expected to be independent of the choice of these slicing parameters that are introduced in the intermediate stages of the calculation. In Fig. 3.4, we show the dependency of the transverse momentum distribution p_T^Z on the slicing parameter δ_s keeping the ratio of δ_s to δ_c fixed at a value of 100. This distribution is obtained using the hard truncation scheme for a particular choice of the model parameters $M_s = 3$ TeV and $\delta = 4$. It can be seen from Fig. 3.4, that both the 2-body and the 3-body contributions vary with δ_s but their sum is fairly stable against the variation of δ_s over a wide range. Similar observation has been found while varying δ_c by keeping the ratio of these two slicing parameters fixed. This ensures the proper implementation of the slicing method in our NLO computation.

Another useful check on the computation is to reproduce the cross sections for the associated production of the photon and the graviton at the LHC [93]. In order to do this, we recalculated both real emission as well as virtual contributions for this process and the corresponding soft and collinear pieces. We found that the following replacements: (i) $\frac{(C_V^2+C_A^2)}{4} \to Q_f^2$, (ii) $m_Z \to 0$, (iii) $T_Z \to e$, in the two body and three body real emission matrix elements of the Z boson with graviton production processes correctly reproduce the corresponding matrix elements for the photon with graviton production process. Here, Q_f is the charge of the fermion and e is the electromagnetic coupling. Using our symbolic program, we find that the analytical expression containing virtual contributions of this process agrees with one given in the appendix of [93]. In addition, using these recalculated quantities, we further reconfirmed all the numerical results in [93] after taking their choice of parameters, cuts *etc.* It is important to note that the NLO cross sections or the K-factors are subject to the choice of the event selection or more precisely the cuts on the particles in the final state. In our calculation, however, the gauge bosons being massive, we present our results according to the cuts given in eq. (3.28) and (3.29).

In Fig. 3.5, the total cross section for the associated production of Z boson and the graviton is shown as a function of p_T^{min} to NLO in QCD at the LHC. The cross sections are given for both truncated as well as untruncated cases and with the choice of model parameters $M_s = 3$ TeV and $d = 2$. A similar plot is shown for $d = 4$ in Fig. 3.6. The cross section for $d = 2$ is larger compared to that for $d = 4$ because the density of the graviton modes drops as d increases. The K-factors are found to have a mild dependency on p_T^{min}, varying from 1.6 to 1.4. In Fig. 3.7, we have shown the variation of the truncated as well as untruncated total cross sections with respect to the scale M_s for the case $d = 2$. The difference between the truncated and the untruncated cross sections is mainly due to the contributions coming from the region $Q > M_s$. However, with increasing M_s the parton fluxes corresponding to Q in this region rapidly fall down and hence the difference between the two cross sections decreases with increase in M_s. Such a behaviour is evident from Fig. 3.7 and 3.8 for $d = 2$ and $d = 4$ respectively. The corresponding K-factors are also shown in Fig. 3.9. In the rest of our calculation we choose $p_T^{min} = 400$ GeV and $M_s = 3$ TeV.

Next, we present LO and NLO transverse momentum distributions of the Z boson (p_T^Z) in Fig. 3.10 for $d = 2, 4, 6$ and the corresponding missing transverse momentum distributions (p_T^{miss}) in the left panel of Fig. 3.11 for $d = 2, 4$. The QCD corrections enhance both p_T^Z and p_T^{miss} distributions. Note that the shape of the p_T^Z distribution remains unaffected while this is not the case for p_T^{miss} distribution. Such a pattern can be understood from the definition of p_T^{miss} mentioned before. Thereafter, we present the rapidity distributions of the Z bosons. The rapidity of massive gauge bosons is defined by,

$$Y = \frac{1}{2} \log \left(\frac{E + p_z}{E - p_z} \right) \qquad , \tag{3.30}$$

where E and p_z are the energy and the longitudinal momentum components of the gauge boson in the lab frame. In the right panel of Fig. 3.11, we have plotted the rapidity distribution of the Z boson both at LO and at NLO for two different choices of the factorization scale: $\mu_F = p_T^Z/2$ and $2p_T^Z$. This distribution is obtained by integrating over the transverse momentum of the Z boson from 700 GeV to 750 GeV, for $d = 4$. Note that the NLO corrections increase the cross section. As expected, the inclusion of $\mathcal{O}(\alpha_s)$ corrections reduces the dependence on the arbitrary factorisation scale μ_F. The percentage of uncertainty in the cross sections at the central rapidity region $Y = 0$, due the variation of the scale from $\mu_F = p_T^Z/2$ to $\mu_F = 2p_T^Z$, is 18.9 at LO and it gets reduced to 8.6 at NLO.

3.3.2 Charged Gauge Boson

In this section we discuss the impact of NLO QCD corrections on the associated production of charged gauge bosons ($W^{\pm}$) and the graviton at the LHC. The matrix elements for the $W^{\pm}$ case are identical to those for the Z boson case except for the masses of the gauge bosons and their couplings to the quarks as seen in eq. (3.2). Further, in the case of charged gauge bosons, the parton fluxes will also be different from those of the neutral gauge boson. The parton fluxes for the quark anti-quark annihilation process in the case of Z boson are of the form $q\bar{q}$ ($q = u, d, s, c, b$), while they are of the form $u\bar{d}$ ($d\bar{u}$) for $W^+(W^-)$. For $W^{\pm}$ boson production cross sections, we consider the mixing of quarks among different quark generations, as allowed by the CKM matrix elements V_{ij}, with ($i = u, c, t$) and ($j = d, s, b$). In view of this, in the above parton fluxes u and d correspond to any up-type and down-type quarks respectively. The CKM matrix elements are given by [104],

$$\begin{aligned} |V_{ud}| = 0.97425 \;, \quad |V_{us}| = 0.2252 \;, \quad |V_{ub}| = 3.89 \times 10^{-3} \quad &, \\ |V_{cd}| = 0.230 \;, \quad |V_{cs}| = 1.023 \;, \quad |V_{cb}| = 40.6 \times 10^{-3} \quad &. \end{aligned} \tag{3.31}$$

Since all our calculations are done in the massless limit of the partons, we have not included the top quark contribution in our calculation and set all V_{tj}'s to zero.

Similar to the case of Z boson, we will present the total cross sections as well as the differential distributions for the associated production of $W^{\pm}$ boson and a graviton. In Fig. 3.12 and 3.20, we have shown the stability of the transverse momentum distributions of W^- and W^+ respectively with the slicing parameter δ_s. These distributions are obtained for the choice of $p_T^W = 500$ GeV, keeping the ratio δ_s/δ_c fixed at 100. It can be seen from the figures that the sum of the 2-body and 3-body contributions is fairly stable against the variation of the slicing parameters.

This ensures proper implementation of the slicing method in our numerical code, taking into account the appropriate parton fluxes for $W^{\pm}$. Next, we present the total cross sections as a function of p_T^{min} as well as M_s. In Fig. 3.13 and 3.14, we show truncated as well as untruncated total cross sections for W^- case, as a function of p_T^{min}, for $d = 2$ and $d = 4$ respectively. It can be seen from these figures that the QCD corrections have enhanced the leading order cross sections considerably, but there is no significant change in the shape of the cross sections. Similar plots are shown for W^+ in Fig. 3.21 and 3.22.

In Fig. 3.15 and 3.16, we show the total cross sections for W^- as a function of M_s for $d = 2$ and $d = 4$ respectively. A set of similar plots for W^+ is shown in Fig. 3.23 and 3.24. Note that, in each of the above cases, the cross sections for W^+ are somewhat higher than the corresponding ones for W^-. This difference in the total cross sections can be understood from the respective parton fluxes for W^- and W^+ at the LHC. The corresponding K-factors are shown in Fig. 3.17 for W^- and in Fig. 3.25 for W^+. For the choice of the parameters we have considered, the K-factors are found to vary from 1.4 to 1.7 in case of W^-, while they range from 1.05 to 1.65 for W^+. Note that the K-factors for W^- case are comparable but a little higher than those for W^+, which again can be accounted for the differences in the parton fluxes. The fact that the valence quark contributions are negligible and the parton fluxes at LO for W^+ are higher compared to those for W^- explains the behaviour of the above factors.

Further, in Fig. 3.18 and 3.26, we present the transverse momentum distribution of W^- and W^+ respectively as a function of the number of extra dimensions d and for $M_s = 3$ TeV. Similarly, we show the missing transverse momentum distribution of the graviton when produced in association with W^- in the left panel of Fig. 3.19. In the right panel, we present the scale uncertainties in the rapidity distribution of W^- by varying the factorization scale from $\mu_F = p_T^{W^-}/2$ to $\mu_F = 2p_T^{W^-}$. This rapidity distribution is obtained by integrating over the transverse momentum $p_T^{W^-}$ from 700 GeV to 750 GeV. Similar plots are shown for W^+ in Fig. 3.27. Note that the uncertainty resulting from the variation of factorisation scale μ_F gets reduced as we include $\mathcal{O}(\alpha_s)$ corrections. The percentage of uncertainty at the central rapidity $Y^{W^\pm} = 0$ is decreased from 19.1 to 9.3 in the case of W^-, whereas it gets reduced from 18.8 to 8.3 in the case of W^+.

3.4 Conclusion

In this chapter, we have systematically computed the full NLO QCD corrections to the associated production of the vector gauge boson and the graviton in theories with large extra dimensions at the LHC. This process plays an important role in probing the extra dimensions at the collider experiments, thanks to the large parton fluxes available at the LHC. We have used a semi-analytical two cutoff phase space slicing method to compute these corrections. We have quantified the UV sensitivity of the theoretical predictions by studying the cross sections in the truncated as well as the untruncated cases. In both the cases, the radiative corrections are found to have enhanced the cross sections significantly but do not appreciably change their shapes. The K-factors for the neutral gauge boson are found to vary from 1.2 to 1.6 depending on the number of extra dimensions d, while they vary from 1.3 to 1.8 for the case of charged gauge bosons. Although, the choice of the model parameters has the potential to change the cross sections calculated in truncated or untruncated cases significantly, we notice that the K-factors remain almost the same in these two cases. In addition to the total cross sections, we have also studied the differential distributions of the vector gauge bosons and found that the radiative corrections are significant and they do not affect their shapes except for the missing transverse momentum distribution. At the hadron colliders, as we already know, LO predictions often suffer from large uncertainties resulting from the choice of factorisation scale. Reducing these uncertainties is one of the main motivations for doing NLO computation. We have shown that this is indeed the case for the rapidity distributions of the gauge bosons by varying the factorization scale from $\mu_F = p_T/2$ to $\mu_F = 2p_T$, leading to reduction in the percentage of scale uncertainty to 9% from 19%. As we have already discussed, by performing fixed order NLO calculation, we usually get observables which are highly inclusive in nature. In order to acquire an exclusive description of the final state, we need to match the fixed order NLO result with the parton shower effect. The next chapter is designed to discuss the diphoton production process at the LHC in both SM and ADD model at the NLO+PS accuracy.

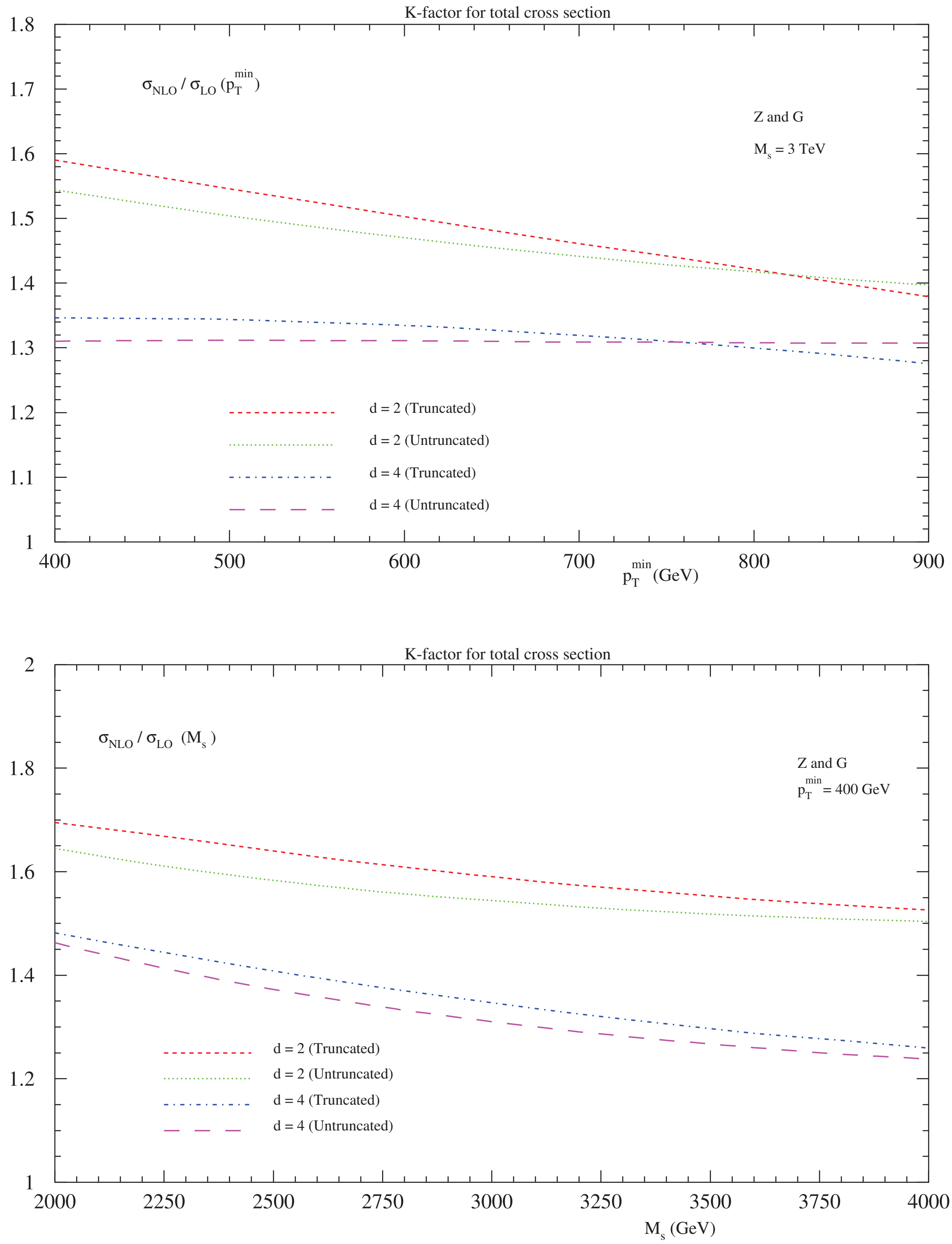

Figure 3.9: K-factors of the total cross section for the associated production of Z boson and graviton, given as a function of p_T^{min} (top) and the scale M_s (bottom).

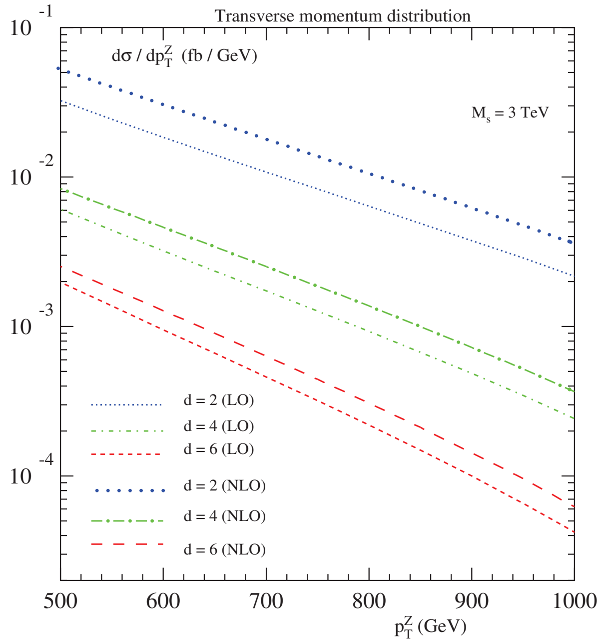

Figure 3.10: Transverse momentum distribution of Z boson for $M_s = 3$ TeV is shown for different values of the number of extra dimensions d.

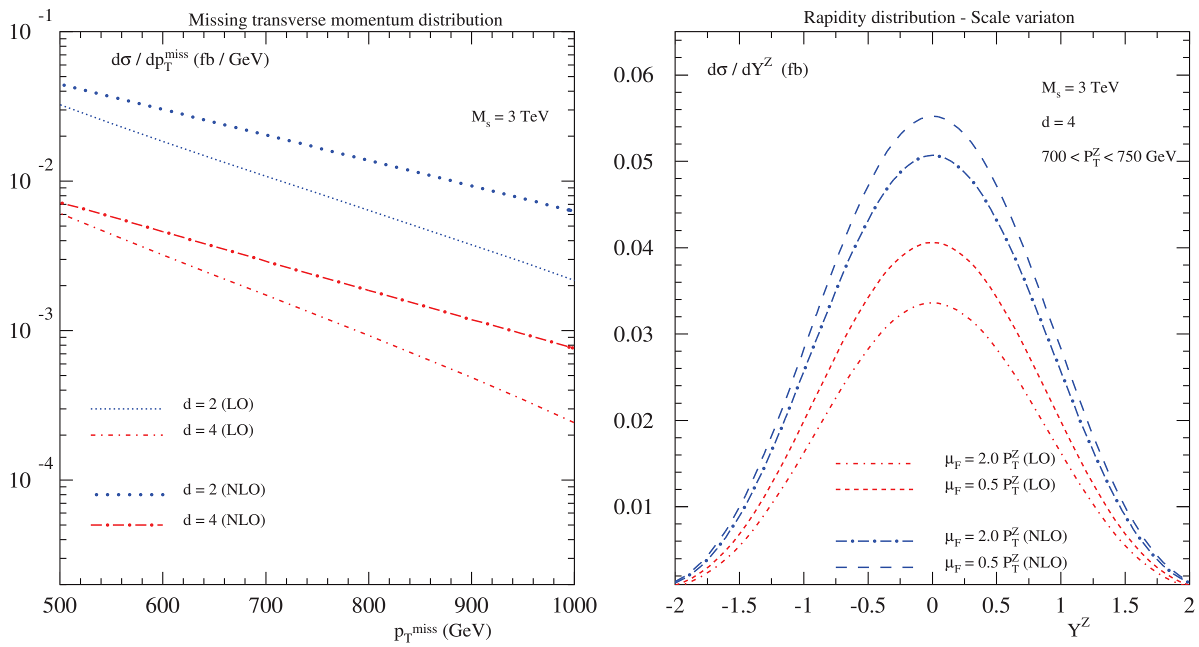

Figure 3.11: Missing transverse momentum distribution of the graviton produced in association with Z boson for $M_s = 3$ TeV (left). The scale uncertainties in the rapidity distribution of Z boson for $M_s = 3$ TeV and $d = 4$ (right).

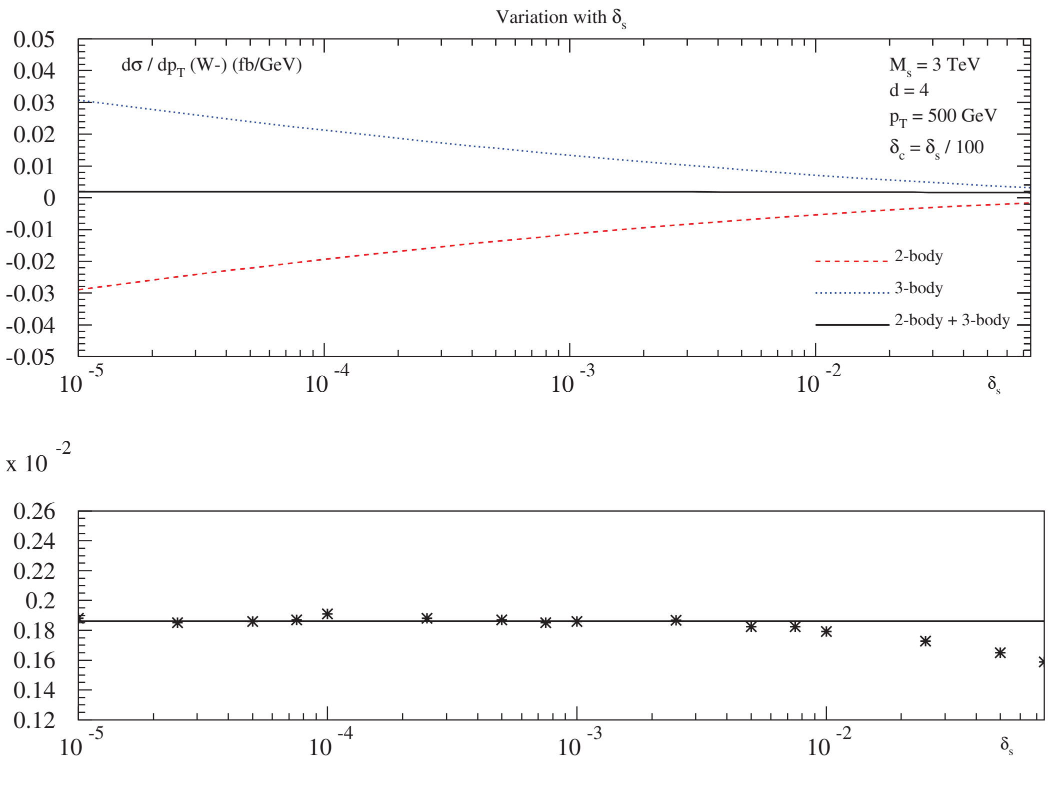

Figure 3.12: Variation of the transverse momentum distribution of W^- boson with δ_s for $M_s = 3$ TeV and $d = 4$, keeping the ratio $\delta_s/\delta_c = 100$ fixed.

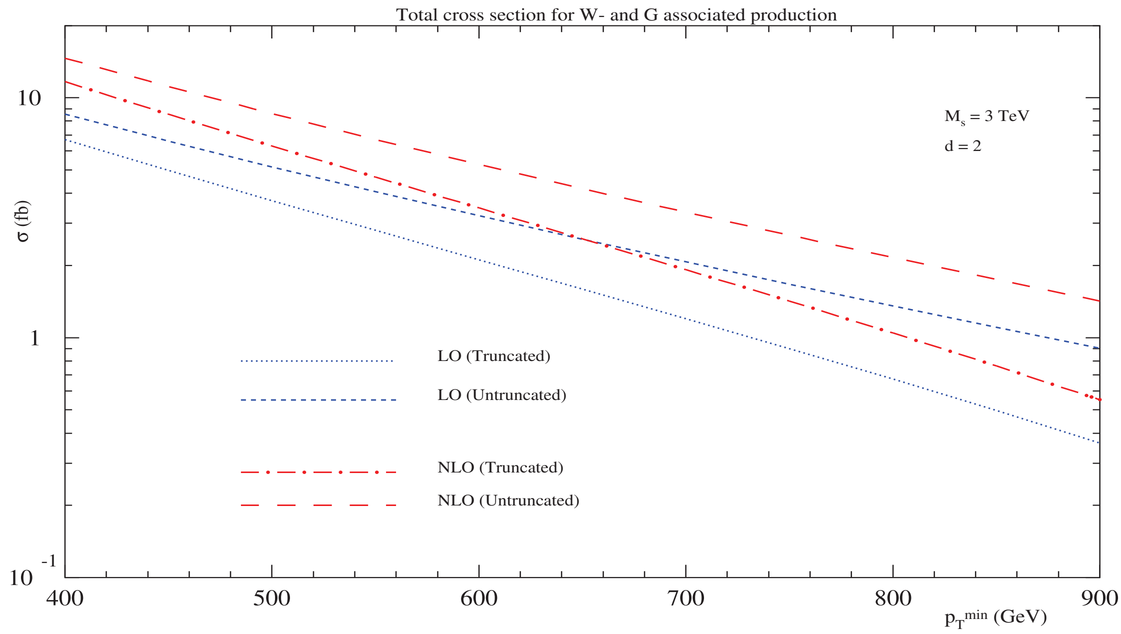

Figure 3.13: Total cross section for the associated production of W^- boson and graviton as a function of p_T^{min} for $M_s = 3$ TeV and $d = 2$.

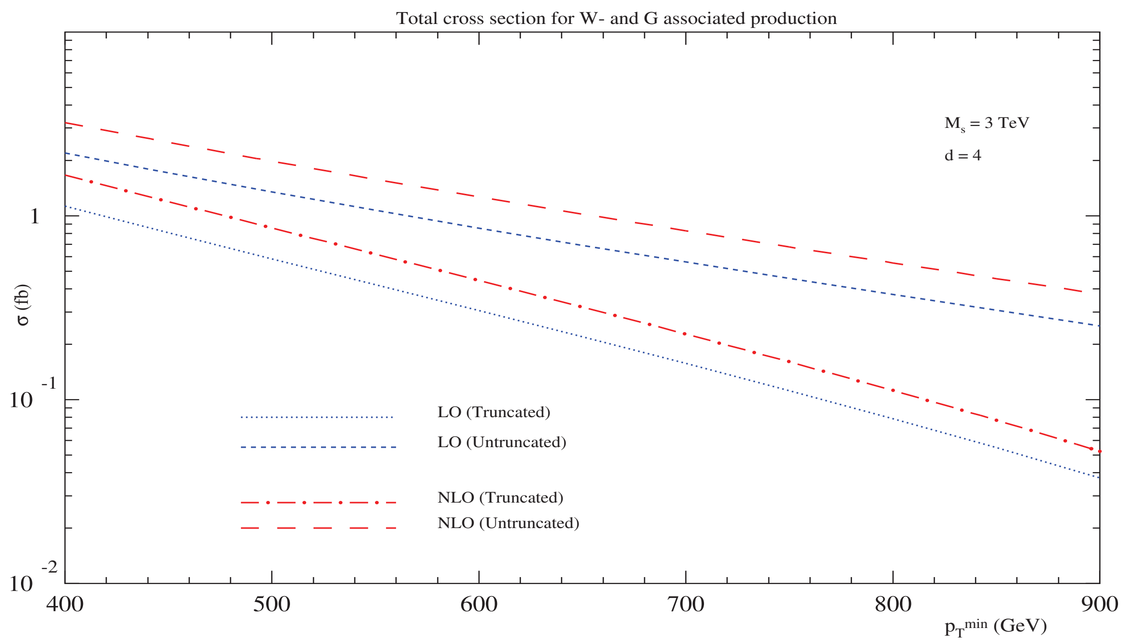

Figure 3.14: Total cross section for the associated production of W^- boson and graviton, shown as a function of p_T^{min} for $M_s = 3$ TeV and $d = 4$.

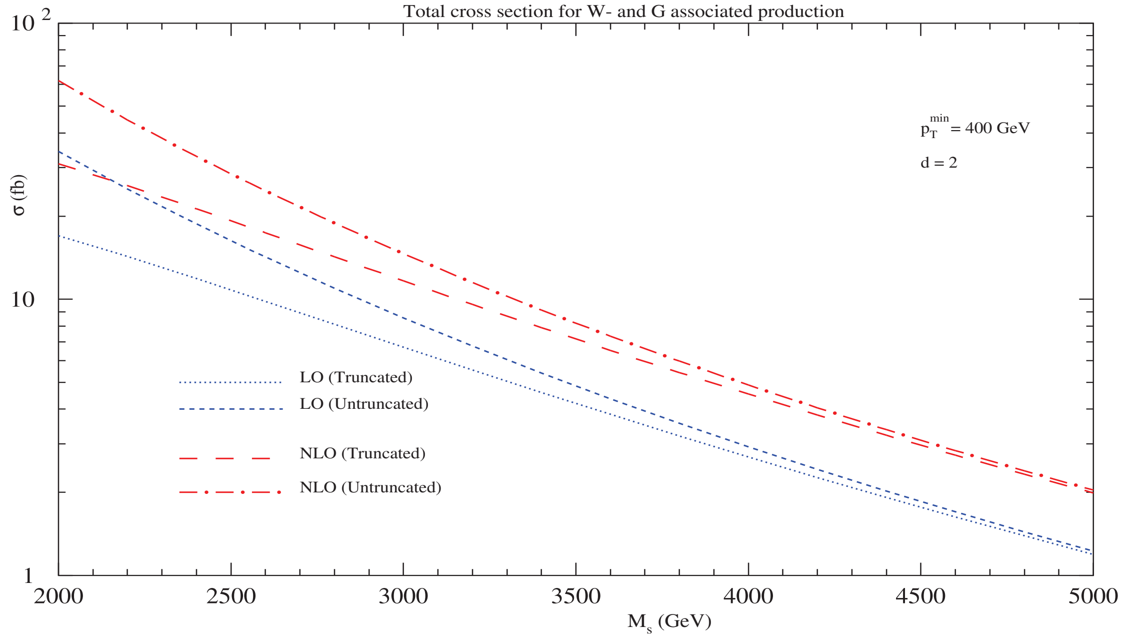

Figure 3.15: Total cross section for the associated production of W^- boson and graviton, given as a function of M_s for $d = 2$.

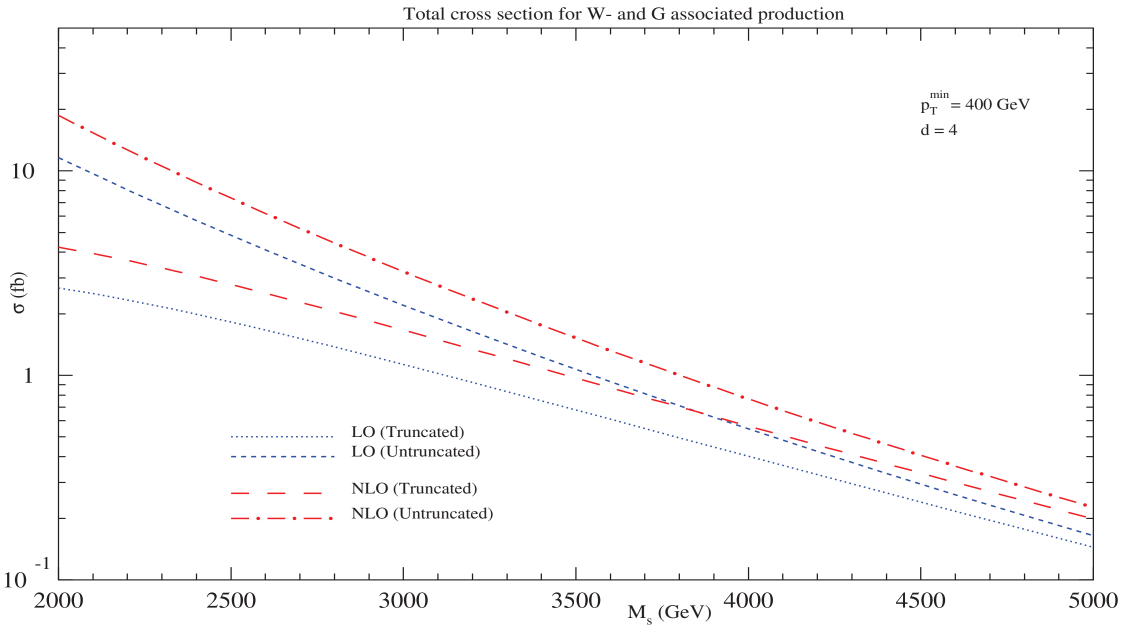

Figure 3.16: Total cross section for the associated production of W^- boson and graviton, shown as a function of M_s for $d = 4$.

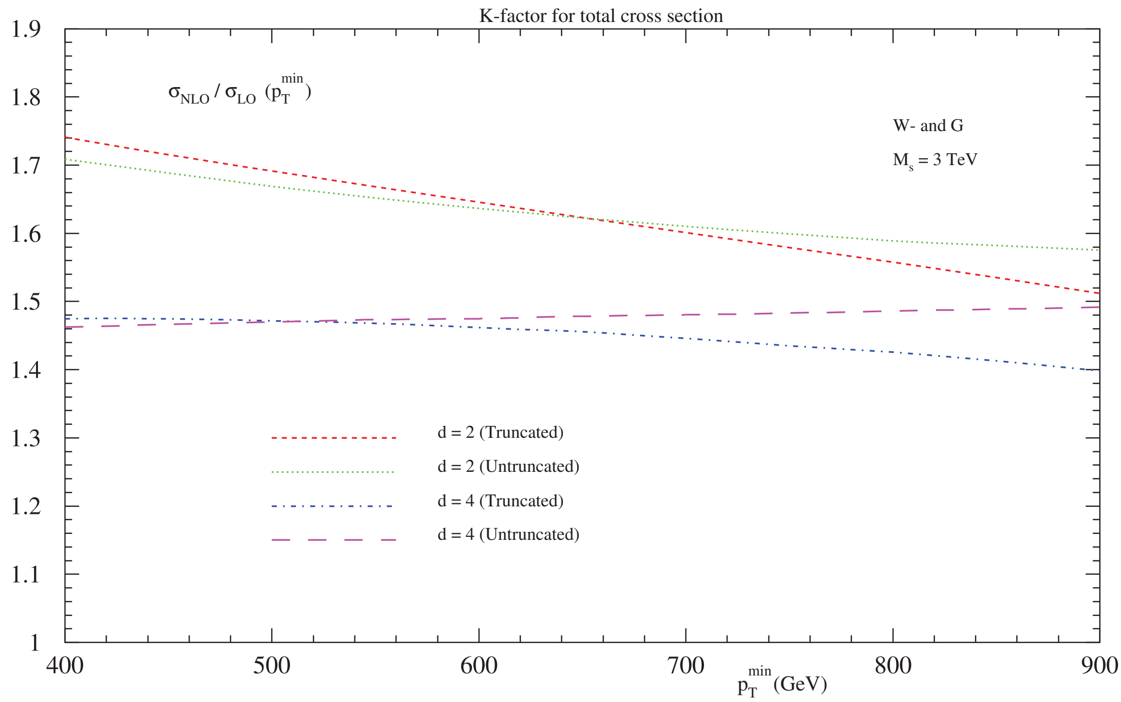

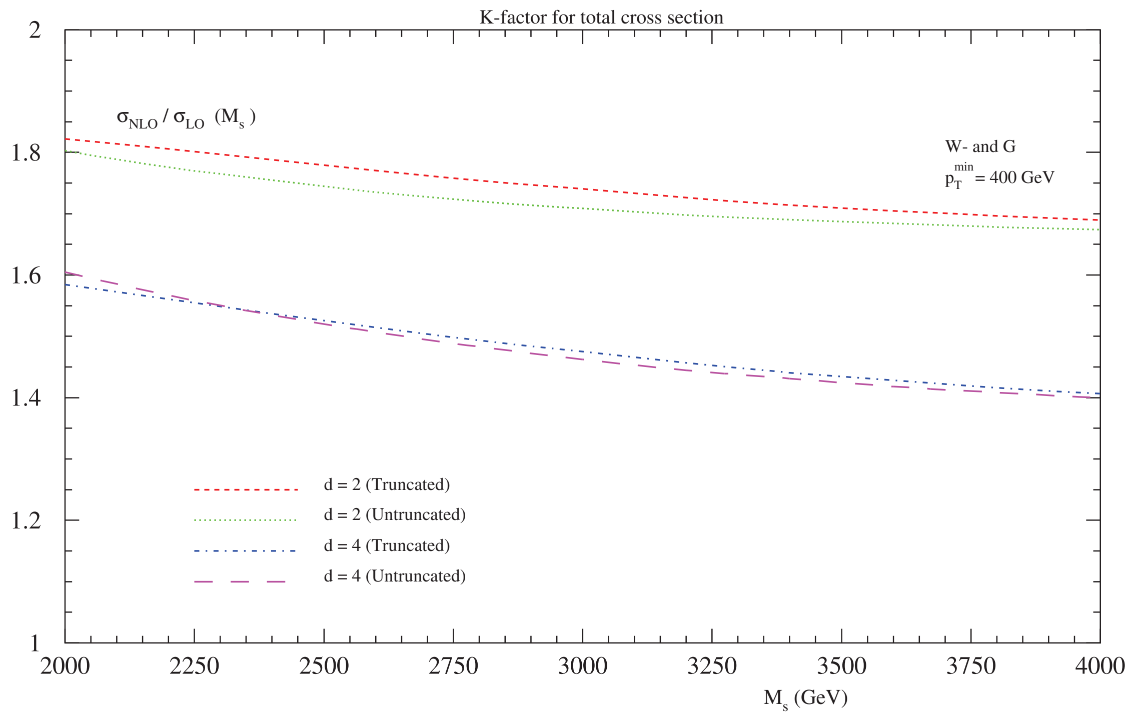

Figure 3.17: K-factors of the total cross section for the associated production of W^- boson and graviton, given as a function of p_T^{min} (top) and the scale M_s (bottom).

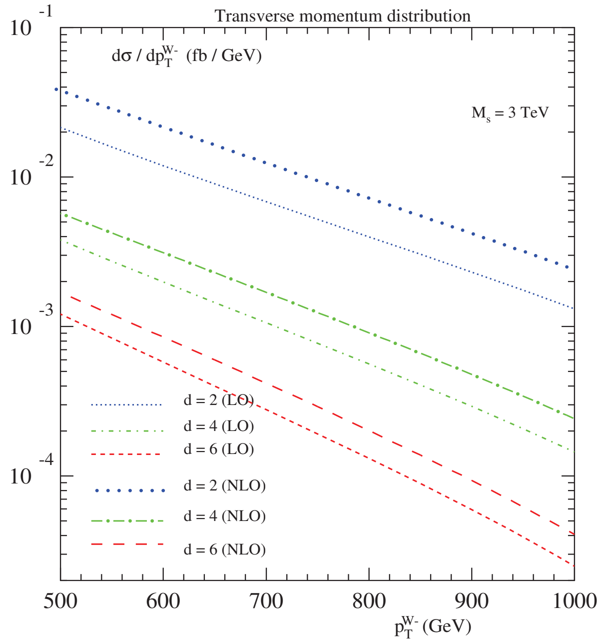

Figure 3.18: Transverse momentum distribution of W^- boson for $M_s = 3$ TeV is shown for different values of the number of extra dimensions d.

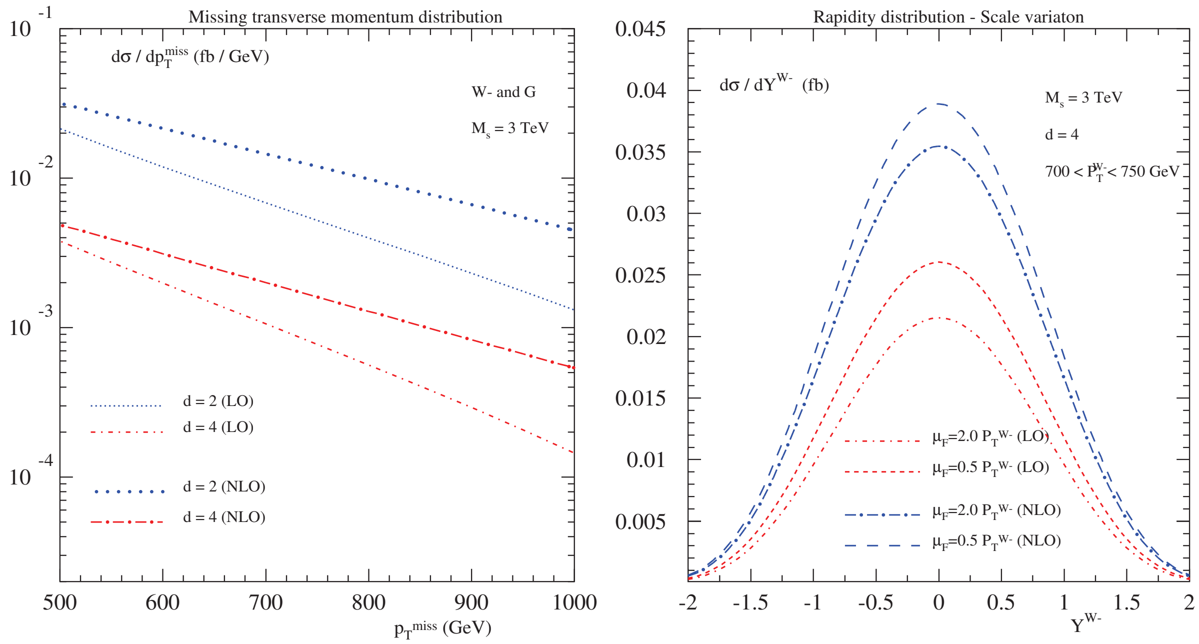

Figure 3.19: Missing transverse momentum distribution of the graviton produced in association with W^- boson for $M_s = 3$ TeV (left). The scale uncertainties in the rapidity distribution of W^- boson for $M_s = 3$ TeV and $d = 4$ (right).

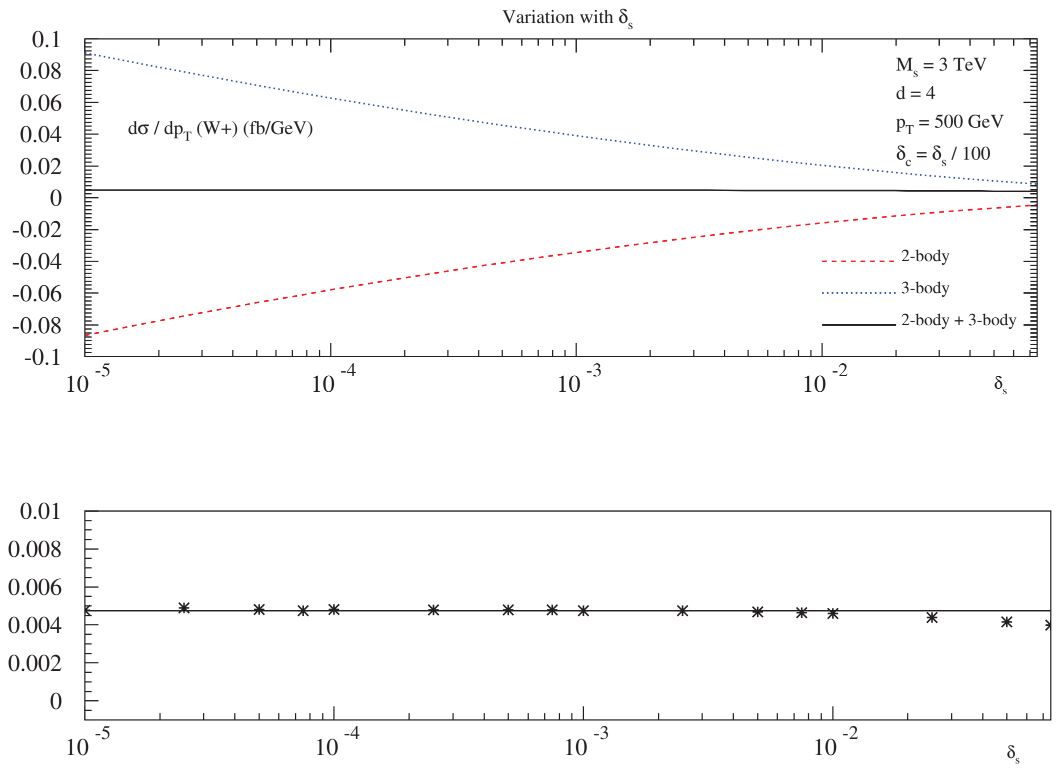

Figure 3.20: Variation of the transverse momentum distribution of W^+ boson with δ_s for $M_s = 3$ TeV and $d = 4$, keeping the ratio $\delta_s/\delta_c = 100$ fixed.

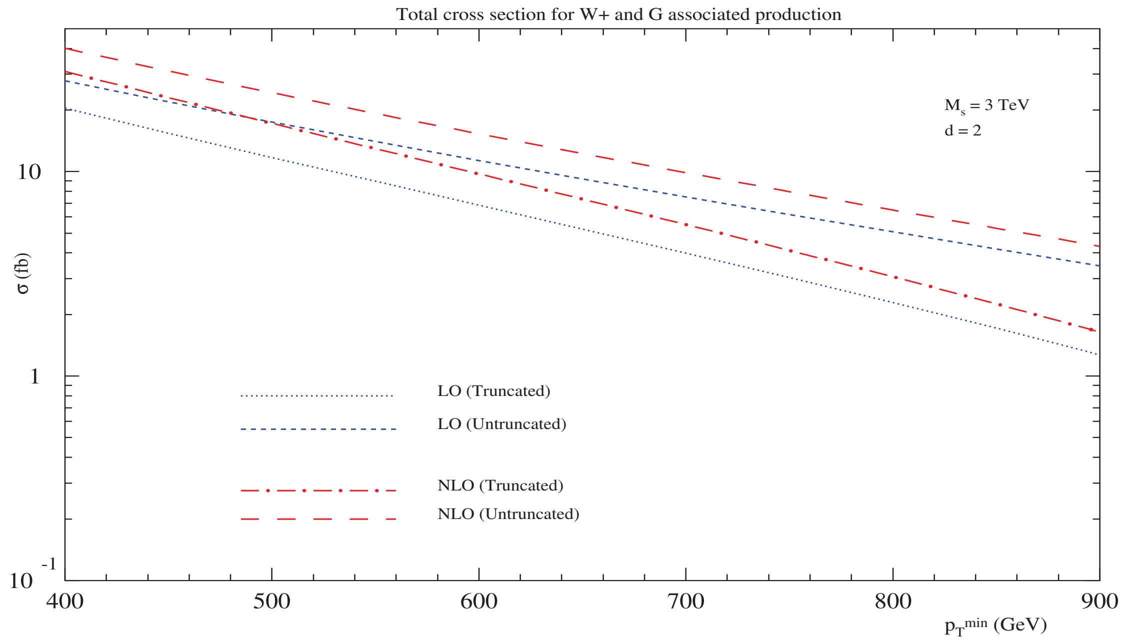

Figure 3.21: Total cross section for the associated production of W^+ boson and graviton, shown as a function of p_T^{min} for $M_s = 3$ TeV and $d = 2$.

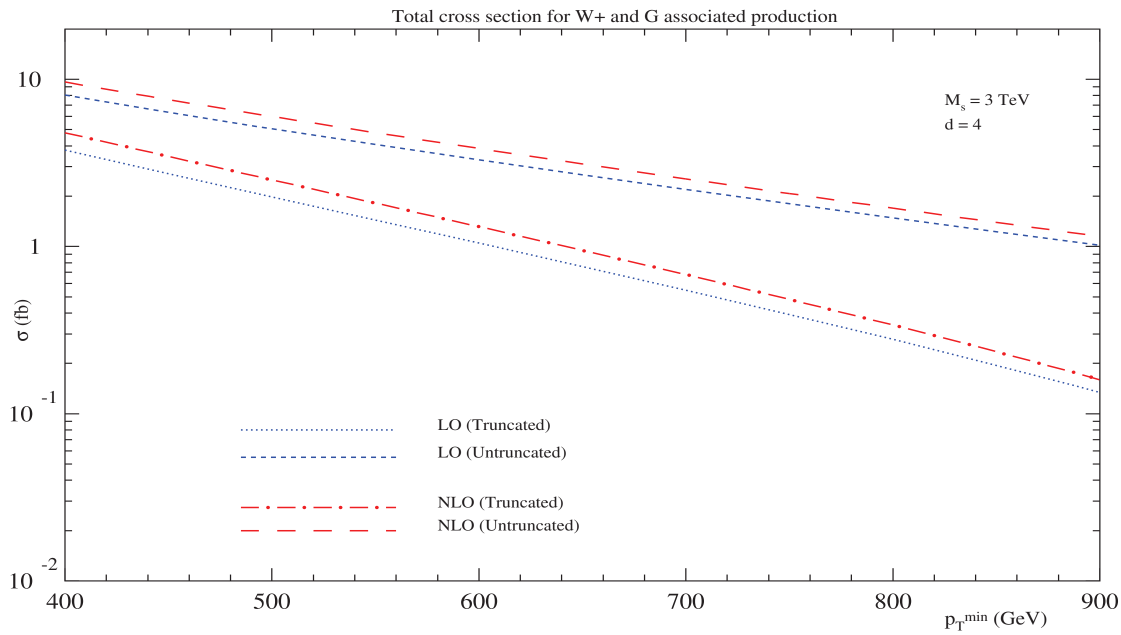

Figure 3.22: Total cross section for the associated production of W^+ boson and graviton, shown as a function of p_T^{min} for $M_s = 3$ TeV and $d = 4$.

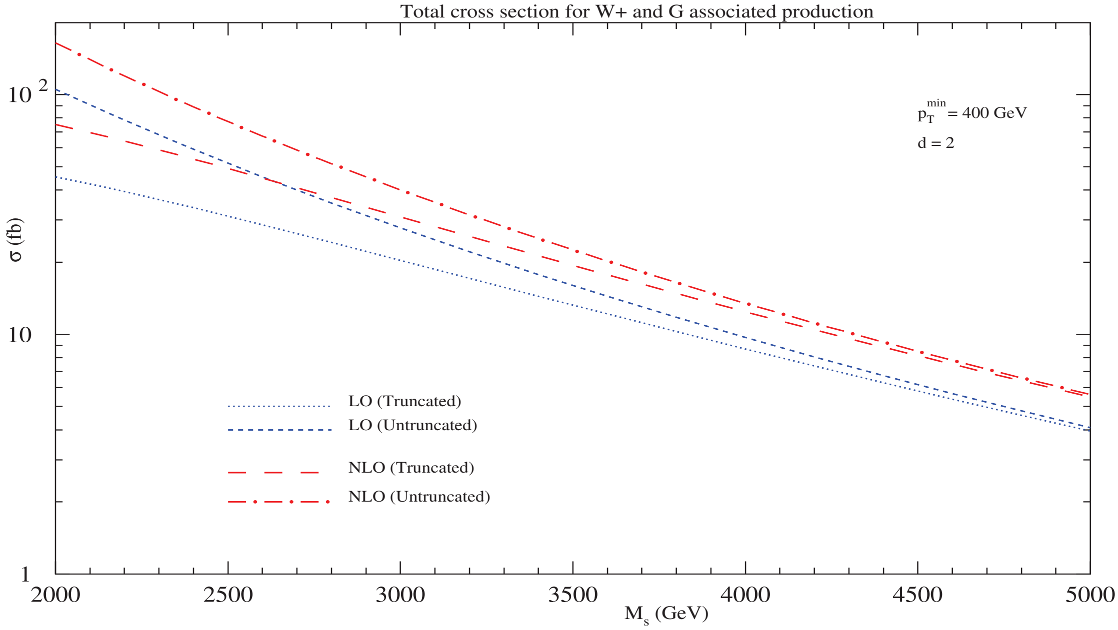

Figure 3.23: Total cross section for the associated production of W^+ boson and graviton, shown as a function of M_s for $d = 2$.

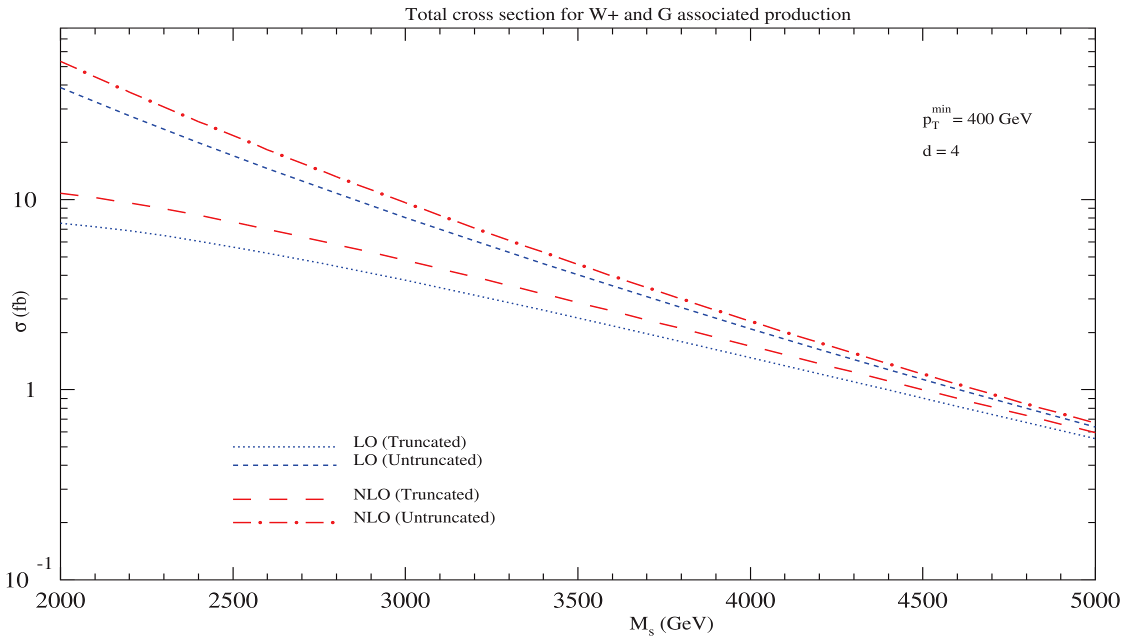

Figure 3.24: Total cross section for the associated production of W^+ boson and graviton, shown as a function of M_s for $d = 4$.

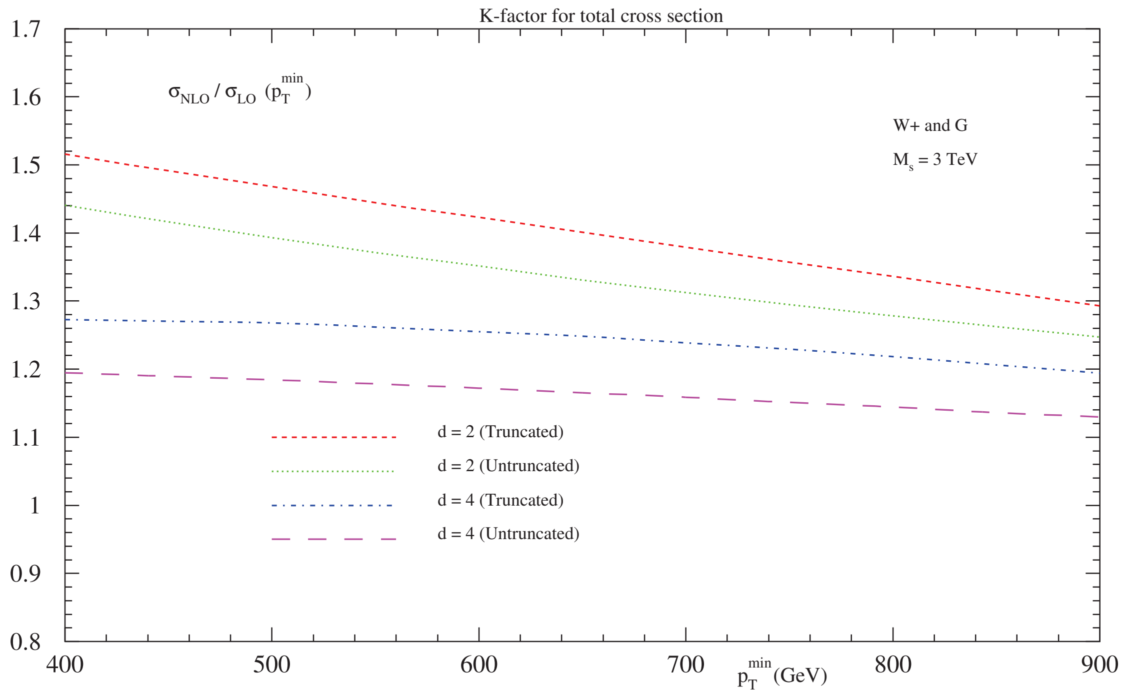

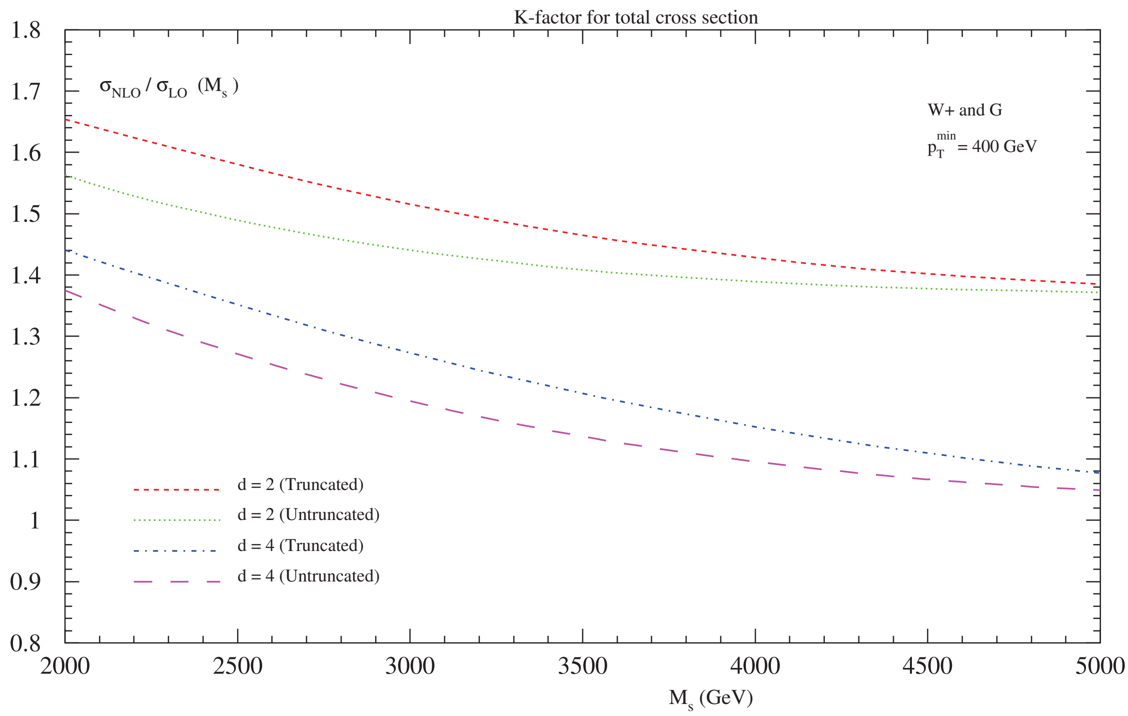

Figure 3.25: K-factors of the total cross section for the associated production of W^+ boson and graviton, given as a function of p_T^{min} (top) and the scale M_s (bottom).

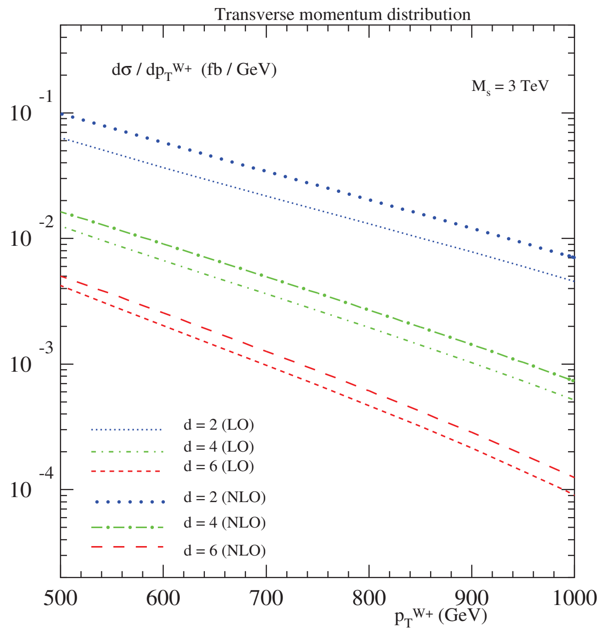

Figure 3.26: Transverse momentum distribution of W^+ boson for $M_s = 3$ TeV is shown for different values of the number of extra dimensions d.

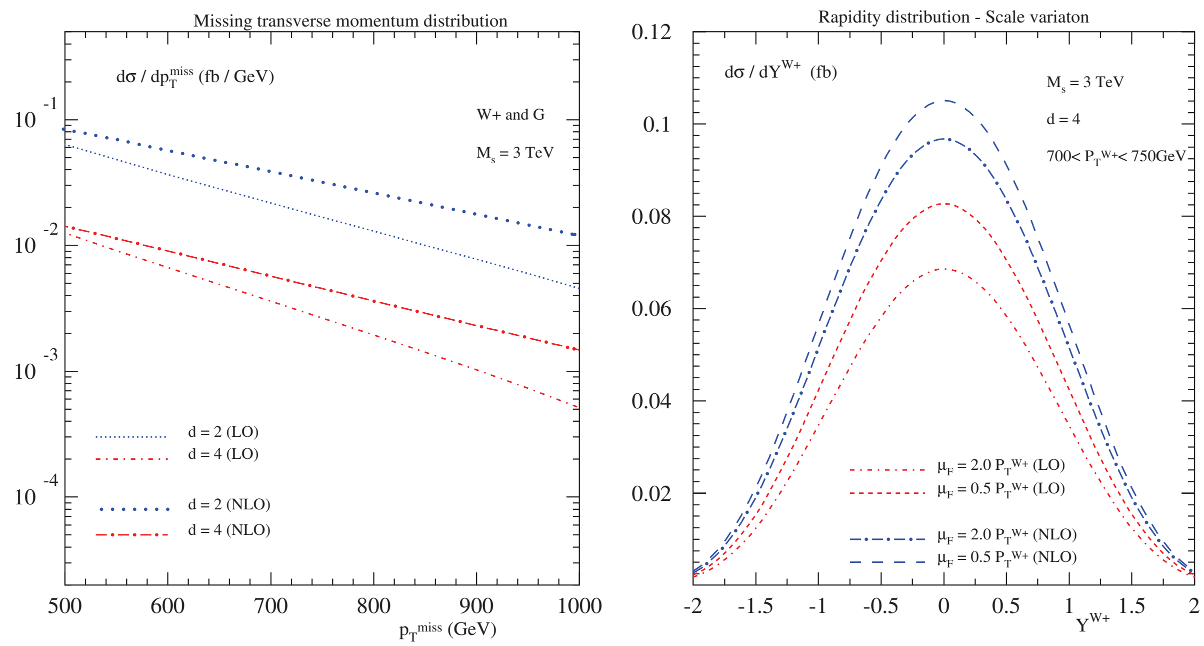

Figure 3.27: Missing transverse momentum distribution of the graviton produced in association with W^+ boson for $M_s = 3$ TeV (left). The scale uncertainties in the rapidity distribution of W^+ boson for $M_s = 3$ TeV and $d = 4$ (right).

Chapter 4

Diphoton Production

4.1 Introduction

Improved theoretical predictions to higher orders in QCD have been performed for cross sections of pair production processes *viz.* di-lepton [50, 51, 52], di-gauge boson ($\gamma\gamma$ [56, 57], ZZ [59] and W^+W^- [60]), which in the LED model could result from the exchange of a virtual KK mode in addition to the usual SM contribution. The real emission of KK modes lead to large missing E_T signals *viz.*, mono-jet [92], mono-photon [93], mono-Z boson and mono-$W^{\pm}$ boson [106, 107]. NLO QCD corrections in some of the above processes are quite substantial and their inclusion in the computation also lead to a reduction of theoretical uncertainties, making it possible for the experiments to put more stringent bounds on the extra dimension model parameters.

The diphoton final state is an important signal for extra dimension searches, as the branching ratio of a KK mode decay to diphoton is twice than that of a decay to individual charged lepton pair. The quantitative impacts of the NLO QCD correction to the diphoton final state for extra dimension searches have been studied in [56, 57], where various IR safe observables were studied using phase space slicing method. The factorisation scale dependence gets reduced when $\mathcal{O}(\alpha_s)$ corrections are included. Fixed order calculation truncated to NLO, at best yields results for sufficiently inclusive observable. Combining fixed order NLO and PS Monte Carlo [32, 33], would extend the coverage of the kinematical region to consistently include resummation in the collinear limit and also produce a more exclusive description of the final state to make it as realistic as possible to the experimental situation. The flexibility to incorporate hadronisation models and capabilities to simulate realistic final state configurations, that can undergo detector simulations, are the main advantages for the experimental collaborations.

ATLAS [76] and CMS [75] have analysed the diphoton invariant mass spectrum, using a constant K-factor for the full range of the invariant mass distribution to put lower bounds on extra dimension scale to NLO accuracy. However, this choice is not sensitive to possible distortions of distributions that can arise at NLO. Our present analysis will further help to put more stringent bounds on the model parameters. Bounds on M_S for different extra dimensions d have been obtained by ATLAS and CMS collaborations [75, 76]. For our present analysis, we choose the following values: $M_S = 3.7$ TeV (d=2), 3.8 TeV (d=3), 3.2 TeV (d=4), 2.9 TeV (d=5), 2.7 TeV (d=6). For relevant observables, we consider the fixed order results to NLO accuracy and include PS. Factorisation, renormalisation scale uncertainties and PDF uncertainties are also estimated in an automated way [108]. For photon isolation, both smooth cone isolation and the experimental isolation criteria are considered.

4.2 NLO+PS

Since the KK modes couple universally to the SM particles through the energy momentum tensor, both the $q\bar{q}$ and gg channel would contribute to the diphoton final state at leading order (LO). In the SM, the gg channel starts only at NNLO level via the finite box contribution through quark loop and the large gluon-gluon flux at the LHC makes this contribution potentially comparable to the LO results. In the invariant mass region of interest to extra dimension searches, the box diagram contribution is not significant enough [56, 57].

All the partonic contributions to NLO in QCD have been calculated for the diphoton final state [56, 57], for both ADD [36, 37, 38] and RS [42] extra dimension models. QCD radiative corrections through virtual one loop gluon and real emission of gluons to the $q\ \bar{q} \to \gamma\ \gamma$ subprocess, would contribute to both SM and extra dimension models. The $q(\bar{q})\ g \to q(\bar{q})\ \gamma\ \gamma$ begins to contribute for both SM and extra dimension models at NLO. The LO $g\ g \to \gamma\ \gamma$ extra dimension process will also get one loop virtual gluon and real gluon emission radiative corrections. There will also be interference between the SM and extra dimension model to give contributions up to $\mathcal{O}(\alpha_s)$ and in this analysis all of them are taken care of. We have included the $\mathcal{O}(\alpha_s)$ corrections as a result of the interference between the SM box diagram contribution and LO extra dimension contribution to the $g\ g \to \gamma\ \gamma$ subprocess for completeness, though it is quite suppressed in the region of interest to extra dimension models and contributes only about 0.1% to the gg subprocess.

The $q(\bar{q})\ g \to q(\bar{q})\ \gamma\ \gamma$ NLO contribution has an additional QED collinear singularity when the photon gets collinear to the emitting quark and can be absorbed into the fragmentation function which gives the probability of a parton fragmenting into a photon. Parton fragmentation functions are additional non perturbative inputs which are not very well known. At the LHC, secondary photons as a result of hadron decaying into collinear photons and jets faking as photon are taken care of by photon isolation criteria [75, 76] which also substantially reduces the fragmentation contribution. Since the fragmentation is essentially a collinear effect, the fragmentation function can be avoided by the smooth cone isolation proposed by Frixione [109], which ensures that in no region of the phase space the soft radiation is eliminated. The smooth cone isolation is able to eliminate the not so well known fragmentation contribution and at the same time, it ensures IR safe observable. Centered in the direction of the photon in the pseudo rapidity (η) and azimuthal angle (ϕ) plane, a cone of radius $r = \sqrt{(\eta - \eta_\gamma)^2 + (\phi - \phi_\gamma)^2}$ is defined. The hadronic activity $H(r)$ is defined as the sum of hadronic transverse energy in a circle of radius $r < r_0$ and E_T^γ is the transverse energy of the photon. For all cones with $r \leq r_0$, the isolation criterion $H(r) < H(r)_{\max}$ has to be satisfied, where $H(r)_{\max}$ is defined as,

$$H(r)_{\max} = \epsilon_\gamma \; E_T^\gamma \left(\frac{1 - \cos r}{1 - \cos r_0} \right)^n \; . \tag{4.1}$$

Efforts for the experimental implementation of the smooth cone isolation is on going.

Automation is an essential ingredient of this work. We have chosen to work in the aMC@NLO framework [110], which automatises the MC@NLO formalism [32] to match NLO computations with parton showers. In this chapter, we present results matched to HERWIG [16]. For the NLO computation, isolation of IR poles and phase space integration are carried out by MadFKS [111], which automatises the FKS subtraction method [112] using the MadGraph [113] matrix-element generator, whereas for one-loop amplitudes the results of [56, 57] are used. The automation within the MadGraph framework requires a new HELAS [114] subroutine to calculate helicity amplitudes with massive spin-2 particles [115, 116]. In addition, for our present analysis, we have implemented the sum over the KK modes of the virtual graviton (see eq. (1.10)) in it (see Appendix D for details). We use this framework to generate the events for 8 TeV run at the LHC. For the invariant mass distributions we have reproduced the results of [56, 57] using the fixed order results obtained from this set-up. Also numerical cancellation of the singularities from the real and virtual terms have been explicitly checked.

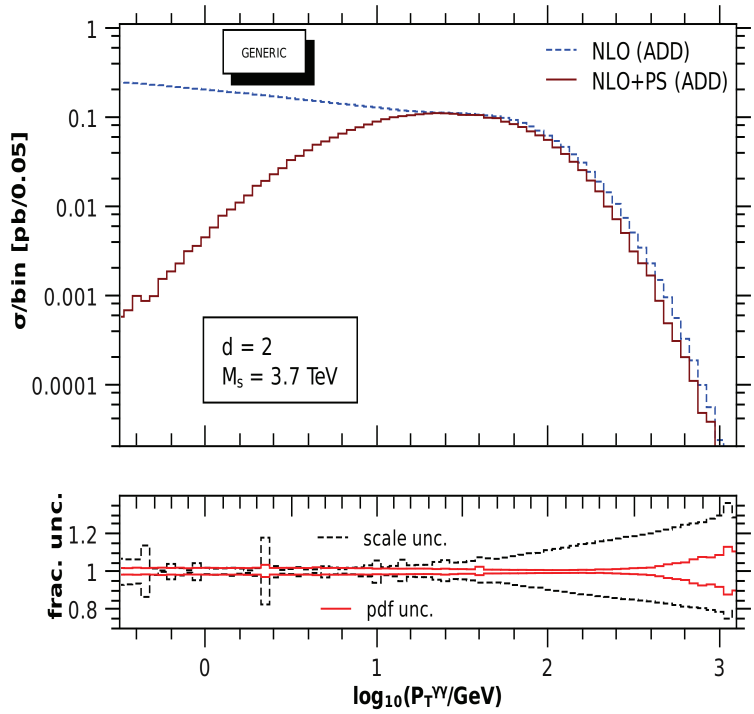

Figure 4.1: Transverse momentum ($P_T^{\gamma\gamma}$) distributions of the diphoton for the fixed order NLO and NLO+PS. The ADD model parameters used are $d = 2$ and $M_S = 3.7$ TeV. The lower inset displays the fractional scale and PDF uncertainties of the NLO+PS (ADD) results.

4.3 Numerical Results

In this section, we present the results for various kinematic distributions of photon pair in SM and ADD model. We have included all the subprocess contributions to NLO. The following input parameters are used: $\alpha_{em}^{-1} = 132.507$, $G_F = 1.16639 \times 10^{-5}$

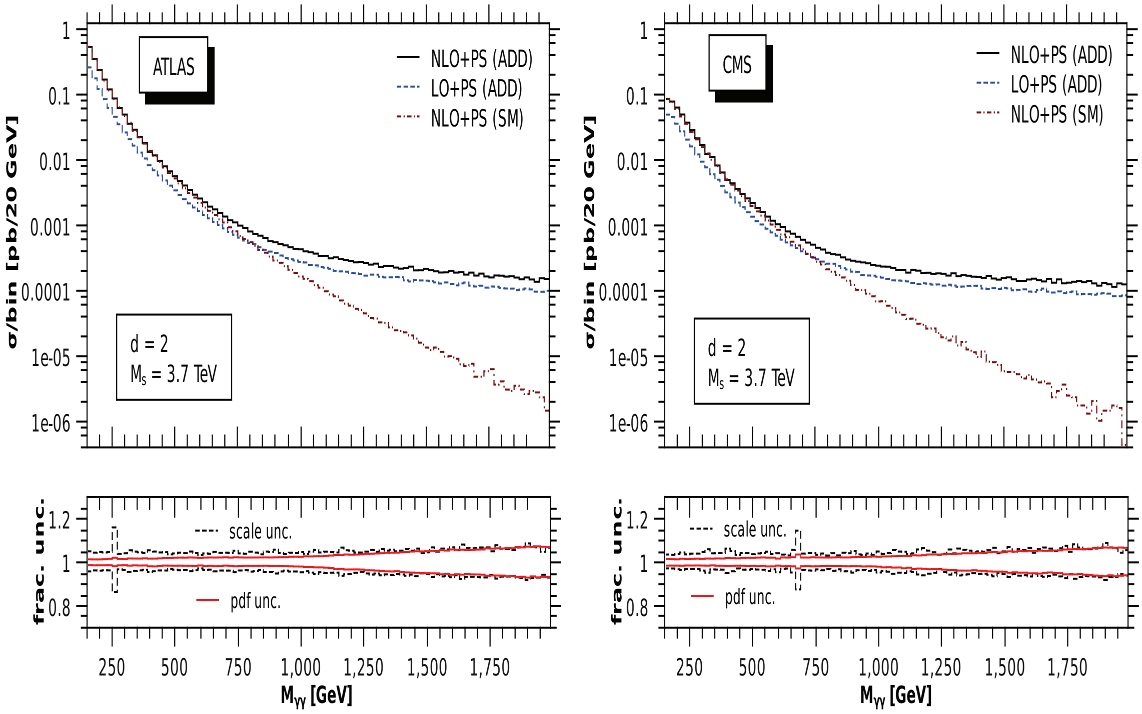

Figure 4.2: Invariant mass ($M_{\gamma\gamma}$) distributions for ATLAS (left panel) and CMS (right panel) for $d = 2$ and $M_S = 3.7$ TeV. The SM contribution to NLO+PS and ADD to LO+PS and NLO+PS have been plotted. For the NLO+PS (ADD) results, the lower insets display the fractional scale and PDF uncertainties.

GeV^{-2}, $m_Z = 91.188$ GeV and MSTW2008(n)lo68cl [117] for the (N)LO PDF. Our calculation is LO in the electroweak coupling and therefore the dependence on the scale in this coupling constant is beyond the precision of our results. In our electroweak scheme, m_W and $\sin^2\theta_W$ are computed from m_Z, α_{em} and G_F; this value for the α_{em} gives a W-boson mass ($m_W = 80.419$ GeV) that is close to the experimental value. The MSTW PDF also sets the value of the strong coupling $\alpha_s(m_Z)$ at LO and NLO in QCD. The renormalisation and factorisation scales are chosen as $\mu_F = \mu_R = M_{\gamma\gamma}$, the invariant mass of the photon pair. The events that have to be showered are generated using the following generation cuts: $|\eta_{\gamma_{1,2}}| < 2.6$, $P_T^{\gamma_{1,2}} > 20$ GeV, diphoton invariant mass 100 GeV $< M_{\gamma\gamma} < M_S$ and the photon isolation is done using the Frixione isolation with $r_0 = 0.38$, $\epsilon_\gamma = 1$ and $n = 2$. More specific analysis cuts are applied subsequently while showering the events in order to produce unbiased results.

The dependence of the prediction of an observable on the factorisation and renormalisation scales, is a result of the uncalculated higher order contributions, which can be estimated by varying μ_F and μ_R independently around the central value $\mu_F = \mu_R = M_{\gamma\gamma}$. The variation is done by the following assignment $\mu_F = \xi_F\ M_{\gamma\gamma}$ and $\mu_R = \xi_R\ M_{\gamma\gamma}$, where the values for (ξ_F, ξ_R) used are (1,1), (1/2,1/2), (1/2,1), (1,1/2), (1,2), (2,1), (2,2). The various ratios of μ_F, μ_R and $M_{\gamma\gamma}$ that appear as arguments of logarithms in the perturbative expansion to NLO are within the range [1/2,2]. The variation of both μ_F and μ_R are taken as the envelope of the above individual variations. Variation of only μ_F would involve the choice $\xi_R = 1$ & varying ξ_F and vice-versa for variation of only μ_R. The PDF uncertainties are estimated in the Hessian method using the prescription given by MSTW [117]. Fractional uncertainty defined as the ratio of the variation about the central value divided by the central value, is a good indicator of the scale and PDF uncertainties and is plotted in the lower insets of various figures. As described in [108], the generation of these uncertainty bands can be done at virtually no extra CPU cost within the aMC@NLO framework.

To begin with, we compare the fixed order NLO result with NLO+PS for the transverse momentum of the diphoton $\log_{10} P_T^{\gamma\gamma}$ using 'generic' cuts: $M_{\gamma\gamma} > 140$ GeV, $|\eta_\gamma| < 2.5$, $P_T^{\gamma_1} > 40$ GeV, $P_T^{\gamma_2} > 25$ GeV and $r_0 = 0.4$. In Fig. 4.1, $\log_{10} P_T^{\gamma\gamma}$ distribution is plotted for $d = 2$ with appropriate M_S value. It is clear that at low $P_T^{\gamma\gamma}$ values, NLO+PS correctly resums the Sudakov logarithms, leading to a suppression of the cross section, while the fixed order NLO result diverges for $P_T^{\gamma\gamma} \to 0$. At high $P_T^{\gamma\gamma}$, the NLO fixed order and NLO+PS results are in agreement. In the lower inset of Fig. 4.1, we have presented the scale and PDF variations of the NLO+PS, which increase with $P_T^{\gamma\gamma}$ as observed in [118].

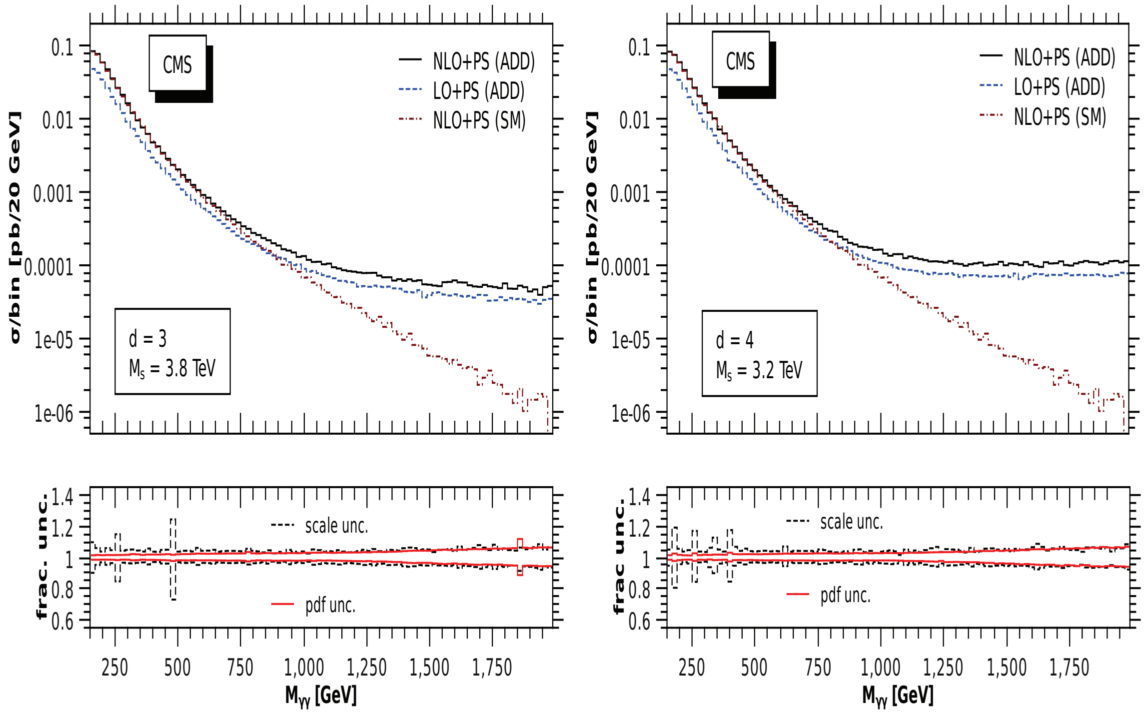

Figure 4.3: Invariant mass ($M_{\gamma\gamma}$) distributions for $d = 3$ (left panel) and $d = 4$ (right panel) are plotted for ADD and SM contributions to NLO+PS accuracy. The lower insets give the corresponding fractional scale and PDF uncertainties for NLO+PS (ADD).

We now present the results for the various kinematical distributions to NLO accuracy with PS (labelled as NLO+PS), for analysis specific cuts. Both the experiments ATLAS and CMS have looked for diphoton invariant mass in the region 140 GeV $< M_{\gamma\gamma} < M_S$. ATLAS cuts [76]: the rapidity of the individual photons are in the region $|\eta_\gamma| < 2.37$, with an exclusion region $1.37 < |\eta_\gamma| < 1.52$, the transverse momentum of the individual photons $P_T^\gamma > 25$ GeV and for photon isolation: sum of transverse energy of hadrons $\sum E_T(H) < 5$ GeV with $\Delta r < 0.4$, where $\Delta r = \sqrt{\Delta\phi^2 + \Delta\eta^2}$ is a cone in the rapidity − azimuthal angle plane. For CMS the corresponding cuts are [75]: $|\eta_\gamma| < 1.44$, $P_T^\gamma > 70$ GeV, photon isolation: (i) sum of the energy of hadrons $\sum E(H) < 0.05 E^\gamma$ with $\Delta r < 0.15$, (ii) sum of transverse energy of hadrons $\sum E_T(H) < 2.2$ GeV $+ 0.0025\ E_T^\gamma$ with $0.15 < \Delta r < 0.4$. We have further checked that, in addition to the ATLAS and CMS photon isolation, if we also include the Frixione isolation criteria, there are no appreciable changes in the final results.

In Fig. 4.2, we have plotted invariant mass distributions $d\sigma/dM_{\gamma\gamma}$ of photon pair in the SM as well as in the ADD model for ATLAS (left panel) and CMS (right panel). For ADD model we have obtained the distributions for $M_S = 3.7$ TeV and $d = 2$. The central value curves correspond to the choice $\mu_F = \mu_R = M_{\gamma\gamma}$, have been plotted for the ADD (NLO+PS) and purely SM (NLO+PS) contribution. The label ADD refers to the total contribution coming from SM, ADD and the interference between them. The corresponding ADD (LO+PS) contribution gives an indication of the quantitative impact of the NLO QCD correction. At larger invariant mass of the photon pair, the ADD effect is dominant. To demonstrate the sensitivity of our predictions to the choice of scale and PDF uncertainties, in the lower insets fractional uncertainties by varying (a) both μ_F and μ_R and (b) PDF error sets, are plotted. The difference in the distributions in Fig. 4.2 for ATLAS and CMS can be attributed to the very different cuts used for their analysis. In Fig. 4.3, the corresponding plots for $d = 3, 4$ are plotted for the CMS cuts. The choice of M_S used for the plots corresponds to the lower bounds obtained by [75, 76] using the diphoton process. By including higher order corrections, the scale dependence goes down from about 25% at LO, to about 10% at NLO, as can be estimated from the ratio plots. The PDF uncertainty does not change significantly and remains about 8%.

We now consider the fractional scale uncertainties on the invariant mass dis-

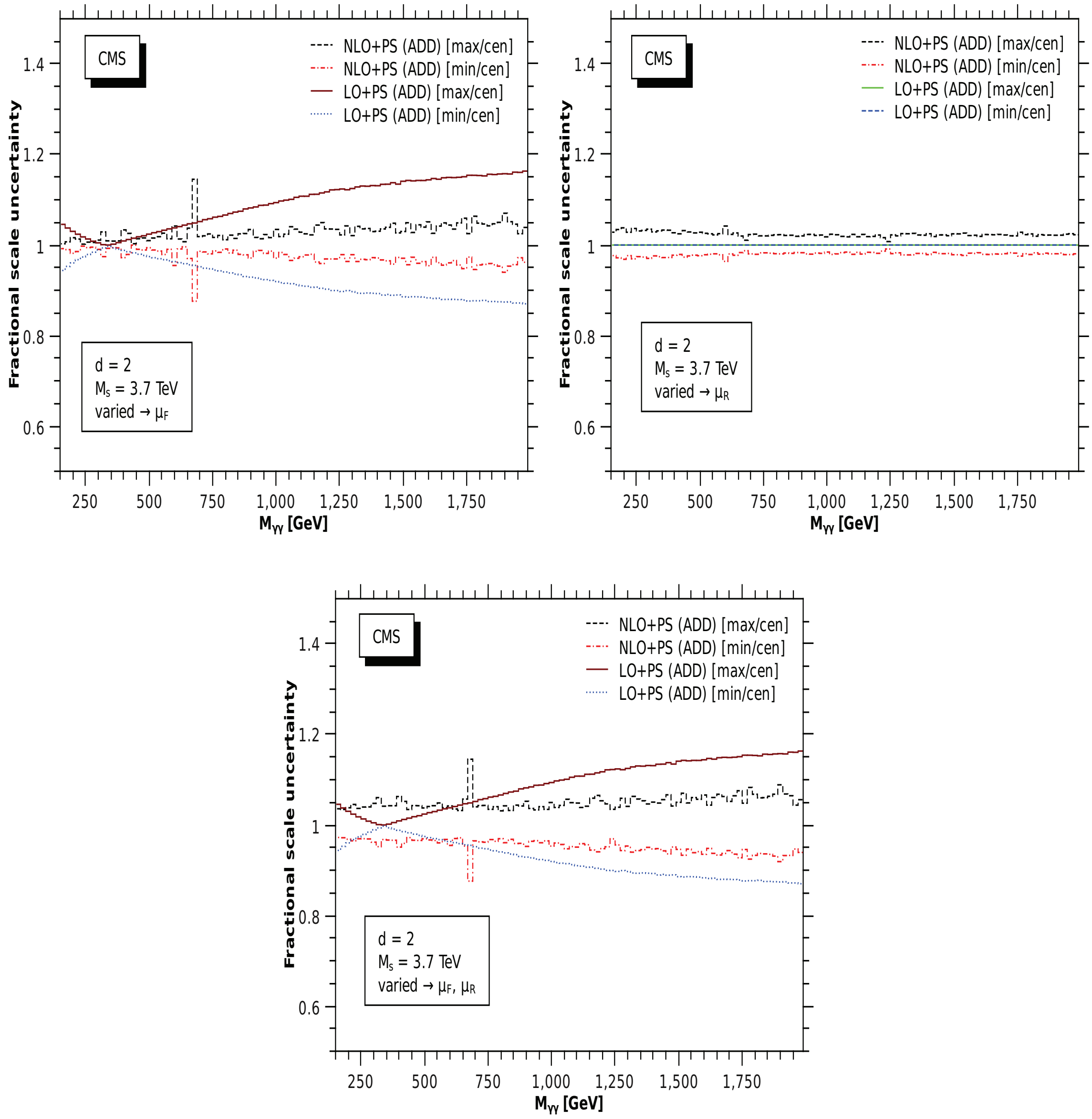

Figure 4.4: For the invariant mass distribution with $d = 2$ and $M_S = 3.7$ TeV, the fractional scale uncertainties as a result of μ_F variation (upper left panel), μ_R variation (upper right panel) and μ_F, μ_R variation (lower panel).

tribution as a result of the variation of the scales μ_F and μ_R (both independently and simultaneously) in going from LO+PS to NLO+PS. Note that the LO cross sections depend only on μ_F through the PDF sets, but at NLO level the scale μ_R enters through $\alpha_s(\mu_R)$ and $\log(\mu_F/\mu_R)$ coming from the partonic cross sections after

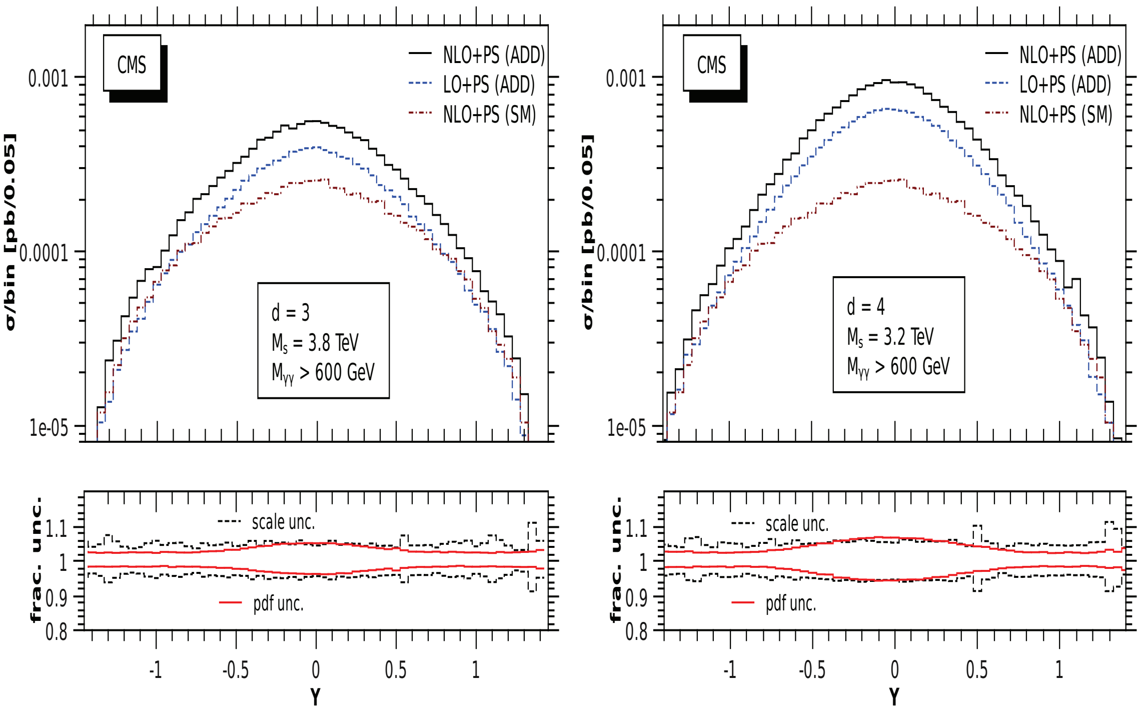

Figure 4.5: Rapidity (Y) distributions of the diphoton pair for $d = 3$ (left panel) and $d = 4$ (right panel) for SM (NLO+PS) and ADD (LO+PS and NLO+PS). The lower insets display the corresponding fractional scale and PDF uncertainties of the NLO+PS (ADD) results.

mass factorisation. As expected the inclusion of NLO QCD correction reduces the factorisation scale dependence resulting from the LO observable which is clear from Fig. 4.4 (upper left panel). In the high $M_{\gamma\gamma}$ region, the uncertainty of about 25% at LO+PS gets reduced to 5% when NLO+PS corrections are included. On the other hand, the μ_R dependence enters only at NLO level (see upper right panel of Fig. 4.4) which will get reduced only if NNLO corrections are included. Hence, we see our NLO corrections are sensitive to the choice of μ_R but the variation is only 5% and is fairly constant for the range of invariant mass considered. If we vary both μ_F and μ_R simultaneously as shown in Fig. 4.4 (lower panel), we find that the reduction in the μ_F scale dependence at NLO level is mildly affected by the μ_R variation in the large invariant mass region. In the small invariant mass region, the LO and NLO results exhibit smaller μ_F dependence compared to the large invariant mass region. But μ_R dependence coming from the NLO results does not change much with the invariant mass $M_{\gamma\gamma}$. Hence variation due to μ_R at small $M_{\gamma\gamma}$ is larger compared to that resulting from μ_F. This explains the behavior at small invariant mass regions where the NLO+PS variation is in excess of the LO+PS (see lower panel of Fig. 4.4).

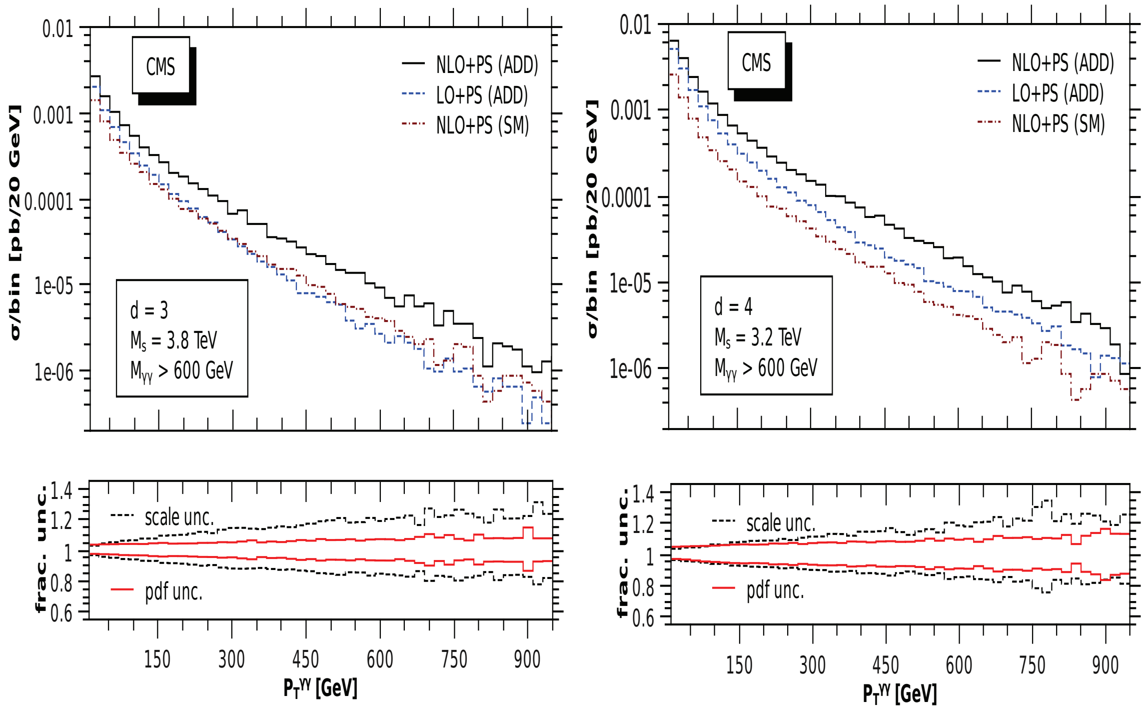

Figure 4.6: Transverse momentum ($P_T^{\gamma\gamma}$) distributions of the diphoton for $d = 3$ (left panel) and $d = 4$ (right panel) along with the corresponding fractional scale and PDF uncertainties (lower inset) of the NLO+PS (ADD) results.

The rapidity (Y) distribution of the diphoton pair is plotted in Fig. 4.5 for $d = 3$ (left panel) and $d = 4$ (right panel). For this analysis we have chosen $M_{\gamma\gamma} > 600$ GeV, the region where the effects of ADD model begins to dominate over the SM diphoton signal at NLO (see Fig. 4.3). The scale and PDF uncertainties to NLO are displayed as insets at the bottom of each figure. The scale uncertainties are usually larger than the PDF uncertainties in the rapidity distribution except for the central rapidity region where they are comparable. For $d = 3$ the scale uncertainties are about 20% around the central rapidity region, which come down to about 10% when NLO+PS corrections are included. The PDF uncertainties for LO+PS and NLO+PS are comparable.

Finally, we plot the transverse momentum distribution in Fig. 4.6 for $d = 3$ (left panel) and $d = 4$ (right panel), for the SM and ADD model to NLO+PS accuracy, with $M_{\gamma\gamma} > 600$ GeV. The ADD results are also plotted for LO+PS. The scale and PDF uncertainties are displayed as insets at the bottom of the plots for NLO+PS (ADD).

4.4 Conclusion

In this chapter, we have presented the diphoton final state in the LED model to NLO in QCD and matching to PS is implemented using the aMC@NLO framework. All the subprocesses that contribute to the diphoton final state from both the SM and ADD model are considered to NLO in QCD. This is the first time MC@NLO formalism has been used for a processes in the ADD model and we hope it would significantly help extra dimension searches at the LHC to constrain the ADD model parameters. Using a set of generic cuts, we first demonstrated the importance of NLO+PS over the fixed order NLO computations, by considering the $P_T^{\gamma\gamma}$ distribution. We have presented our results for various observables *viz.*, invariant mass, rapidity and transverse momentum of the diphoton, both for the ATLAS and CMS detector specific cuts to NLO+PS accuracy. It is important to note that there is substantial enhancement of the various distributions due to the inclusion of NLO corrections and both the theoretical and PDF uncertainties have been estimated.

There is a significant decrease in theoretical uncertainties from over 20% at LO to about 10% when NLO corrections are included. The results are presented for different number of extra spatial dimensions $d = 2 - 6$ with respective values of the fundamental scale M_S that have been experimentally bounded. The event files for $d = 2-6$ are available on the website `http://amcatnlo.cern.ch`. Nevertheless, the complete code is also uploaded on the website `http://amcatnlo.cern.ch` so that it could be used by the experimental collaborations in the large extra dimension searches at the LHC.

Chapter 5

Summary

Needless to say, LHC is a QCD machine and proper illustration of an experimental outcome demands theoretical predictions involving higher order QCD corrections to separate it out from plenty of QCD backgrounds. In this thesis, it has been our main objective to discuss mainly the aspects of NLO QCD corrections with a few important and interesting processes in both SM and BSM in the context of LHC. To present it in a more vivid way, we have gradually stepped towards NLO calculation and then to NLO+PS matching, starting with a LO study.

We have studied triple gauge boson production processes at LO in both SM and LED model for 14 TeV LHC run. In fact, these processes are potential backgrounds of many new physics signals. We have calculated squared amplitudes of the partonic subprocesses of $\gamma\gamma\gamma$, $\gamma\gamma Z$, γZZ and ZZZ productions in three parts: (i) pure SM, (ii) pure LED, (iii) interference between SM and LED, using the symbolic manipulation system FORM. Moreover, we have carried out a number of investigations including gauge invariance check to ensure the correctness of these analytical results. These results are then imported in a FORTRAN based Monte Carlo code, where we have used VEGAS for the purpose of doing phase space integration. With this set-up, we finally obtain numerical results for the total cross sections as well as differential distributions of many kinematical observables for all of the above mentioned processes with the flexibility in choosing cuts, PDF sets *etc*. Later on, we have re-calculated all these numerical results with the help of MadGraph5 package, using proper model description in it and implementing KK mode summation of the graviton propagator in the spin-2 HELAS routines and found excellent agreement with our previous results.

Complete NLO QCD correction to the production of vector gauge boson in association with LED graviton, which essentially plays a vital role in searching new physics signal, has been studied in the context of 14 TeV LHC. In experiment, gravitons express themselves as missing transverse energies, which undoubtedly resemble with the signature coming from SM neutrinos or some other particles that arise in different BSM scenarios, thereby making the process more interesting and compelling us to do its $\mathcal{O}(\alpha_s)$ QCD correction. All the squared matrix elements of the partonic subprocesses at the Born level as well as at the $\mathcal{O}(\alpha_s)$ corrected level *i.e.*, amplitude square of the real emission Feynman diagrams with an extra radiation and the interference between the Born and the virtual Feynman diagrams, are calculated in $n = (4 + \epsilon)$ space-time dimensions using the symbolic manipulation programme FORM and they have been passed through several other tests along with the gauge invariance check. In addition, we have used FORM extensively also in regulating and at the same time, in reducing one loop integrals that arise in the virtual corrections. While performing NLO computation, the complete cross section has been split up into two categories: (*i*) 2-body phase space contribution, which is coming from the Born term, virtual corrections and the real emissions in the soft and collinear limit, (*ii*) 3-body phase space contribution, which solely originates from the divergence free hard finite part of the real emission corrections. We have implemented the two cutoff phase space slicing method in our numerical FORTRAN code to deal with the real emission contribution and used VEGAS as the integrator in that code. We have explicitly checked IR safety of the final result and also found that the final result is independent of the choice of cutoff parameters while adding the 2-body and 3-body phase space contributions. We have presented truncated as well as untruncated differential distributions of several observables using this present framework and also showed that the scale dependence gets reduced at the NLO. This framework is totally general in nature and it can be used to study any other process of interest involving one loop calculation at the NLO level using the two cutoff phase space slicing method with numerous freedom in working with different models, importing various PDF sets, defining several kinematical variables & observables and so on.

Results of diphoton production in the SM and LED model have been produced in NLO+PS accuracy, which would indisputably be required in extra dimension searches at the LHC. We have used aMC@NLO for this purpose, where the real emission contribution is dealt with FKS subtraction scheme and the matching of fixed order NLO results with the HERWIG6 parton shower Monte Carlo is done following the MC@NLO formalism in an automated way. We have implemented the KK mode summation of the graviton propagator in the spin-2 HELAS routines and provided the one loop corrected results within this framework externally. Cancellations of double and single poles coming from the real and virtual contributions have been checked in each and every phase space points while studying fixed order results. We have presented NLO+PS accurate numerical results of differential distributions for a choice of kinematical observables with the estimation of scale and PDF uncertainties for 8 TeV LHC. The complete stand-alone code can be downloaded from `http://amcatnlo.cern.ch` to run it for different LHC center of mass energy with the flexibility in making all the required changes in parameter values, cuts, PDF *etc.* to obtain desired results. This present framework can easily be fitted for the study of any process in the ADD model. Besides, with appropriate changes in the model and the graviton propagator description, this complete layout can easily be moulded to study processes in RS scenario.

Appendices

Appendix A

Expressions: Matrix Element Square for $q\bar{q} \to \gamma\gamma\gamma$

$$\sum_{spin} |\overline{M}|^2_{\text{SM}} = \frac{1}{4}\frac{1}{3}\frac{e^6\ Q_f^6}{t_{13}t_{14}t_{23}t_{24}(s_{12}+t_{13}+t_{14})(s_{12}+t_{23}+t_{24})}\times$$

$$16s_{12}\big(2s_{12}^4+4s_{12}^3(t_{13}+t_{14}+t_{23}+t_{24})+3s_{12}^2(t_{13}+t_{14}+t_{23}+t_{24})^2+s_{12}(t_{13}+t_{14}+t_{23}+t_{24})^3+\big(t13^2+t_{13}t_{14}+{t_{14}}^2+{t_{23}}^2+t_{23}t_{24}+{t_{24}}^2\big)(t_{13}(2t_{23}+t_{24})+t_{14}(t_{23}+2t_{24}))\big) \tag{A.1}$$

$$\sum_{spin} |\overline{M}|^2_{\text{LED}} = \frac{1}{4}\frac{1}{3}\frac{e^2\ Q_f^2\ \kappa^4}{2s_{12}t_{13}t_{14}(s_{12}+t_{13}+t_{14})t_{23}t_{24}(s_{12}+t_{23}+t_{24})}\times$$

$$\mathcal{D}_{45}{}^2t_{14}(s_{12}+t_{13}+t_{14})t_{24}(s_{12}+t_{23}+t_{24})\big(4s_{12}^4+(8t_{13}+9t_{14}+8t_{23}+9t_{24})s_{12}^3+\big(6{t_{13}}^2+(14t_{14}+12t_{23}+13t_{24})t_{13}+9{t_{14}}^2+6{t_{23}}^2+9{t_{24}}^2+13t_{14}t_{23}+16t_{14}t_{24}+14t_{23}t_{24}\big)s_{12}^2+\big(2{t_{13}}^3+(7t_{14}+6(t_{23}+t_{24}))\,{t_{13}}^2+\big(9{t_{14}}^2+13t_{23}t_{14}+16t_{24}t_{14}+6{t_{23}}^2+9{t_{24}}^2+13t_{23}t_{24}\big)t_{13}+4{t_{14}}^3+3{t_{14}}^2(3t_{23}+4t_{24})+(t_{23}+t_{24})\big(2{t_{23}}^2+5t_{24}t_{23}+4{t_{24}}^2\big)+2t_{14}\big(3{t_{23}}^2+8t_{24}t_{23}+6{t_{24}}^2\big)\big)s_{12}+2\big({t_{13}}^2+2t_{14}t_{13}+2{t_{14}}^2+{t_{23}}^2+2{t_{24}}^2+2t_{23}t_{24}\big)(t_{13}(t_{23}+$$

$$t_{24})+t_{14}(t_{23}+2t_{24}))\big)(s_{12}+t_{13}+t_{23})^2+t_{13}t_{23}\big(\mathcal{D}_{35}{}^2(s_{12}+t_{13}+t_{14})(s_{12}+t_{23}+t_{24})\big(4s_{12}^4+(9t_{13}+8t_{14}+9t_{23}+8t_{24})s_{12}^3+\big(9t_{13}{}^2+(14t_{14}+16t_{23}+13t_{24})t_{13}+6t_{14}{}^2+9t_{23}{}^2+6t_{24}{}^2+13t_{14}t_{23}+12t_{14}t_{24}+14t_{23}t_{24}\big)s_{12}^2+\big(4t_{13}{}^3+3(3t_{14}+4t_{23}+3t_{24})t_{13}{}^2+\big(7t_{14}{}^2+16t_{23}t_{14}+13t_{24}t_{14}+12t_{23}{}^2+6t_{24}{}^2+16t_{23}t_{24}\big)t_{13}+2t_{14}{}^3+6t_{14}{}^2(t_{23}+t_{24})+(t_{23}+t_{24})\big(4t_{23}{}^2+5t_{24}t_{23}+2t_{24}{}^2\big)+t_{14}\big(9t_{23}{}^2+13t_{24}t_{23}+6t_{24}{}^2\big)\big)s_{12}+2\big(2t_{13}{}^2+2t_{14}t_{13}+t_{14}{}^2+2t_{23}{}^2+t_{24}{}^2+2t_{23}t_{24}\big)(t_{14}(t_{23}+t_{24})+t_{13}(2t_{23}+t_{24}))\big)(s_{12}+t_{14}+t_{24})^2+2\mathcal{D}_{35}\mathcal{D}_{34}t_{13}t_{23}\big(t_{13}{}^2+t_{23}{}^2\big)\big((s_{12}+t_{13}+2t_{14})t_{24}{}^3+\big(2s_{12}^2+(2t_{13}+7t_{14}+2t_{23})s_{12}+4t_{14}(t_{13}+t_{14})+(t_{13}+3t_{14})t_{23}\big)t_{24}{}^2+\big(s_{12}^3+(t_{13}+6t_{14}+2t_{23})s_{12}^2+\big(7t_{14}{}^2+6t_{23}t_{14}+t_{23}{}^2+t_{13}(6t_{14}+t_{23})\big)s_{12}+t_{14}\big(t_{13}{}^2+3t_{14}t_{13}+2t_{14}{}^2+t_{23}{}^2+4(t_{13}+t_{14})t_{23}\big)\big)t_{24}+t_{14}(s_{12}+t_{13}+t_{14})(s_{12}(s_{12}+t_{13}+t_{14})+(s_{12}+t_{14})t_{23})\big)+\mathcal{D}_{34}{}^2t_{14}t_{24}(s_{12}+t_{13}+t_{14}+t_{23}+t_{24})^2\big((t_{13}t_{14}+t_{23}t_{24})s_{12}^2+(t_{13}+t_{14}+t_{23}+t_{24})(t_{13}t_{14}+t_{23}t_{24})s_{12}+2(t_{13}t_{23}+t_{14}t_{24})\big(t_{13}{}^2+t_{14}{}^2+t_{23}{}^2+t_{24}{}^2\big)\big)\big)+2\mathcal{D}_{45}\big(\mathcal{D}_{34}t_{14}{}^2\big(t_{14}{}^2+t_{24}{}^2\big)\big((t_{13}+t_{23})s_{12}^3+\big(2t_{13}{}^2+(2t_{14}+6t_{23}+t_{24})t_{13}+t_{23}(t_{14}+2(t_{23}+t_{24}))\big)s_{12}^2+\big(t_{13}{}^3+(2t_{14}+7t_{23}+2t_{24})t_{13}{}^2+\big(t_{14}{}^2+(6t_{23}+t_{24})t_{14}+t_{23}(7t_{23}+6t_{24})\big)t_{13}+t_{23}\big((t_{23}+t_{24})^2+t_{14}(2t_{23}+t_{24})\big)\big)s_{12}+t_{13}t_{23}t_{24}{}^2+t_{23}\big((2t_{13}+t_{14})t_{23}{}^2+4t_{13}(t_{13}+t_{14})t_{23}+t_{13}(t_{13}+t_{14})(2t_{13}+t_{14})\big)+\big((t_{13}+t_{14})t_{13}{}^2+4(t_{13}+t_{14})t_{23}t_{13}+(3t_{13}+t_{14})t_{23}{}^2\big)t_{24}\big)t_{24}{}^2+\mathcal{D}_{35}(s_{12}+t_{13}+t_{14})^2(s_{12}+t_{23}+t_{24})^2\big(2s_{12}^2+2(t_{13}+t_{14}+t_{23}+t_{24})s_{12}+(t_{13}+t_{14})^2+(t_{23}+t_{24})^2\big)\big((t_{13}t_{14}+t_{23}t_{24})s_{12}^2+(t_{13}+t_{14}+t_{23}+t_{24})(t_{13}t_{14}+t_{23}t_{24})s_{12}+t_{13}t_{23}t_{24}{}^2+t_{13}t_{14}{}^2t_{23}+t_{14}\big(t_{13}{}^2+4t_{23}t_{13}+t_{23}{}^2\big)t_{24}\big)\big) \tag{A.2}$$

$$\sum_{spin}|\overline{M}|^2_{\rm INT}=\ \frac{1}{4}\,\frac{1}{3}\,\frac{2\ e^4\ Q_f^4\ \kappa^2}{s_{12}t_{13}t_{14}t_{23}t_{24}(s_{12}+t_{13}+t_{14})(s_{12}+t_{23}+t_{24})}\times$$

$$2\big(\mathcal{D}_{45}\big(t_{24}\big(t_{23}(s_{12}(s_{12}+t_{13})-2t_{13}t_{14})+s_{12}(s_{12}+t_{13})^2\big)+t_{14}(s_{12}+t_{23})(s_{12}(s_{12}+t_{13}+t_{14})+t_{23}(s_{12}+t_{14}))+t_{24}{}^2(s_{12}+t_{13})^2\big)\big(2s_{12}^4+4s_{12}^3(t_{13}+$$

$$t_{14} + t_{23} + t_{24}) + 3s_{12}^2(t_{13} + t_{14} + t_{23} + t_{24})^2 + s_{12}(t_{13} + t_{14} + t_{23} + t_{24})^3 + t_{13}{}^3(t_{23} + t_{24}) + 3t_{13}{}^2 t_{14}(t_{23} + t_{24}) + t_{13}(t_{23} + t_{24})\big(3t_{14}{}^2 + (t_{23} + t_{24})^2\big) + t_{14}(t_{23} + 2t_{24})\big(t_{14}{}^2 + t_{23}{}^2 + t_{23}t_{24} + t_{24}{}^2\big)\big) + \mathcal{D}_{35}\big(2s_{12}^4 + 4s_{12}^3(t_{13} + t_{14} + t_{23} + t_{24}) + 3s_{12}^2(t_{13} + t_{14} + t_{23} + t_{24})^2 + s_{12}(t_{13} + t_{14} + t_{23} + t_{24})^3 + t_{23}(2t_{13} + t_{14})\big(t_{13}{}^2 + t_{13}t_{14} + t_{14}{}^2 + t_{23}{}^2\big) + t_{24}(t_{13} + t_{14})\big((t_{13} + t_{14})^2 + 3t_{23}{}^2\big) + 3t_{23}t_{24}{}^2(t_{13} + t_{14}) + t_{24}{}^3(t_{13} + t_{14})\big)\big(s_{12}^3(t_{13} + t_{23}) + s_{12}^2\big(t_{13}{}^2 + t_{13}(t_{14} + 2t_{24}) + t_{23}(2t_{14} + t_{23} + t_{24})\big) + s_{12}\big(t_{14}t_{24}(t_{13} + t_{23}) + t_{13}t_{24}(2t_{13} + t_{24}) + t_{14}{}^2 t_{23} + 2t_{14}t_{23}{}^2\big) + (t_{14}t_{23} - t_{13}t_{24})^2\big) + \mathcal{D}_{34}\big(t_{13}{}^3 t_{23} + t_{13}t_{23}{}^3 + t_{14}t_{24}\big(t_{14}{}^2 + t_{24}{}^2\big)\big)\big(s_{12}^2(t_{13}t_{24} + t_{14}t_{23}) + s_{12}(t_{13} + t_{14} + t_{23} + t_{24})(t_{13}t_{24} + t_{14}t_{23}) + (t_{14}t_{23} - t_{13}t_{24})^2\big)\big) \tag{A.3}$$

Because of three indentical photons in the final state, an additional symmetry factor of $\frac{1}{3!}$ has to be considered while calculating cross section.

Appendix B

Tensor Reduction

B.1 4-point 4-rank Tensor Reduction

B.1.1 Co-efficients of $D_{\mu\nu\rho\lambda}$

$$P^{\mu\nu\rho}_{1,1,1} D_{\mu\nu\rho\lambda} \begin{pmatrix} p_1^\lambda \\ p_2^\lambda \\ p_3^\lambda \end{pmatrix} = X_{[1,2,3]} \begin{pmatrix} D_{41} \\ D_{44} \\ D_{45} \end{pmatrix} + \begin{pmatrix} 3D_{416} \\ 0 \\ 0 \end{pmatrix} = \begin{pmatrix} R_{441} \\ R_{442} \\ R_{443} \end{pmatrix}$$

$$P^{\mu\nu\rho}_{2,2,2} D_{\mu\nu\rho\lambda} \begin{pmatrix} p_1^\lambda \\ p_2^\lambda \\ p_3^\lambda \end{pmatrix} = X_{[1,2,3]} \begin{pmatrix} D_{49} \\ D_{42} \\ D_{413} \end{pmatrix} + \begin{pmatrix} 0 \\ 3D_{417} \\ 0 \end{pmatrix} = \begin{pmatrix} R_{444} \\ R_{445} \\ R_{446} \end{pmatrix}$$

$$P^{\mu\nu\rho}_{3,3,3} D_{\mu\nu\rho\lambda} \begin{pmatrix} p_1^\lambda \\ p_2^\lambda \\ p_3^\lambda \end{pmatrix} = X_{[1,2,3]} \begin{pmatrix} D_{412} \\ D_{415} \\ D_{43} \end{pmatrix} + \begin{pmatrix} 0 \\ 0 \\ 3D_{418} \end{pmatrix} = \begin{pmatrix} R_{447} \\ R_{448} \\ R_{449} \end{pmatrix}$$

$$P^{\mu\nu\rho}_{1,1,2} D_{\mu\nu\rho\lambda} \begin{pmatrix} p_1^\lambda \\ p_2^\lambda \\ p_3^\lambda \end{pmatrix} = X_{[1,2,3]} \begin{pmatrix} D_{44} \\ D_{46} \\ D_{47} \end{pmatrix} + \begin{pmatrix} 2D_{419} \\ D_{416} \\ 0 \end{pmatrix} = \begin{pmatrix} R_{4410} \\ R_{4411} \\ R_{4412} \end{pmatrix}$$

$$P^{\mu\nu\rho}_{1,1,3} D_{\mu\nu\rho\lambda} \begin{pmatrix} p_1^\lambda \\ p_2^\lambda \\ p_3^\lambda \end{pmatrix} = X_{[1,2,3]} \begin{pmatrix} D_{45} \\ D_{47} \\ D_{48} \end{pmatrix} + \begin{pmatrix} 2D_{420} \\ 0 \\ D_{416} \end{pmatrix} = \begin{pmatrix} R_{4413} \\ R_{4414} \\ R_{4415} \end{pmatrix}$$

$$P^{\mu\nu\rho}_{2,2,3} D_{\mu\nu\rho\lambda} \begin{pmatrix} p_1^\lambda \\ p_2^\lambda \\ p_3^\lambda \end{pmatrix} = X_{[1,2,3]} \begin{pmatrix} D_{410} \\ D_{413} \\ D_{414} \end{pmatrix} + \begin{pmatrix} 0 \\ 2D_{421} \\ D_{417} \end{pmatrix} = \begin{pmatrix} R_{4416} \\ R_{4417} \\ R_{4418} \end{pmatrix}$$

$$P^{\mu\nu\rho}_{2,3,3} D_{\mu\nu\rho\lambda} \begin{pmatrix} p_1^\lambda \\ p_2^\lambda \\ p_3^\lambda \end{pmatrix} = X_{[1,2,3]} \begin{pmatrix} D_{411} \\ D_{414} \\ D_{415} \end{pmatrix} + \begin{pmatrix} 0 \\ D_{418} \\ 2D_{421} \end{pmatrix} = \begin{pmatrix} R_{4419} \\ R_{4420} \\ R_{4421} \end{pmatrix}$$

$$P^{\mu\nu} P^{\rho}_{1} D_{\mu\nu\rho\lambda} \begin{pmatrix} p_1^\lambda \\ p_2^\lambda \\ p_3^\lambda \end{pmatrix} = X_{[1,2,3]} \begin{pmatrix} D_{416} \\ D_{419} \\ D_{420} \end{pmatrix} + \begin{pmatrix} D_{422} \\ 0 \\ 0 \end{pmatrix} = \begin{pmatrix} R_{4422} \\ R_{4423} \\ R_{4424} \end{pmatrix}$$

$$P^{\mu\nu}P_2^{\rho}D_{\mu\nu\rho\lambda}\begin{pmatrix} p_1^{\lambda} \\ p_2^{\lambda} \\ p_3^{\lambda} \end{pmatrix} = X_{[1,2,3]}\begin{pmatrix} D_{419} \\ D_{417} \\ D_{421} \end{pmatrix} + \begin{pmatrix} 0 \\ D_{422} \\ 0 \end{pmatrix} = \begin{pmatrix} R_{4425} \\ R_{4426} \\ R_{4427} \end{pmatrix}$$

$$P^{\mu\nu}P_3^{\rho}D_{\mu\nu\rho\lambda}\begin{pmatrix} p_1^{\lambda} \\ p_2^{\lambda} \\ p_3^{\lambda} \end{pmatrix} = X_{[1,2,3]}\begin{pmatrix} D_{420} \\ D_{421} \\ D_{418} \end{pmatrix} + \begin{pmatrix} 0 \\ 0 \\ D_{422} \end{pmatrix} = \begin{pmatrix} R_{4428} \\ R_{4429} \\ R_{4430} \end{pmatrix}$$

$$\begin{aligned} D_{422} &= \left(\frac{n-3}{n-1}\right)P^{\mu\nu}P^{\rho\lambda}D_{\mu\nu\rho\lambda} \\ &= -\frac{1}{2}\left(\frac{1}{n-1}\right)[f_{41}D_{311}+f_{42}D_{312}+f_{43}D_{313}-C_{24}(2,3)] \end{aligned}$$

B.1.2 R_{44} - Functions

$$\begin{aligned}
R_{441} &= \frac{1}{2}[f_{41}D_{31}+C_{31}(1+2,3)+C_0(2,3)] \\
R_{442} &= \frac{1}{2}[f_{42}D_{31}+C_{31}(1,2+3)-C_{31}(1+2,3)] \\
R_{443} &= \frac{1}{2}[f_{43}D_{31}+C_{31}(1,2)-C_{31}(1,2+3)] \\
R_{444} &= \frac{1}{2}[f_{41}D_{32}+C_{31}(1+2,3)-C_{31}(2,3)] \\
R_{445} &= \frac{1}{2}[f_{42}D_{32}+C_{32}(1,2+3)-C_{31}(1+2,3)] \\
R_{446} &= \frac{1}{2}[f_{43}D_{32}+C_{32}(1,2)-C_{32}(1,2+3)] \\
R_{447} &= \frac{1}{2}[f_{41}D_{33}+C_{32}(1+2,3)-C_{32}(2,3)] \\
R_{448} &= \frac{1}{2}[f_{42}D_{33}+C_{32}(1,2+3)-C_{31}(1+2,3)] \\
R_{449} &= \frac{1}{2}[f_{43}D_{33}-C_{32}(1,2+3)]
\end{aligned}$$

$$
\begin{aligned}
R_{4410} &= \frac{1}{2}[f_{41}D_{34} + C_{31}(1+2,3) - C_{11}(2,3)] \\
R_{4411} &= \frac{1}{2}[f_{42}D_{34} + C_{33}(1,2+3) - C_{31}(1+2,3)] \\
R_{4412} &= \frac{1}{2}[f_{43}D_{34} + C_{33}(1,2) - C_{33}(1,2+3)] \\
R_{4413} &= \frac{1}{2}[f_{41}D_{35} + C_{33}(1+2,3) - C_{12}(2,3)] \\
R_{4414} &= \frac{1}{2}[f_{42}D_{35} + C_{33}(1,2+3) - C_{33}(1+2,3)] \\
R_{4415} &= \frac{1}{2}[f_{43}D_{35} + C_{33}(1,2) - C_{33}(1,2+3)] \\
R_{4416} &= \frac{1}{2}[f_{41}D_{38} + C_{33}(1+2,3) - C_{33}(2,3)] \\
R_{4417} &= \frac{1}{2}[f_{42}D_{38} + C_{32}(1,2+3) - C_{33}(1+2,3)] \\
R_{4418} &= \frac{1}{2}[f_{43}D_{38} - C_{32}(1,2+3)] \\
R_{4419} &= \frac{1}{2}[f_{41}D_{39} + C_{34}(1+2,3) - C_{34}(2,3)] \\
R_{4420} &= \frac{1}{2}[f_{42}D_{39} + C_{32}(1,2+3) - C_{34}(1+2,3)] \\
R_{4421} &= \frac{1}{2}[f_{43}D_{39} - C_{32}(1,2+3)] \\
R_{4422} &= \frac{1}{2}[f_{41}D_{311} + C_{35}(1+2,3) + C_{24}(2,3)] \\
R_{4423} &= \frac{1}{2}[f_{42}D_{311} + C_{35}(1,2+3) - C_{35}(1+2,3)] \\
R_{4424} &= \frac{1}{2}[f_{43}D_{311} + C_{35}(1,2) - C_{35}(1,2+3)] \\
R_{4425} &= \frac{1}{2}[f_{41}D_{312} + C_{35}(1+2,3) - C_{35}(2,3)] \\
R_{4426} &= \frac{1}{2}[f_{42}D_{312} + C_{36}(1,2+3) - C_{35}(1+2,3)] \\
R_{4427} &= \frac{1}{2}[f_{43}D_{312} + C_{36}(1,2) - C_{36}(1,2+3)] \\
R_{4428} &= \frac{1}{2}[f_{41}D_{313} + C_{36}(1+2,3) - C_{36}(2,3)] \\
R_{4429} &= \frac{1}{2}[f_{42}D_{313} + C_{36}(1,2+3) - C_{36}(1+2,3)] \\
R_{4430} &= \frac{1}{2}[f_{43}D_{313} - C_{36}(1,2+3)]
\end{aligned}
$$

$$\begin{aligned}
f_{41} &= -p_1^2 \\
f_{42} &= -(p_1+p_2)^2 + p_1^2 \\
f_{43} &= -(p_1+p_2+p_3)^2 + (p_1+p_2)^2
\end{aligned}$$

B.2 5-point Reduction

B.2.1 Co-efficients of E_μ

$$E_\mu \begin{pmatrix} p_1^\mu \\ p_2^\mu \\ p_3^\mu \\ p_4^\mu \end{pmatrix} = X_{[1,2,3,4]} \begin{pmatrix} E_{11} \\ E_{12} \\ E_{13} \\ E_{14} \end{pmatrix} = \begin{pmatrix} R_{511} \\ R_{512} \\ R_{513} \\ R_{514} \end{pmatrix}$$

B.2.2 R_{51} - Functions

$$\begin{aligned}
R511 &= \frac{1}{2}[f_{51}E_0 + D_0(1+2,3,4) - D_0(2,3,4)] \\
R512 &= \frac{1}{2}[f_{52}E_0 + D_0(1,2+3,4) - D_0(1+2,3,4)] \\
R513 &= \frac{1}{2}[f_{53}E_0 + D_0(1,2,3+4) - D_0(1,2+3,4)] \\
R514 &= \frac{1}{2}[f_{54}E_0 + D_0(1,2,3) - D_0(1,2,3+4)]
\end{aligned}$$

B.2.3 Co-efficients of $E_{\mu\nu}$

$$P_1^{\mu} E_{\mu\nu} \begin{pmatrix} p_1^{\nu} \\ p_2^{\nu} \\ p_3^{\nu} \\ p_4^{\nu} \end{pmatrix} = X_{[1,2,3,4]} \begin{pmatrix} E_{21} \\ E_{25} \\ E_{26} \\ E_{27} \end{pmatrix} + \begin{pmatrix} E_{211} \\ 0 \\ 0 \\ 0 \end{pmatrix} = \begin{pmatrix} R_{521} \\ R_{522} \\ R_{523} \\ R_{524} \end{pmatrix}$$

$$P_2^{\mu} E_{\mu\nu} \begin{pmatrix} p_1^{\nu} \\ p_2^{\nu} \\ p_3^{\nu} \\ p_4^{\nu} \end{pmatrix} = X_{[1,2,3,4]} \begin{pmatrix} E_{25} \\ E_{22} \\ E_{28} \\ E_{29} \end{pmatrix} + \begin{pmatrix} 0 \\ E_{211} \\ 0 \\ 0 \end{pmatrix} = \begin{pmatrix} R_{525} \\ R_{526} \\ R_{527} \\ R_{528} \end{pmatrix}$$

$$P_3^{\mu} E_{\mu\nu} \begin{pmatrix} p_1^{\nu} \\ p_2^{\nu} \\ p_3^{\nu} \\ p_4^{\nu} \end{pmatrix} = X_{[1,2,3,4]} \begin{pmatrix} E_{26} \\ E_{28} \\ E_{23} \\ E_{210} \end{pmatrix} + \begin{pmatrix} 0 \\ 0 \\ E_{211} \\ 0 \end{pmatrix} = \begin{pmatrix} R_{529} \\ R_{5210} \\ R_{5211} \\ R_{5212} \end{pmatrix}$$

$$P_4^{\mu} E_{\mu\nu} \begin{pmatrix} p_1^{\nu} \\ p_2^{\nu} \\ p_3^{\nu} \\ p_4^{\nu} \end{pmatrix} = X_{[1,2,3,4]} \begin{pmatrix} E_{27} \\ E_{29} \\ E_{210} \\ E_{24} \end{pmatrix} + \begin{pmatrix} 0 \\ 0 \\ 0 \\ E_{211} \end{pmatrix} = \begin{pmatrix} R_{5213} \\ R_{5214} \\ R_{5215} \\ R_{5216} \end{pmatrix}$$

$$E_{211} = P^{\mu\nu} E_{\mu\nu}$$

$$= -\frac{1}{2}\left(\frac{1}{n-4}\right)[f_{51}E_{11} + f_{52}E_{12} + f_{53}E_{13} + f_{54}E_{14} - D_0(2,3,4)]$$

B.2.4 R_{52} - Functions

$$\begin{aligned}
R_{521} &= \frac{1}{2}[f_{51}E_{11} + D_{11}(1+2,3,4) + D_0(2,3,4)] \\
R_{522} &= \frac{1}{2}[f_{52}E_{11} + D_{11}(1,2+3,4) - D_{11}(1+2,3,4)] \\
R_{523} &= \frac{1}{2}[f_{53}E_{11} + D_{11}(1,2,3+4) - D_{11}(1,2+3,4)] \\
R_{524} &= \frac{1}{2}[f_{54}E_{11} + D_{11}(1,2,3) - D_{11}(1,2,3+4)] \\
R_{525} &= \frac{1}{2}[f_{51}E_{12} + D_{11}(1+2,3,4) - D_{11}(2,3,4)] \\
R_{526} &= \frac{1}{2}[f_{52}E_{12} + D_{12}(1,2+3,4) - D_{11}(1+2,3,4)] \\
R_{527} &= \frac{1}{2}[f_{53}E_{12} + D_{12}(1,2,3+4) - D_{12}(1,2+3,4)] \\
R_{528} &= \frac{1}{2}[f_{54}E_{12} + D_{12}(1,2,3) - D_{12}(1,2,3+4)] \\
R_{529} &= \frac{1}{2}[f_{51}E_{13} + D_{12}(1+2,3,4) - D_{12}(2,3,4)] \\
R_{5210} &= \frac{1}{2}[f_{52}E_{13} + D_{12}(1,2+3,4) - D_{12}(1+2,3,4)] \\
R_{5211} &= \frac{1}{2}[f_{53}E_{13} + D_{13}(1,2,3+4) - D_{12}(1,2+3,4)] \\
R_{5212} &= \frac{1}{2}[f_{54}E_{13} + D_{13}(1,2,3) - D_{13}(1,2,3+4)] \\
R_{5213} &= \frac{1}{2}[f_{51}E_{14} + D_{13}(1+2,3,4) - D_{13}(2,3,4)] \\
R_{5214} &= \frac{1}{2}[f_{52}E_{14} + D_{13}(1,2+3,4) - D_{13}(1+2,3,4)] \\
R_{5215} &= \frac{1}{2}[f_{53}E_{14} + D_{13}(1,2,3+4) - D_{13}(1,2+3,4)] \\
R_{5216} &= \frac{1}{2}[f_{54}E_{14} - D_{13}(1,2,3+4)]
\end{aligned}$$

B.2.5 Co-efficients of $E_{\mu\nu\rho}$

$$P^{\mu\nu}_{1,1}E_{\mu\nu\rho}\begin{pmatrix} p^\rho_1 \\ p^\rho_2 \\ p^\rho_3 \\ p^\rho_4 \end{pmatrix} = X_{[1,2,3,4]}\begin{pmatrix} E_{31} \\ E_{35} \\ E_{36} \\ E_{37} \end{pmatrix} + \begin{pmatrix} 2E_{321} \\ 0 \\ 0 \\ 0 \end{pmatrix} = \begin{pmatrix} R_{531} \\ R_{532} \\ R_{533} \\ R_{534} \end{pmatrix}$$

$$P^{\mu\nu}_{2,2}E_{\mu\nu\rho}\begin{pmatrix} p^\rho_1 \\ p^\rho_2 \\ p^\rho_3 \\ p^\rho_4 \end{pmatrix} = X_{[1,2,3,4]}\begin{pmatrix} E_{38} \\ E_{32} \\ E_{314} \\ E_{315} \end{pmatrix} + \begin{pmatrix} 0 \\ 2E_{322} \\ 0 \\ 0 \end{pmatrix} = \begin{pmatrix} R_{535} \\ R_{536} \\ R_{537} \\ R_{538} \end{pmatrix}$$

$$P^{\mu\nu}_{3,3}E_{\mu\nu\rho}\begin{pmatrix} p^\rho_1 \\ p^\rho_2 \\ p^\rho_3 \\ p^\rho_4 \end{pmatrix} = X_{[1,2,3,4]}\begin{pmatrix} E_{39} \\ E_{316} \\ E_{33} \\ E_{319} \end{pmatrix} + \begin{pmatrix} 0 \\ 0 \\ 2E_{323} \\ 0 \end{pmatrix} = \begin{pmatrix} R_{539} \\ R_{5310} \\ R_{5311} \\ R_{5312} \end{pmatrix}$$

$$P^{\mu\nu}_{4,4}E_{\mu\nu\rho}\begin{pmatrix} p^\rho_1 \\ p^\rho_2 \\ p^\rho_3 \\ p^\rho_4 \end{pmatrix} = X_{[1,2,3,4]}\begin{pmatrix} E_{310} \\ E_{317} \\ E_{320} \\ E_{34} \end{pmatrix} + \begin{pmatrix} 0 \\ 0 \\ 0 \\ 2E_{324} \end{pmatrix} = \begin{pmatrix} R_{5313} \\ R_{5314} \\ R_{5315} \\ R_{5316} \end{pmatrix}$$

$$P_{1,2}^{\mu\nu} E_{\mu\nu\rho} \begin{pmatrix} p_1^\rho \\ p_2^\rho \\ p_3^\rho \\ p_4^\rho \end{pmatrix} = X_{[1,2,3,4]} \begin{pmatrix} E_{35} \\ E_{38} \\ E_{311} \\ E_{312} \end{pmatrix} + \begin{pmatrix} E_{322} \\ E_{321} \\ 0 \\ 0 \end{pmatrix} = \begin{pmatrix} R_{5317} \\ R_{5318} \\ R_{5319} \\ R_{5320} \end{pmatrix}$$

$$P_{3,4}^{\mu\nu} E_{\mu\nu\rho} \begin{pmatrix} p_1^\rho \\ p_2^\rho \\ p_3^\rho \\ p_4^\rho \end{pmatrix} = X_{[1,2,3,4]} \begin{pmatrix} E_{313} \\ E_{318} \\ E_{319} \\ E_{320} \end{pmatrix} + \begin{pmatrix} 0 \\ 0 \\ E_{324} \\ E_{323} \end{pmatrix} = \begin{pmatrix} R_{5321} \\ R_{5322} \\ R_{5323} \\ R_{5324} \end{pmatrix}$$

$$P^{\mu\nu} E_{\mu\nu\rho} \begin{pmatrix} p_1^\rho \\ p_2^\rho \\ p_3^\rho \\ p_4^\rho \end{pmatrix} = X_{[1,2,3,4]} \begin{pmatrix} E_{321} \\ E_{322} \\ E_{323} \\ E_{324} \end{pmatrix} = \begin{pmatrix} R_{5325} \\ R_{5326} \\ R_{5327} \\ R_{5328} \end{pmatrix}$$

B.2.6 R_{53} - Functions

$$\begin{aligned}
R_{531} &= \frac{1}{2}[f_{51}E_{21} + D_{21}(1+2,3,4) - D_0(2,3,4)] \\
R_{532} &= \frac{1}{2}[f_{52}E_{21} + D_{21}(1,2+3,4) - D_{21}(1+2,3,4)] \\
R_{533} &= \frac{1}{2}[f_{53}E_{21} + D_{21}(1,2,3+4) - D_{21}(1,2+3,4)] \\
R_{534} &= \frac{1}{2}[f_{54}E_{21} + D_{21}(1,2,3) - D_{21}(1,2,3+4)] \\
R_{535} &= \frac{1}{2}[f_{51}E_{22} + D_{21}(1+2,3,4) - D_{21}(2,3,4)] \\
R_{536} &= \frac{1}{2}[f_{52}E_{22} + D_{22}(1,2+3,4) - D_{21}(1+2,3,4)] \\
R_{537} &= \frac{1}{2}[f_{53}E_{22} + D_{22}(1,2,3+4) - D_{22}(1,2+3,4)]
\end{aligned}$$

$$
\begin{aligned}
R_{538} &= \frac{1}{2}[f_{54}E_{22} + D_{22}(1,2,3) - D_{22}(1,2,3+4)] \\
R_{539} &= \frac{1}{2}[f_{51}E_{23} + D_{22}(1+2,3,4) - D_{22}(2,3,4)] \\
R_{5310} &= \frac{1}{2}[f_{52}E_{23} + D_{22}(1,2+3,4) - D_{22}(1+2,3,4)] \\
R_{5311} &= \frac{1}{2}[f_{53}E_{23} + D_{23}(1,2,3+4) - D_{22}(1,2+3,4)] \\
R_{5312} &= \frac{1}{2}[f_{54}E_{23} + D_{23}(1,2,3) - D_{23}(1,2,3+4)] \\
R_{5313} &= \frac{1}{2}[f_{51}E_{24} + D_{23}(1+2,3,4) - D_{23}(2,3,4)] \\
R_{5314} &= \frac{1}{2}[f_{52}E_{24} + D_{23}(1,2+3,4) - D_{23}(1+2,3,4)] \\
R_{5315} &= \frac{1}{2}[f_{53}E_{24} + D_{23}(1,2,3+4) - D_{23}(1,2+3,4)] \\
R_{5316} &= \frac{1}{2}[f_{54}E_{24} - D_{23}(1,2,3+4)] \\
R_{5317} &= \frac{1}{2}[f_{51}E_{25} + D_{21}(1+2,3,4) + D_{11}(2,3,4)] \\
R_{5318} &= \frac{1}{2}[f_{52}E_{25} + D_{24}(1,2+3,4) - D_{21}(1+2,3,4)] \\
R_{5319} &= \frac{1}{2}[f_{53}E_{25} + D_{24}(1,2,3+4) - D_{24}(1,2+3,4)] \\
R_{5320} &= \frac{1}{2}[f_{54}E_{25} + D_{24}(1,2,3) - D_{24}(1,2,3+4)] \\
R_{5321} &= \frac{1}{2}[f_{51}E_{210} + D_{26}(1+2,3,4) - D_{26}(2,3,4)] \\
R_{5322} &= \frac{1}{2}[f_{52}E_{210} + D_{26}(1,2+3,4) - D_{26}(1+2,3,4)] \\
R_{5323} &= \frac{1}{2}[f_{53}E_{210} + D_{23}(1,2,3+4) - D_{26}(1,2+3,4)] \\
R_{5324} &= \frac{1}{2}[f_{54}E_{210} - D_{23}(1,2,3+4)] \\
R_{5325} &= \frac{1}{2}[f_{51}E_{211} + D_{27}(1+2,3,4) - D_{27}(2,3,4)] \\
R_{5326} &= \frac{1}{2}[f_{52}E_{211} + D_{27}(1,2+3,4) - D_{27}(1+2,3,4)] \\
R_{5327} &= \frac{1}{2}[f_{53}E_{211} + D_{27}(1,2,3+4) - D_{27}(1,2+3,4)] \\
R_{5328} &= \frac{1}{2}[f_{54}E_{211} + D_{27}(1,2,3) - D_{27}(1,2,3+4)]
\end{aligned}
$$

B.2.7 Co-efficients of $E_{\mu\nu\rho\lambda}$

$$P^{\mu\nu\rho}_{1,1,1}E_{\mu\nu\rho\lambda}\begin{pmatrix} p_1^\lambda \\ p_2^\lambda \\ p_3^\lambda \\ p_4^\lambda \end{pmatrix} = X_{[1,2,3,4]}\begin{pmatrix} E_{41} \\ E_{45} \\ E_{46} \\ E_{47} \end{pmatrix} + \begin{pmatrix} 3E_{436} \\ 0 \\ 0 \\ 0 \end{pmatrix} = \begin{pmatrix} R_{541} \\ R_{542} \\ R_{543} \\ R_{544} \end{pmatrix}$$

$$P^{\mu\nu\rho}_{2,2,2}E_{\mu\nu\rho\lambda}\begin{pmatrix} p_1^\lambda \\ p_2^\lambda \\ p_3^\lambda \\ p_4^\lambda \end{pmatrix} = X_{[1,2,3,4]}\begin{pmatrix} E_{414} \\ E_{42} \\ E_{424} \\ E_{425} \end{pmatrix} + \begin{pmatrix} 0 \\ 3E_{440} \\ 0 \\ 0 \end{pmatrix} = \begin{pmatrix} R_{545} \\ R_{546} \\ R_{547} \\ R_{548} \end{pmatrix}$$

$$P^{\mu\nu\rho}_{3,3,3}E_{\mu\nu\rho\lambda}\begin{pmatrix} p_1^\lambda \\ p_2^\lambda \\ p_3^\lambda \\ p_4^\lambda \end{pmatrix} = X_{[1,2,3,4]}\begin{pmatrix} E_{420} \\ E_{429} \\ E_{43} \\ E_{433} \end{pmatrix} + \begin{pmatrix} 0 \\ 0 \\ 3E_{443} \\ 0 \end{pmatrix} = \begin{pmatrix} R_{549} \\ R_{5410} \\ R_{5411} \\ R_{5412} \end{pmatrix}$$

$$P^{\mu\nu\rho}_{4,4,4}E_{\mu\nu\rho\lambda}\begin{pmatrix} p_1^\lambda \\ p_2^\lambda \\ p_3^\lambda \\ p_4^\lambda \end{pmatrix} = X_{[1,2,3,4]}\begin{pmatrix} E_{423} \\ E_{432} \\ E_{435} \\ E_{44} \end{pmatrix} + \begin{pmatrix} 0 \\ 0 \\ 0 \\ 3E_{445} \end{pmatrix} = \begin{pmatrix} R_{5413} \\ R_{5414} \\ R_{5415} \\ R_{5416} \end{pmatrix}$$

$$P^{\mu\nu\rho}_{1,1,2}E_{\mu\nu\rho\lambda}\begin{pmatrix} p_1^\lambda \\ p_2^\lambda \\ p_3^\lambda \\ p_4^\lambda \end{pmatrix} = X_{[1,2,3,4]}\begin{pmatrix} E_{45} \\ E_{48} \\ E_{411} \\ E_{412} \end{pmatrix} + \begin{pmatrix} 2E_{437} \\ E_{436} \\ 0 \\ 0 \end{pmatrix} = \begin{pmatrix} R_{5417} \\ R_{5418} \\ R_{5419} \\ R_{5420} \end{pmatrix}$$

$$P^{\mu\nu\rho}_{1,1,3}E_{\mu\nu\rho\lambda}\begin{pmatrix} p_1^\lambda \\ p_2^\lambda \\ p_3^\lambda \\ p_4^\lambda \end{pmatrix} = X_{[1,2,3,4]}\begin{pmatrix} E_{46} \\ E_{411} \\ E_{49} \\ E_{413} \end{pmatrix} + \begin{pmatrix} 2E_{438} \\ 0 \\ E_{436} \\ 0 \end{pmatrix} = \begin{pmatrix} R_{5421} \\ R_{5422} \\ R_{5423} \\ R_{5424} \end{pmatrix}$$

$$P^{\mu\nu\rho}_{1,2,2}E_{\mu\nu\rho\lambda}\begin{pmatrix} p_1^\lambda \\ p_2^\lambda \\ p_3^\lambda \\ p_4^\lambda \end{pmatrix} = X_{[1,2,3,4]}\begin{pmatrix} E_{48} \\ E_{414} \\ E_{415} \\ E_{416} \end{pmatrix} + \begin{pmatrix} E_{440} \\ 2E_{437} \\ 0 \\ 0 \end{pmatrix} = \begin{pmatrix} R_{5425} \\ R_{5426} \\ R_{5427} \\ R_{5428} \end{pmatrix}$$

$$P^{\mu\nu\rho}_{1,3,3}E_{\mu\nu\rho\lambda}\begin{pmatrix} p_1^\lambda \\ p_2^\lambda \\ p_3^\lambda \\ p_4^\lambda \end{pmatrix} = X_{[1,2,3,4]}\begin{pmatrix} E_{49} \\ E_{417} \\ E_{420} \\ E_{421} \end{pmatrix} + \begin{pmatrix} E_{443} \\ 0 \\ 2E_{438} \\ 0 \end{pmatrix} = \begin{pmatrix} R_{5429} \\ R_{5430} \\ R_{5431} \\ R_{5432} \end{pmatrix}$$

$$P^{\mu\nu\rho}_{1,2,3}E_{\mu\nu\rho\lambda}\begin{pmatrix} p_1^\lambda \\ p_2^\lambda \\ p_3^\lambda \\ p_4^\lambda \end{pmatrix} = X_{[1,2,3,4]}\begin{pmatrix} E_{411} \\ E_{415} \\ E_{417} \\ E_{418} \end{pmatrix} + \begin{pmatrix} E_{441} \\ E_{438} \\ E_{437} \\ 0 \end{pmatrix} = \begin{pmatrix} R_{5433} \\ R_{5434} \\ R_{5435} \\ R_{5436} \end{pmatrix}$$

$$P^{\mu\nu\rho}_{2,2,3}E_{\mu\nu\rho\lambda}\begin{pmatrix} p_1^\lambda \\ p_2^\lambda \\ p_3^\lambda \\ p_4^\lambda \end{pmatrix} = X_{[1,2,3,4]}\begin{pmatrix} E_{415} \\ E_{424} \\ E_{426} \\ E_{427} \end{pmatrix} + \begin{pmatrix} 0 \\ 2E_{441} \\ E_{440} \\ 0 \end{pmatrix} = \begin{pmatrix} R_{5437} \\ R_{5438} \\ R_{5439} \\ R_{5440} \end{pmatrix}$$

$$P^{\mu\nu\rho}_{2,3,3}E_{\mu\nu\rho\lambda}\begin{pmatrix} p_1^\lambda \\ p_2^\lambda \\ p_3^\lambda \\ p_4^\lambda \end{pmatrix} = X_{[1,2,3,4]}\begin{pmatrix} E_{417} \\ E_{426} \\ E_{429} \\ E_{430} \end{pmatrix} + \begin{pmatrix} 0 \\ E_{443} \\ 2E_{441} \\ 0 \end{pmatrix} = \begin{pmatrix} R_{5441} \\ R_{5442} \\ R_{5443} \\ R_{5444} \end{pmatrix}$$

$$P^{\mu\nu\rho}_{1,4,4}E_{\mu\nu\rho\lambda}\begin{pmatrix} p_1^\lambda \\ p_2^\lambda \\ p_3^\lambda \\ p_4^\lambda \end{pmatrix} = X_{[1,2,3,4]}\begin{pmatrix} E_{410} \\ E_{419} \\ E_{422} \\ E_{423} \end{pmatrix} + \begin{pmatrix} E_{445} \\ 0 \\ 0 \\ 2E_{439} \end{pmatrix} = \begin{pmatrix} R_{5445} \\ R_{5446} \\ R_{5447} \\ R_{5448} \end{pmatrix}$$

$$P^{\mu\nu\rho}_{2,4,4}E_{\mu\nu\rho\lambda}\begin{pmatrix} p_1^\lambda \\ p_2^\lambda \\ p_3^\lambda \\ p_4^\lambda \end{pmatrix} = X_{[1,2,3,4]}\begin{pmatrix} E_{419} \\ E_{428} \\ E_{431} \\ E_{432} \end{pmatrix} + \begin{pmatrix} 0 \\ E_{445} \\ 0 \\ 2E_{442} \end{pmatrix} = \begin{pmatrix} R_{5449} \\ R_{5450} \\ R_{5451} \\ R_{5452} \end{pmatrix}$$

$$P^{\mu\nu\rho}_{3,4,4}E_{\mu\nu\rho\lambda}\begin{pmatrix} p_1^\lambda \\ p_2^\lambda \\ p_3^\lambda \\ p_4^\lambda \end{pmatrix} = X_{[1,2,3,4]}\begin{pmatrix} E_{422} \\ E_{431} \\ E_{434} \\ E_{435} \end{pmatrix} + \begin{pmatrix} 0 \\ 0 \\ E_{445} \\ 2E_{444} \end{pmatrix} = \begin{pmatrix} R_{5453} \\ R_{5454} \\ R_{5455} \\ R_{5456} \end{pmatrix}$$

$$P^{\mu\nu}P^{\rho}_{1}E_{\mu\nu\rho\lambda}\begin{pmatrix} p_1^\lambda \\ p_2^\lambda \\ p_3^\lambda \\ p_4^\lambda \end{pmatrix} = X_{[1,2,3,4]}\begin{pmatrix} E_{436} \\ E_{437} \\ E_{438} \\ E_{439} \end{pmatrix} + \begin{pmatrix} E_{446} \\ 0 \\ 0 \\ 0 \end{pmatrix} = \begin{pmatrix} R_{5457} \\ R_{5458} \\ R_{5459} \\ R_{5460} \end{pmatrix}$$

$$P^{\mu\nu}P^{\rho}_{2}E_{\mu\nu\rho\lambda}\begin{pmatrix} p_1^\lambda \\ p_2^\lambda \\ p_3^\lambda \\ p_4^\lambda \end{pmatrix} = X_{[1,2,3,4]}\begin{pmatrix} E_{437} \\ E_{440} \\ E_{441} \\ E_{442} \end{pmatrix} + \begin{pmatrix} 0 \\ E_{446} \\ 0 \\ 0 \end{pmatrix} = \begin{pmatrix} R_{5461} \\ R_{5462} \\ R_{5463} \\ R_{5464} \end{pmatrix}$$

$$P^{\mu\nu} P_3^{\rho} E_{\mu\nu\rho\lambda} \begin{pmatrix} p_1^\lambda \\ p_2^\lambda \\ p_3^\lambda \\ p_4^\lambda \end{pmatrix} = X_{[1,2,3,4]} \begin{pmatrix} E_{438} \\ E_{441} \\ E_{443} \\ E_{444} \end{pmatrix} + \begin{pmatrix} 0 \\ 0 \\ E_{446} \\ 0 \end{pmatrix} = \begin{pmatrix} R_{5465} \\ R_{5466} \\ R_{5467} \\ R_{5468} \end{pmatrix}$$

$$P^{\mu\nu} P_4^{\rho} E_{\mu\nu\rho\lambda} \begin{pmatrix} p_1^\lambda \\ p_2^\lambda \\ p_3^\lambda \\ p_4^\lambda \end{pmatrix} = X_{[1,2,3,4]} \begin{pmatrix} E_{439} \\ E_{442} \\ E_{444} \\ E_{445} \end{pmatrix} + \begin{pmatrix} 0 \\ 0 \\ 0 \\ E_{446} \end{pmatrix} = \begin{pmatrix} R_{5469} \\ R_{5470} \\ R_{5471} \\ R_{5472} \end{pmatrix}$$

$$\begin{aligned} E_{446} &= \left(\frac{1}{2n-7}\right) P^{\mu\nu} P^{\rho\lambda} E_{\mu\nu\rho\lambda} \\ &= -\frac{1}{2}\left(\frac{1}{n-2}\right)[f_{51}E_{321} + f_{52}E_{322} + f_{53}E_{323} + f_{54}E_{324} - D_{27}(2,3,4)] \end{aligned}$$

B.2.8 R_{54} - Functions

$$\begin{aligned} R_{541} &= \frac{1}{2}[f_{51}E_{31} + D_{31}(1+2,3,4) + D_0(2,3,4)] \\ R_{542} &= \frac{1}{2}[f_{52}E_{31} + D_{31}(1,2+3,4) - D_{31}(1+2,3,4)] \\ R_{543} &= \frac{1}{2}[f_{53}E_{31} + D_{31}(1,2,3+4) - D_{31}(1,2+3,4)] \\ R_{544} &= \frac{1}{2}[f_{54}E_{31} + D_{31}(1,2,3) - D_{31}(1,2,3+4)] \\ R_{545} &= \frac{1}{2}[f_{51}E_{32} + D_{31}(1+2,3,4) - D_{31}(2,3,4)] \\ R_{546} &= \frac{1}{2}[f_{52}E_{32} + D_{32}(1,2+3,4) - D_{31}(1+2,3,4)] \\ R_{547} &= \frac{1}{2}[f_{53}E_{32} + D_{32}(1,2,3+4) - D_{32}(1,2+3,4)] \\ R_{548} &= \frac{1}{2}[f_{54}E_{32} + D_{32}(1,2,3) - D_{32}(1,2,3+4)] \end{aligned}$$

$$
\begin{aligned}
R_{549} &= \frac{1}{2}[f_{51}E_{33} + D_{32}(1+2,3,4) - D_{32}(2,3,4)] \\
R_{5410} &= \frac{1}{2}[f_{52}E_{33} + D_{32}(1,2+3,4) - D_{32}(1+2,3,4)] \\
R_{5411} &= \frac{1}{2}[f_{53}E_{33} + D_{33}(1,2,3+4) - D_{32}(1,2+3,4)] \\
R_{5412} &= \frac{1}{2}[f_{54}E_{33} + D_{33}(1,2,3) - D_{33}(1,2,3+4)] \\
R_{5413} &= \frac{1}{2}[f_{51}E_{34} + D_{33}(1+2,3,4) - D_{33}(2,3,4)] \\
R_{5414} &= \frac{1}{2}[f_{52}E_{34} + D_{33}(1,2+3,4) - D_{33}(1+2,3,4)] \\
R_{5415} &= \frac{1}{2}[f_{53}E_{34} + D_{33}(1,2,3+4) - D_{33}(1,2+3,4)] \\
R_{5416} &= \frac{1}{2}[f_{54}E_{34} - D_{33}(1,2,3+4)] \\
R_{5417} &= \frac{1}{2}[f_{51}E_{35} + D_{31}(1+2,3,4) - D_{11}(2,3,4)] \\
R_{5418} &= \frac{1}{2}[f_{52}E_{35} + D_{34}(1,2+3,4) - D_{31}(1+2,3,4)] \\
R_{5419} &= \frac{1}{2}[f_{53}E_{35} + D_{34}(1,2,3+4) - D_{34}(1,2+3,4)] \\
R_{5420} &= \frac{1}{2}[f_{54}E_{35} + D_{34}(1,2,3) - D_{34}(1,2,3+4)] \\
R_{5421} &= \frac{1}{2}[f_{51}E_{36} + D_{34}(1+2,3,4) - D_{12}(2,3,4)] \\
R_{5422} &= \frac{1}{2}[f_{52}E_{36} + D_{34}(1,2+3,4) - D_{34}(1+2,3,4)] \\
R_{5423} &= \frac{1}{2}[f_{53}E_{36} + D_{35}(1,2,3+4) - D_{34}(1,2+3,4)] \\
R_{5424} &= \frac{1}{2}[f_{54}E_{36} + D_{35}(1,2,3) - D_{35}(1,2,3+4)] \\
R_{5425} &= \frac{1}{2}[f_{51}E_{38} + D_{31}(1+2,3,4) + D_{21}(2,3,4)] \\
R_{5426} &= \frac{1}{2}[f_{52}E_{38} + D_{36}(1,2+3,4) - D_{31}(1+2,3,4)] \\
R_{5427} &= \frac{1}{2}[f_{53}E_{38} + D_{36}(1,2,3+4) - D_{36}(1,2+3,4)] \\
R_{5428} &= \frac{1}{2}[f_{54}E_{38} + D_{36}(1,2,3) - D_{36}(1,2,3+4)] \\
R_{5429} &= \frac{1}{2}[f_{51}E_{39} + D_{36}(1+2,3,4) + D_{22}(2,3,4)] \\
R_{5430} &= \frac{1}{2}[f_{52}E_{39} + D_{36}(1,2+3,4) - D_{36}(1+2,3,4)]
\end{aligned}
$$

$$
\begin{aligned}
R_{5431} &= \frac{1}{2}[f_{53}E_{39} + D_{37}(1,2,3+4) - D_{36}(1,2+3,4)] \\
R_{5432} &= \frac{1}{2}[f_{54}E_{39} + D_{37}(1,2,3) - D_{37}(1,2,3+4)] \\
R_{5433} &= \frac{1}{2}[f_{51}E_{311} + D_{34}(1+2,3,4) + D_{24}(2,3,4)] \\
R_{5434} &= \frac{1}{2}[f_{52}E_{311} + D_{36}(1,2+3,4) - D_{34}(1+2,3,4)] \\
R_{5435} &= \frac{1}{2}[f_{53}E_{311} + D_{310}(1,2,3+4) - D_{36}(1,2+3,4)] \\
R_{5436} &= \frac{1}{2}[f_{54}E_{311} + D_{310}(1,2,3) - D_{310}(1,2,3+4)] \\
R_{5437} &= \frac{1}{2}[f_{51}E_{314} + D_{34}(1+2,3,4) - D_{34}(2,3,4)] \\
R_{5438} &= \frac{1}{2}[f_{52}E_{314} + D_{32}(1,2+3,4) - D_{34}(1+2,3,4)] \\
R_{5439} &= \frac{1}{2}[f_{53}E_{314} + D_{38}(1,2,3+4) - D_{32}(1,2+3,4)] \\
R_{5440} &= \frac{1}{2}[f_{54}E_{314} + D_{38}(1,2,3) - D_{38}(1,2,3+4)] \\
R_{5441} &= \frac{1}{2}[f_{51}E_{316} + D_{36}(1+2,3,4) - D_{36}(2,3,4)] \\
R_{5442} &= \frac{1}{2}[f_{52}E_{316} + D_{32}(1,2+3,4) - D_{36}(1+2,3,4)] \\
R_{5443} &= \frac{1}{2}[f_{53}E_{316} + D_{39}(1,2,3+4) - D_{32}(1,2+3,4)] \\
R_{5444} &= \frac{1}{2}[f_{54}E_{316} + D_{39}(1,2,3) - D_{39}(1,2,3+4)] \\
R_{5445} &= \frac{1}{2}[f_{51}E_{310} + D_{37}(1+2,3,4) + D_{23}(2,3,4)] \\
R_{5446} &= \frac{1}{2}[f_{52}E_{310} + D_{37}(1,2+3,4) - D_{37}(1+2,3,4)] \\
R_{5447} &= \frac{1}{2}[f_{53}E_{310} + D_{37}(1,2,3+4) - D_{37}(1,2+3,4)] \\
R_{5448} &= \frac{1}{2}[f_{54}E_{310} - D_{37}(1,2,3+4)] \\
R_{5449} &= \frac{1}{2}[f_{51}E_{317} + D_{37}(1+2,3,4) - D_{37}(2,3,4)] \\
R_{5450} &= \frac{1}{2}[f_{52}E_{317} + D_{39}(1,2+3,4) - D_{37}(1+2,3,4)] \\
R_{5451} &= \frac{1}{2}[f_{53}E_{317} + D_{39}(1,2,3+4) - D_{39}(1,2+3,4)] \\
R_{5452} &= \frac{1}{2}[f_{54}E_{317} - D_{39}(1,2,3+4)]
\end{aligned}
$$

$$R_{5453} = \frac{1}{2}[f_{51}E_{320} + D_{39}(1+2,3,4) - D_{39}(2,3,4)]$$
$$R_{5454} = \frac{1}{2}[f_{52}E_{320} + D_{39}(1,2+3,4) - D_{39}(1+2,3,4)]$$
$$R_{5455} = \frac{1}{2}[f_{53}E_{320} + D_{33}(1,2,3+4) - D_{39}(1,2+3,4)]$$
$$R_{5456} = \frac{1}{2}[f_{54}E_{320} - D_{33}(1,2,3+4)]$$
$$R_{5457} = \frac{1}{2}[f_{51}E_{321} + D_{311}(1+2,3,4) + D_{27}(2,3,4)]$$
$$R_{5458} = \frac{1}{2}[f_{52}E_{321} + D_{311}(1,2+3,4) - D_{311}(1+2,3,4)]$$
$$R_{5459} = \frac{1}{2}[f_{53}E_{321} + D_{311}(1,2,3+4) - D_{311}(1,2+3,4)]$$
$$R_{5460} = \frac{1}{2}[f_{54}E_{321} + D_{311}(1,2,3) - D_{311}(1,2,3+4)]$$
$$R_{5461} = \frac{1}{2}[f_{51}E_{322} + D_{311}(1+2,3,4) - D_{311}(2,3,4)]$$
$$R_{5462} = \frac{1}{2}[f_{52}E_{322} + D_{312}(1,2+3,4) - D_{311}(1+2,3,4)]$$
$$R_{5463} = \frac{1}{2}[f_{53}E_{322} + D_{312}(1,2,3+4) - D_{312}(1,2+3,4)]$$
$$R_{5464} = \frac{1}{2}[f_{54}E_{322} + D_{312}(1,2,3) - D_{312}(1,2,3+4)]$$
$$R_{5465} = \frac{1}{2}[f_{51}E_{323} + D_{312}(1+2,3,4) - D_{312}(2,3,4)]$$
$$R_{5466} = \frac{1}{2}[f_{52}E_{323} + D_{312}(1,2+3,4) - D_{312}(1+2,3,4)]$$
$$R_{5467} = \frac{1}{2}[f_{53}E_{323} + D_{313}(1,2,3+4) - D_{312}(1,2+3,4)]$$
$$R_{5468} = \frac{1}{2}[f_{54}E_{323} + D_{313}(1,2,3) - D_{313}(1,2,3+4)]$$
$$R_{5469} = \frac{1}{2}[f_{51}E_{324} + D_{313}(1+2,3,4) - D_{313}(2,3,4)]$$
$$R_{5470} = \frac{1}{2}[f_{52}E_{324} + D_{313}(1,2+3,4) - D_{313}(1+2,3,4)]$$
$$R_{5471} = \frac{1}{2}[f_{53}E_{324} + D_{313}(1,2,3+4) - D_{313}(1,2+3,4)]$$
$$R_{5472} = \frac{1}{2}[f_{54}E_{324} - D_{313}(1,2,3+4)]$$

$$
\begin{aligned}
f_{51} &= -p_1^2 \\
f_{52} &= -(p_1+p_2)^2 + p_1^2 \\
f_{53} &= -(p_1+p_2+p_3)^2 + (p_1+p_2)^2 \\
f_{54} &= -(p_1+p_2+p_3+p_4)^2 + (p_1+p_2+p_3)^2
\end{aligned}
$$

Appendix C

Expressions: Real Graviton Production

C.1 Finite Part of the Virtual Contribution

All the V_i's appearing in eq. (3.12) are given below:

$$V_1 = \frac{1}{(t^2u(m_z^2-s))}\times$$

$$\Big((-2m^8t+2m^6(m_Z^2(-6t+u)+t(7t+2u))-m^4(18m_Z^4t-2m_Z^2(24t^2+6tu-u^2)+3t(10t^2+8tu+u^2))+m^2t(-8m_Z^6+26t^3+36t^2u+15tu^2+u^3+2m_Z^4(21t+5u)-2m_Z^2(30t^2+23tu+u^2))-4t^2(-2m_Z^6+2t^3+4t^2u+3tu^2+u^3+m_Z^4(6t+4u)-m_Z^2(6t^2+8tu+3u^2))\Big) \tag{C.1}$$

$$V_2 = \frac{1}{(t^2u(m_Z^2-s))}\times$$

$$\Big(16(2m^8t + 2m^6(m_Z^2(6t-u) - t(7t+2u)) + m^4(18m_Z^4t - 2m_Z^2(24t^2 + 6tu - u^2) + 3t(10t^2 + 8tu + u^2)) - m^2t(-8m_Z^6 + 26t^3 + 36t^2u + 15tu^2 + u^3 + 2m_Z^4(21t+5u) - 2m_Z^2(30t^2 + 23tu + u^2)) + 4t^2(-2m_Z^6 + 2t^3 + 4t^2u + 3tu^2 + u^3 + m_Z^4(6t+4u) - m_Z^2(6t^2 + 8tu + 3u^2)))\Big) \tag{C.2}$$

$$V_3 = V_2|_{t\leftrightarrow u} \tag{C.3}$$

$$V_4 = V_1|_{t\leftrightarrow u} \tag{C.4}$$

$$V_5 = \frac{1}{(2t^2u^2(-m^2+t+u))}\times$$

$$\Big((4m^8tu - 2m^6(9tu(t+u) + m_Z^2(t^2 - 12tu + u^2)) + m^4(36m_Z^4tu + 3tu(11t^2 + 16tu + 11u^2) + 2m_Z^2(t^3 - 30t^2u - 30tu^2 + u^3)) + 4tu(-2m_Z^6(t+u) + (t+u)^2(2t^2 + tu + 2u^2) + m_Z^4(6t^2 + 8tu + 6u^2) - m_Z^2(6t^3 + 11t^2u + 11tu^2 + 6u^3)) - m^2tu(-16m_Z^6 + 52m_Z^4(t+u) - 2m_Z^2(31t^2 + 46tu + 31u^2) + 3(9t^3 + 17t^2u + 17tu^2 + 9u^3)))\Big) \tag{C.5}$$

$$V_6 = \frac{1}{(2t^2u^2(-m^2+t+u))}\times$$

$$\Big((4m^8tu - 2m^6(9tu(t+u) + m_Z^2(t^2 - 12tu + u^2)) + m^4(36m_Z^4tu + 3tu(11t^2 + 16tu + 11u^2) + 2m_Z^2(t^3 - 30t^2u - 30tu^2 + u^3)) + 4tu(-2m_Z^6(t+u) + (t+u)^2(2t^2 + tu + 2u^2) + m_Z^4(6t^2 + 8tu + 6u^2) - m_Z^2(6t^3 + 11t^2u + 11tu^2 + 6u^3)) - m^2tu(-16m_Z^6 + 52m_Z^4(t+u) - 2m_Z^2(31t^2 + 46tu + 31u^2) + 3(9t^3 + 17t^2u + 17tu^2 + 9u^3)))\Big) \tag{C.6}$$

$$V_7 = V_6 \tag{C.7}$$

$$V_8 = \frac{1}{((m^2-t)^2(m_Z^2-t)^2t^2(m^2-t-u)u)}\times$$
$$\Big((m^{12}m_Z^2t(-3m_Z^2+2t)-3m^{10}m_Z^2(m_Z^4(6t-u)+t^2(6t+u)-m_Z^2t(13t+u))+m^8(-27m_Z^8t+12t^4u+3m_Z^6(38t^2+5tu-u^2)+m_Z^2t^2(48t^2+11tu+3u^2)-m_Z^4t(138t^2+50tu+3u^2))-4t^5u(4m_Z^6-2m_Z^4(5t+4u)-t(2t^2+5tu+3u^2)+m_Z^2(8t^2+13tu+4u^2))+m^4t^2(12m_Z^{10}-2m_Z^8(39t+7u)+m_Z^6(160t^2+61tu+5u^2)+t^2u(56t^2+69tu+12u^2)+m_Z^2t(34t^3-107t^2u-99tu^2-12u^3)-2m_Z^4(64t^3+t^2u-2tu^2+3u^3))+m^6t(-12m_Z^{10}-27m_Z^6t(8t+3u)-6t^3u(7t+4u)+m_Z^8(89t+15u)+m_Z^2t(-58t^3+29t^2u+16tu^2-2u^3)+m_Z^4(198t^3+94t^2u+23tu^2+3u^3))+m^2t^3(4m_Z^8(4t-u)+4m_Z^4t(8t^2-22tu-17u^2)+4m_Z^6(-10t^2+6tu+u^2)-t^2u(34t^2+65tu+27u^2)+2m_Z^2t(-4t^3+51t^2u+69tu^2+18u^3)))\Big) \tag{C.8}$$

$$V_9 = V_8|_{t\leftrightarrow u} \tag{C.9}$$

$$V_{10} = \frac{1}{(tu(m^2-t-u)(-4m^2m_Z^2+(t+u)^2)^2)}\times$$
$$\Big(16(104m^{12}m_Z^4(t+u)+4m^{10}m_Z^2(96m_Z^4(t+u)-2m_Z^2(73t^2+74tu+73u^2)-3(t^3+13t^2u+13tu^2+u^3))+4(t+u)^5(-2m_Z^6(t+u)+(t+u)^2(2t^2+tu+2u^2)+m_Z^4(6t^2+8tu+6u^2)-m_Z^2(6t^3+11t^2u+11tu^2+6u^3))+m^4(3(t+u)^5(11t^2+16tu+11u^2)-16m_Z^{10}(17t^2+10tu+17u^2)-8m_Z^4(t+u)^3(25t^2+132tu+25u^2)-12m_Z^6(t+u)^2(43t^2-108tu+43u^2)+4m_Z^2(t+u)^4(49t^2+40tu+49u^2)+48m_Z^8(16t^3+11t^2u+11tu^2+16u^3))-$$

$$m^2(t+u)^2(-16m_Z^8(4t^2+11tu+4u^2)+2m_Z^2(t+u)^3(9t^2-26tu+9u^2)+3(t+u)^4(9t^2+8tu+9u^2)-4m_Z^4(t+u)^2(45t^2+26tu+45u^2)+8m_Z^6(25t^3+64t^2u+64tu^2+25u^3))+4m^8(146m_Z^8(t+u)+(t+u)^5+26m_Z^2(t+u)^2(t^2+5tu+u^2)-24m_Z^6(17t^2+16tu+17u^2)+4m_Z^4(69t^3+59t^2u+59tu^2+69u^3))+2m^6(136m_Z^{10}(t+u)-9(t+u)^6-12m_Z^8(59t^2+54tu+59u^2)-m_Z^2(t+u)^3(123t^2+286tu+123u^2)-2m_Z^4(t+u)^2(157t^2-374tu+157u^2)+m_Z^6(986t^3+866t^2u+866tu^2+986u^3)))\pi^2\Big) \tag{C.10}$$

$$V_{11} = \frac{1}{(t^2u^2(m^2-t-u)(-4m^2m_Z^2+(t+u)^2)^2)}\times$$

$$\Big((-96m^{12}m_Z^4tu-4t^2u^2(t+u)^3(-6m_Z^6+16m_Z^4(t+u)-15m_Z^2(t+u)^2+5(t+u)^3)+4m^{10}m_Z^2(120m_Z^2tu(t+u)+tu(-3t^2+34tu-3u^2)+12m_Z^4(t^2-12tu+u^2))+m^2tu(2m_Z^2(t+u)^4(t^2+18tu+u^2)+(t+u)^5(3t^2+64tu+3u^2)+2m_Z^4(t+u)^3(9t^2-272tu+9u^2)-4m_Z^6(t+u)^2(11t^2-196tu+11u^2)+24m_Z^8(t^3-13t^2u-13tu^2+u^3))+m^4(192m_Z^{10}tu(t+u)-9tu(t+u)^4(t^2+8tu+u^2)-8m_Z^8tu(71t^2+30tu+71u^2)-2m_Z^4tu(t+u)^2(167t^2-1060tu+167u^2)+4m_Z^6tu(167t^3-227t^2u-227tu^2+167u^3)-m_Z^2(t+u)^3(3t^4-20t^3u+674t^2u^2-20tu^3+3u^4))-2m^8(432m_Z^8tu+tu(t+u)^2(3t^2-4tu+3u^2)+2m_Z^2tu(-15t^3+179t^2u+179tu^2-15u^3)+8m_Z^6(3t^3-97t^2u-97tu^2+3u^3)+4m_Z^4(3t^4+118t^3u+66t^2u^2+118tu^3+3u^4))+m^6(-384m_Z^{10}tu+1312m_Z^8tu(t+u)+4tu(t+u)^3(3t^2+5tu+3u^2)-4m_Z^6tu(391t^2+294tu+391u^2)+m_Z^2(t+u)^2(3t^4-70t^3u+1230t^2u^2-70tu^3+3u^4)+8m_Z^4(3t^5+111t^4u-122t^3u^2-122t^2u^3+111tu^4+3u^5))))\Big) \tag{C.11}$$

$$V_{12} = \frac{1}{(3(m^2-t)t^2(-m_Z^2+t)(m^2-u))}\times$$

$$\frac{1}{(u^2(-m_Z^2+u)(m_Z^2-s)^2(4m^2m_Z^2-(t+u)^2))}\times$$

$\big((-12m^{16}m_Z^2tu(22m_Z^4+20tu-21m_Z^2(t+u))+3m^{14}(20t^2u^2(t+u)^2+44m_Z^8(t^2-12tu+u^2)-10m_Z^4tu(29t^2+118tu+29u^2)+m_Z^6(-44t^3+852t^2u+852tu^2-44u^3)-21m_Z^2tu(t^3-13t^2u-13tu^2+u^3))+4t^3u^3(t+u)^2(64m_Z^{10}-176m_Z^8(t+u)+8m_Z^6(23t^2+49tu+23u^2)-3tu(7t^3+5t^2u+5tu^2+7u^3)-6m_Z^4(16t^3+51t^2u+51tu^2+16u^3)+m_Z^2(24t^4+111t^3u+134t^2u^2+111tu^3+24u^4))-3m^{12}(792m_Z^{10}tu+4m_Z^8(33t^3-601t^2u-601tu^2+33u^3)+t^2u^2(79t^3+257t^2u+257tu^2+79u^3)+m_Z^6(-121t^4+2026t^3u+5262t^2u^2+2026tu^3-121u^4)+m_Z^2tu(-73t^4+142t^3u+574t^2u^2+142tu^3-73u^4)-m_Z^4(11t^5+326t^4u+3015t^3u^2+3015t^2u^3+326tu^4+11u^5))-3m^{10}(352m_Z^{12}tu-2428m_Z^{10}tu(t+u)-t^2u^2(t+u)^2(127t^2+386tu+127u^2)-22m_Z^8(6t^4-167t^3u-430t^2u^2-167tu^3+6u^4)+m_Z^6(99t^5-1796t^4u-9887t^3u^2-9887t^2u^3-1796tu^4+99u^5)+m_Z^2tu(104t^5+521t^4u+707t^3u^2+707t^2u^3+521tu^4+104u^5)+m_Z^4(33t^6+87t^5u+2369t^4u^2+6046\,t^3u^3+2369\,t^2u^4+87\,tu^5+33\,u^6))+m^8(2112m_Z^{12}tu(t+u)-16m_Z^{10}tu(453t^2+1241tu+453u^2)+m_Z^8(-132t^5+6321t^4u+36839\,t^3u^2+36839\,t^2u^3+6321\,tu^4-132u^5)-3t^2u^2(107t^5+809t^4u+1912\,t^3u^2+1912\,t^2u^3+809\,tu^4+107\,u^5)+m_Z^6(33\,t^6-1209\,t^5u-20115\,t^4u^2-42434\,t^3u^3-20115\,t^2u^4-1209\,tu^5+33u^6)+3m_Z^2tu(84t^6+943\,t^5u+3098\,t^4u^2+4694t^3u^3+3098\,t^2u^4+943tu^5+84u^6)+3m_Z^4(33t^7-77\,t^6u-544\,t^5u^2+1792\,t^4u^3+1792\,t^3u^4-544t^2u^5-77tu^6+33u^7))+m^2t^2u^2(-1024m_Z^{12}tu-m_Z^6(t+u)^3(1033t^2+3430tu+1033u^2)-32m_Z^{10}(14t^3-37t^2u-37tu^2+14u^3)+3tu(t+u)^2(41t^4+170t^3u+194t^2u^2+170tu^3+41u^4)+8m_Z^8(142t^4+405t^3u+478t^2u^2+405tu^3+142u^4)+m_Z^4(483t^6+4326t^5u+13853t^4u^2+20660t^3u^3+$

$13853t^2u^4 + 4326tu^5 + 483u^6) - 2m_Z^2(69t^7 + 660t^6u + 2578t^5u^2 + 5301t^4u^3+5301t^3u^4+2578t^2u^5+660tu^6+69u^7))+m^6(-32m_Z^{12}tu(33t^2+131tu+33u^2)+4m_Z^{10}tu(537t^3+4225t^2u+4225tu^2+537u^3)+3t^2u^2(t+u)^2(49t^4+469t^3u+862t^2u^2+469tu^3+49u^4)-4m_Z^8tu(126t^4+4141t^3u+9014t^2u^2+4141tu^3+126u^4)+m_Z^6(33t^7-630t^6u+775t^5u^2+14222t^4u^3+14222t^3u^4+775t^2u^5-630tu^6+33u^7)-3m_Z^2tu(43t^7+686t^6u+3478t^5u^2+7861t^4u^3+7861t^3u^4+3478t^2u^5+686tu^6+43u^7)+m_Z^4(-33t^8+171t^7u+5013t^6u^2+15053t^5u^3+18824t^4u^4+15053t^3u^5+5013t^2u^6+171tu^7-33u^8))+m^4tu(2080m_Z^{12}tu(t+u)-6tu(t+u)^3(5t^4+96t^3u+172t^2u^2+96tu^3+5u^4)+8m_Z^{10}(24t^4-485t^3u-1382t^2u^2-485tu^3+24u^4)-m_Z^8(423t^5+375t^4u-8054t^3u^2-8054t^2u^3+375tu^4+423u^5)+m_Z^6(237t^6+3942t^5u+10563t^4u^2+11668t^3u^3+10563t^2u^4+3942tu^5+237u^6)-m_Z^4(39t^7+2514t^6u+14408t^5u^2+29959t^4u^3+29959t^3u^4+14408t^2u^5+2514tu^6+39u^7)+m_Z^2(33t^8+777t^7u+5388t^6u^2+16631t^5u^3+24742t^4u^4+16631t^3u^5+5388t^2u^6+777tu^7+33u^8))))\Big)$

(C.12)

$$V_{13} = \frac{1}{((m_Z^2-t)^2t^2(m_Z^2-u)^2u^2(-m^2+t+u)(-4m^2m_Z^2+(t+u)^2)^2)}\times$$

$\Big(m_Z^2(-16m^{12}m_Z^4tu(6m_Z^6-8m_Z^4(t+u)-2tu(t+u)+m_Z^2(3t^2+8tu+3u^2))+8m^{10}m_Z^2(6m_Z^{10}(t^2-12tu+u^2)+m_Z^8(-12t^3+149t^2u+149tu^2-12u^3)+3m_Z^4tu(t^3+45t^2u+45tu^2+u^3)-t^2u^2(2t^3+t^2u+tu^2+2u^3)+m_Z^2tu(3t^4-2t^3u-54t^2u^2-2tu^3+3u^4)+m_Z^6(6t^4-80t^3u-284t^2u^2-80tu^3+6u^4))+4t^2u^2(t+u)^3(6m_Z^{12}-28m_Z^{10}(t+u)+2tu(t+u)^2(t^2+3tu+u^2)+m_Z^8(49t^2+110tu+49u^2)-m_Z^6(41t^3+155t^2u+155tu^2+41u^3)+m_Z^4(17t^4+97t^3u+166t^2u^2+97tu^3+17u^4)-m_Z^2(3t^5+26t^4u+71t^3u^2+71t^2u^3+26tu^4+3u^5))-m^8(864m_Z^{14}tu+24m_Z^{12}(2t^3-117t^2u-$

$117tu^2+2u^3)-4m_Z^8tu(293t^3+1581t^2u+1581tu^2+293u^3)+m_Z^{10}(-72t^4+3012t^3u+7672t^2u^2+3012tu^3-72u^4)-2t^2u^2(t^5+15t^4u-20t^3u^2-20t^2u^3+15tu^4+u^5)-4m_Z^4tu(t^5+19t^4u-54t^3u^2-54t^2u^3+19tu^4+u^5)+m_Z^2tu(3t^6+36t^5u-23t^4u^2-688t^3u^3-23t^2u^4+36tu^5+3u^6)+2m_Z^6(12t^6+57t^5u+812t^4u^2+1470t^3u^3+812t^2u^4+57tu^5+12u^6))-m^2tu(4m_Z^{12}(t+u)^2(23t^2-352tu+23u^2)-24m_Z^{14}(t^3-13t^2u-13tu^2+u^3)+2tu(t+u)^4(t^4+13t^3u+38t^2u^2+13tu^3+u^4)+2m_Z^8(t+u)^2(59t^4-542t^3u-2218t^2u^2-542tu^3+59u^4)-2m_Z^{10}(73t^5-845t^4u-3284t^3u^2-3284t^2u^3-845tu^4+73u^5)-m_Z^2(t+u)^3(3t^6+48t^5u+237t^4u^2+236t^3u^3+237t^2u^4+48tu^5+3u^6)+2m_Z^4(t+u)^2(6t^6+87t^5u+104t^4u^2-238t^3u^3+104t^2u^4+87tu^5+6u^6)+m_Z^6(-49t^7-73t^6u+2017t^5u^2+6457t^4u^3+6457t^3u^4+2017t^2u^5-73tu^6-49u^7))+m^6(-384m_Z^{16}tu+1936m_Z^{14}tu(t+u)-4m_Z^{12}tu(859t^2+1806tu+859u^2)-t^2u^2(t+u)^2(3t^4+64t^3u-130t^2u^2+64tu^3+3u^4)+8m_Z^{10}(3t^5+347t^4u+1095t^3u^2+1095t^2u^3+347tu^4+3u^5)-m_Z^8(45t^6+1146t^5u+3887t^4u^2+3460t^3u^3+3887t^2u^4+1146tu^5+45u^6)+m_Z^2tu(3t^7+115t^6u+165t^5u^2-1811t^4u^3-1811t^3u^4+165t^2u^5+115tu^6+3u^7)+2m_Z^6(9t^7+142t^6u+348t^5u^2-1971t^4u^3-1971t^3u^4+348t^2u^5+142tu^6+9u^7)+m_Z^4(3t^8-32t^7u-340t^6u^2+2156t^5u^3+6490t^4u^4+2156t^3u^5-340t^2u^6-32tu^7+3u^8))+m^4(192m_Z^{16}tu(t+u)-8m_Z^{14}tu(101t^2+138tu+101u^2)+4m_Z^{12}tu(333t^3+379t^2u+379tu^2+333u^3)+2m_Z^{10}tu(-581t^4+30t^3u+2118t^2u^2+30tu^3-581u^4)+3t^2u^2(t+u)^3(t^4+18t^3u-2t^2u^2+18tu^3+u^4)-m_Z^2tu(t+u)^2(3t^6+96t^5u+209t^4u^2-1132t^3u^3+209t^2u^4+96tu^5+3u^6)-m_Z^8(3t^7-613t^6u+921t^5u^2+11961t^4u^3+11961t^3u^4+921t^2u^5-613tu^6+3u^7)+m_Z^6(6t^8-177t^7u+12t^6u^2+8745t^5u^3+18124t^4u^4+8745t^3u^5+12t^2u^6-177tu^7+6u^8)-m_Z^4(3t^9-13t^8u-338t^7u^2+1474t^6u^3+8410t^5u^4+8410t^4u^5+$

$$1474t^3u^6 - 338t^2u^7 - 13tu^8 + 3u^9))))\Big)$$

(C.13)

$$V_{14} = \frac{1}{((m^2-t)^2t^2(m^2-u)^2(m^2-t-u)u^2(-4m^2m_Z^2+(t+u)^2)^2)}\times$$

$$\Big(m^2(96m^{18}m_Z^4tu - 4m^{16}m_Z^2(158m_Z^2tu(t+u)+tu(-3t^2+34tu-3u^2)+ 12m_Z^4(t^2-12tu+u^2)) - 4t^3u^3(t+u)^2(12m_Z^6tu+6tu(t+u)^3+m_Z^2(t+ u)^2(t^2-11tu+u^2)-m_Z^4(t^3+7t^2u+7tu^2+u^3))+2m^{14}(432m_Z^8tu+tu(t+ u)^2(3t^2-4tu+3u^2)-4m_Z^2tu(8t^3-113t^2u-113tu^2+8u^3)+4m_Z^6(18t^3- 281t^2u-281tu^2+18u^3)+2m_Z^4(6t^4+411t^3u+578t^2u^2+411tu^3+6u^4))+ m^2t^2u^2(48m_Z^8tu(3t^2-2tu+3u^2)+2(t+u)^4(3t^4+29t^3u+72t^2u^2+29tu^3+ 3u^4) - m_Z^2(t+u)^3(5t^4+124t^3u-102t^2u^2+124tu^3+5u^4)+2m_Z^4(t+ u)^2(7t^4+86t^3u-522t^2u^2+86tu^3+7u^4)-4m_Z^6(3t^5+61t^4u-164t^3u^2- 164t^2u^3+61tu^4+3u^5))+m^{12}(384m_Z^{10}tu-2288m_Z^8tu(t+u)-4tu(t+ u)^3(6t^2+tu+6u^2)-16m_Z^6(9t^4-207t^3u-416t^2u^2-207tu^3+9u^4)- 8m_Z^4(9t^5+284t^4u+356t^3u^2+356t^2u^3+284tu^4+9u^5)-m_Z^2(3t^6-126t^5u+ 2089t^4u^2+4756t^3u^3+2089t^2u^4-126tu^5+3u^6))+m^{10}(-576m_Z^{10}tu(t+ u)+672m_Z^8tu(3t^2+7tu+3u^2)+tu(t+u)^2(39t^4+170t^3u+222t^2u^2+ 170tu^3+39u^4)+16m_Z^6(3t^5-147t^4u-424t^3u^2-424t^2u^3-147tu^4+ 3u^5)+2m_Z^4(36t^6+915t^5u+780t^4u^2-1286t^3u^3+780t^2u^4+915tu^5+ 36u^6)+m_Z^2(9t^7-109t^6u+2141t^5u^2+8903t^4u^3+8903t^3u^4+2141t^2u^5- 109tu^6+9u^7))-m^4tu(48m_Z^8tu(4t^3+3t^2u+3tu^2+4u^3)-m_Z^2tu(t+ u)^2(85t^4-52t^3u-1286t^2u^2-52tu^3+85u^4)+(t+u)^3(3t^6+58t^5u+ 303t^4u^2+492t^3u^3+303t^2u^4+58tu^5+3u^6)-4m_Z^6(3t^6+108t^5u-55t^4u^2- 608t^3u^3-55t^2u^4+108tu^5+3u^6)+m_Z^4(15t^7+353t^6u-501t^5u^2- 5475t^4u^3-5475t^3u^4-501t^2u^5+353tu^6+15u^7))+m^8(192m_Z^{10}tu(t^2+ 4tu+u^2)-32m_Z^8tu(20t^3+97t^2u+97tu^2+20u^3)-3tu(t+u)^3(11t^4+$$

$$80t^3u + 122t^2u^2 + 80tu^3 + 11u^4) + 32m_Z^6tu(27t^4 + 104t^3u + 77t^2u^2 + 104tu^3 + 27u^4) - 2m_Z^4(12t^7 + 423t^6u + 483t^5u^2 - 3970t^4u^3 - 3970t^3u^4 + 483t^2u^5 + 423tu^6 + 12u^7) - m_Z^2(9t^8 - 36t^7u + 880t^6u^2 + 7376t^5u^3 + 13062t^4u^4 + 7376t^3u^5 + 880t^2u^6 - 36tu^7 + 9u^8)) + m^6(-192m_Z^{10}t^2u^2(t + u) + 16m_Z^8tu(3t^4 + 58t^3u + 62t^2u^2 + 58tu^3 + 3u^4) - 4m_Z^6tu(41t^5 + 337t^4u - 308t^3u^2 - 308t^2u^3 + 337tu^4 + 41u^5) + tu(t+u)^2(15t^6 + 194t^5u + 697t^4u^2 + 1016t^3u^3 + 697t^2u^4 + 194tu^5 + 15u^6) + m_Z^4tu(195t^6 + 916t^5u - 4815t^4u^2 - 12032t^3u^3 - 4815t^2u^4 + 916tu^5 + 195u^6) + m_Z^2(3t^9 - t^8u - 20t^7u^2 + 2332t^6u^3 + 7838t^5u^4 + 7838t^4u^5 + 2332t^3u^6 - 20t^2u^7 - tu^8 + 3u^9)))\Big) \tag{C.14}$$

$$V_{15} = \frac{1}{(6t^2u^2(-m^2 + t + u)^2)} \times$$

$$\Big((144m^{10}tu - 6m^8(97tu(t+u) + 12m_Z^2(t^2 - 12tu + u^2)) + 3m^6(432m_Z^4tu + tu(353t^2 + 700tu + 353u^2) + m_Z^2(48t^3 - 746t^2u - 746tu^2 + 48u^3)) + 12m^4(48m_Z^6tu - 208m_Z^4tu(t+u) - tu(89t^3 + 249t^2u + 249tu^2 + 89u^3) + m_Z^2(-6t^4 + 199t^3u + 482t^2u^2 + 199tu^3 - 6u^4)) + m^2tu(-696m_Z^6(t+u) + 40m_Z^4(39t^2 + 107tu + 39u^2) - 6m_Z^2(229t^3 + 817t^2u + 817tu^2 + 229u^3) + 21(27t^4 + 98t^3u + 126t^2u^2 + 98tu^3 + 27u^4)) - 4tu(-2m_Z^6(15t^2 + 86tu + 15u^2) + m_Z^4(90t^3 + 406t^2u + 406tu^2 + 90u^3) - m_Z^2(90t^4 + 381t^3u + 512t^2u^2 + 381tu^3 + 90u^4) + 3(10t^5 + 49t^4u + 69t^3u^2 + 69t^2u^3 + 49tu^4 + 10u^5)))\Big) \tag{C.15}$$

C.2 B_0 Integrals

$$B_0(\mathcal{P}) = \frac{i}{(4\pi)^2}\left[-\frac{2}{\epsilon} + 2 - \gamma_E - f(\mathcal{P})\right] \tag{C.16}$$

where $\mathcal{P} \in \{p_3, p_4, p_5, k, q\}$ and

$$f(\mathcal{P}) = \begin{cases} \ln\left(\frac{-\mathcal{P}^2}{4\pi\mu_r^2}\right) & \text{for } \mathcal{P} = p_3, p_4 \\ \ln\left(\frac{\mathcal{P}^2}{4\pi\mu_r^2}\right) - i\pi & \text{for } \mathcal{P} = p_5, k, q \end{cases} \quad . \tag{C.17}$$

C.3 C_0 Integrals

$$C_0(\mathcal{P}', \mathcal{P}'') = \frac{-i}{(4\pi)^2} \frac{1}{[(\mathcal{P}' - \mathcal{P}'')^2 - \mathcal{P}''^2]} \left[-\frac{2}{\epsilon} \left\{ \ln\left(\frac{-(\mathcal{P}' - \mathcal{P}'')^2}{\mathcal{P}''^2}\right) + i\pi \right\} + \frac{1}{2} \left\{ \left(\gamma_E + \ln\left(\frac{\mathcal{P}''^2}{4\pi\mu_r^2}\right) - i\pi\right)^2 - \left(\gamma_E + \ln\left(\frac{-(\mathcal{P}' - \mathcal{P}'')^2}{4\pi\mu_r^2}\right)\right)^2 \right\} \right] \tag{C.18}$$

where $\mathcal{P}' \in \{p_1, p_2\}$ and $\mathcal{P}'' \in \{k, q\}$.

$$C_0(p_1, p_2) = \frac{-i}{(4\pi)^2} \frac{1}{s} \left[-\frac{4}{\epsilon^2} - \frac{2}{\epsilon} \left\{ \gamma_E + \ln\left(\frac{s}{4\pi\mu_r^2}\right) - i\pi \right\} + \frac{1}{2} \left\{ \frac{\pi^2}{6} - \left(\gamma_E + \ln\left(\frac{s}{4\pi\mu_r^2}\right) - i\pi\right)^2 \right\} \right] \tag{C.19}$$

$$C_0(k, q) = \frac{-i}{(4\pi)^2} \frac{1}{s\beta} \left[2Li_2\left(\frac{2}{1-\alpha+\beta}\right) - 2Li_2\left(\frac{2}{1-\alpha-\beta}\right) - \ln\left(\frac{(1-\alpha)^2 - \beta^2}{4}\right) \left\{ \ln\left(\frac{\alpha-\beta+1}{\alpha-\beta-1}\right) - \ln\left(\frac{\alpha+\beta+1}{\alpha+\beta-1}\right) \right\} \right] \tag{C.20}$$

where $\alpha = \frac{m^2 - m_z^2}{s}$ and $\beta = \frac{1}{s}\sqrt{(t+u)^2 - 4m_z^2 m^2}$.

C.4 D_0 Integrals

$$D_0(p_1, k, q) = \frac{i}{(4\pi)^2} \frac{1}{st} \left[\frac{4}{\epsilon^2} + \frac{2}{\epsilon} \left\{ \gamma_E + \ln\left(\frac{-t}{4\pi\mu_r^2}\right) + \ln\left(\frac{s}{m_z^2}\right) + \ln\left(\frac{-t}{m^2}\right) + i\pi \right\} \right.$$

$$
\begin{aligned}
&+ \left(\gamma_E + \ln\left(\frac{s}{4\pi\mu_r^2}\right) - i\pi\right)^2 + \left(\gamma_E + \ln\left(\frac{-t}{4\pi\mu_r^2}\right)\right)^2 \\
&- \left(\gamma_E + \ln\left(\frac{m_z^2}{4\pi\mu_r^2}\right) - i\pi\right)^2 - \left(\gamma_E + \ln\left(\frac{m^2}{4\pi\mu_r^2}\right) - i\pi\right)^2 \\
&+ \frac{1}{2}\left(\gamma_E + \ln\left(\frac{m_z^2}{s}\right) + \ln\left(\frac{m^2}{4\pi\mu_r^2}\right) - i\pi\right)^2 - \frac{\pi^2}{12} \\
&+ \frac{1}{3}\left(-3\ln^2\left(1 - \frac{t}{m^2}\right) - 3\ln^2\left(\frac{{m_z}^2 - t}{s}\right) - \pi^2\right) - 2Li_2\left(\frac{t}{m^2}\right) \\
&+ \ln^2\left(1 - \frac{m^2}{t}\right) - 2i\pi\ln\left(1 - \frac{m^2}{t}\right) - 2Li_2\left(\frac{t}{{m_z}^2}\right) \\
&+ 2\ln\left(1 - \frac{{m_z}^2}{s}\right)\left(\ln\left(1 - \frac{{m_z}^2}{t}\right) - i\pi\right) \\
&+ \left(\ln\left(1 - \frac{{m_z}^2}{t}\right) - \ln\left(\frac{{m_z}^2 - s}{t}\right)\right) \times \\
&\quad \left(\ln\left(\frac{{m_z}^2 - s}{t}\right) + \log\left(1 - \frac{{m_z}^2}{t}\right) - 2i\pi\right) \\
&- 2\ln\left(\frac{s}{{m_z}^2} - 1\right)\ln\left(1 - \frac{t}{{m_z}^2}\right) + \ln^2\left(1 - \frac{{m_z}^2}{s}\right) \\
&- \ln^2\left(\frac{s}{{m_z}^2}\right) + 2\ln\left(\frac{s}{{m_z}^2}\right)\ln\left(\frac{s}{{m_z}^2} - 1\right)\Bigg]
\end{aligned}
\tag{C.21}
$$

$$
D_0\left(p_2, k, q\right) = D_0\left(p_1, k, q\right)|_{t\to u} \tag{C.22}
$$

$$
\begin{aligned}
D_0\left(k, p_2, q\right) =& \frac{i}{(4\pi)^2}\;\frac{1}{(tu - m_z^2 m^2)}\left[\frac{4}{\epsilon}\left\{\ln\left(\frac{-t}{m_z^2}\right) + \ln\left(\frac{-u}{m^2}\right) + 2i\pi\right\}\right. \\
&- \left(\gamma_E + \ln\left(\frac{m_z^2}{4\pi\mu_r^2}\right) - i\pi\right)^2 - \left(\gamma_E + \ln\left(\frac{m^2}{4\pi\mu_r^2}\right) - i\pi\right)^2 \\
&+ \left(\gamma_E + \ln\left(\frac{-t}{4\pi\mu_r^2}\right)\right)^2 + \left(\gamma_E + \ln\left(\frac{-u}{4\pi\mu_r^2}\right)\right)^2 - \frac{4\pi^2}{3} \\
&+ 2Li_2\left(\frac{(m^2 - t)\left({m_z}^2 - t\right)}{m^2{m_z}^2 - tu}\right) + 2Li_2\left(\frac{(m^2 - u)\left({m_z}^2 - u\right)}{m^2{m_z}^2 - tu}\right) \\
&+ 2Li_2\left(\frac{tu - m^2{m_z}^2}{(m^2 - t)\left(m^2 - u\right)}\right) + 2Li_2\left(\frac{tu - m^2{m_z}^2}{\left({m_z}^2 - t\right)\left({m_z}^2 - u\right)}\right) \\
&+ \ln^2\left(\frac{(m^2 - t)\left(m^2 - u\right)}{tu - m^2{m_z}^2}\right) + \ln^2\left(\frac{\left({m_z}^2 - t\right)\left({m_z}^2 - u\right)}{tu - m^2{m_z}^2}\right)
\end{aligned}
$$

$$
- 2i\pi \left(\ln \left(\frac{(m^2 - t)\,(m^2 - u)}{tu - m^2 {m_z}^2} \right) + \ln \left(\frac{({m_z}^2 - t)\,({m_z}^2 - u)}{tu - m^2 {m_z}^2} \right) \right) \tag{C.23}
$$

Appendix D

ADD & RS Model in MadGraph5

D.1 ADD Model

HLZ formalism [40]

Lagrangian:

$$\mathcal{L}_{\text{HLZ}} = -\frac{\kappa}{2} \sum_{\vec{n}=0}^{\infty} T^{\mu\nu}(x)\ h_{\mu\nu}^{(\vec{n})}(x)$$

where $\kappa = \sqrt{16\pi G_N}$.

Graviton propagator:

$$\mathcal{G}_{\text{HLZ}} = \frac{i\ B_{\mu\nu\alpha\beta}}{k^2 - m^2 + i\epsilon}$$

where

$$\begin{aligned} B_{\mu\nu,\alpha\beta} &= \left(\eta_{\mu\alpha} - \frac{k_\mu k_\alpha}{m^2}\right)\left(\eta_{\nu\beta} - \frac{k_\nu k_\beta}{m^2}\right) \\ &+ \left(\eta_{\mu\beta} - \frac{k_\mu k_\beta}{m^2}\right)\left(\eta_{\nu\alpha} - \frac{k_\nu k_\alpha}{m^2}\right) \\ &- \frac{2}{3}\left(\eta_{\mu\nu} - \frac{k_\mu k_\nu}{m^2}\right)\left(\eta_{\alpha\beta} - \frac{k_\alpha k_\beta}{m^2}\right). \end{aligned}$$

GRW formalism [41]

Lagrangian:

$$\mathcal{L}_{\text{GRW}} = -\frac{1}{\overline{M_P}} \sum_{\vec{n}=0}^{\infty} T^{\mu\nu}(x)\ h'^{(\vec{n})}_{\mu\nu}(x)$$

where $\overline{M_P} = (8\pi G_N)^{-1/2}$.

Graviton Propagator:

$$\mathcal{G}_{\text{GRW}} = \frac{i\ P_{\mu\nu\alpha\beta}}{k^2 - m^2 + i\epsilon}$$

where

$$\begin{aligned} P_{\mu\nu,\alpha\beta} &= \frac{1}{2}\left(\eta_{\mu\alpha}\eta_{\nu\beta} + \eta_{\mu\beta}\eta_{\nu\alpha} - \eta_{\mu\nu}\eta_{\alpha\beta}\right) \\ &- \frac{1}{2m^2}\left(\eta_{\mu\alpha}k_\nu k_\beta + \eta_{\nu\beta}k_\mu k_\alpha + (\alpha \leftrightarrow \beta)\right) \\ &+ \frac{1}{6}\left(\eta_{\mu\nu} + \frac{2\ k_\mu k_\nu}{m^2}\right)\left(\eta_{\alpha\beta} + \frac{2\ k_\alpha k_\beta}{m^2}\right). \end{aligned}$$

In the above, G_N denotes the Newton's constant and k denotes the momentum of a massive spin-2 KK graviton with mass m and rest of the symbols and/or notations are similar to what we have used in section 1.3.1.

We can easily find the inter-relationship between these two formalisms and they are given here under:

$$\frac{1}{\overline{M_P}} = \frac{\kappa}{\sqrt{2}} \quad , \tag{D.1}$$

$$P_{\mu\nu,\alpha\beta} = \frac{1}{2}\, B_{\mu\nu,\alpha\beta} \quad . \tag{D.2}$$

Note that, except the different couplings used in $\mathcal{L}_{\rm HLZ}$ and $\mathcal{L}_{\rm GRW}$ and the difference in the spin-2 graviton propagator as described in the expressions of $\mathcal{G}_{\rm HLZ}$ and $\mathcal{G}_{\rm GRW}$, everything is same in the HLZ and GRW formalisms. Now, whatever be the formalism (HLZ or GRW), the matrix element of a process should come out to be exactly same in both ways by consistent use of a particular formalism. For example, let us consider the following process in LO *i.e.*, $q\bar{q} \to \gamma\gamma$ via a massive spin-2 KK graviton, as depicted in Fig. D.1. In Fig. D.1, V_1 and V_2 denote only the couplings (*i.e.*, $-\frac{\kappa}{2}$

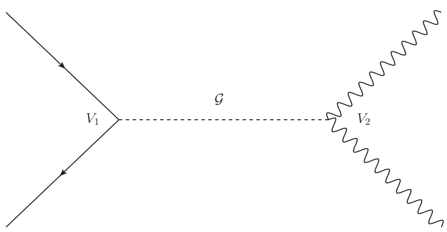

Figure D.1: Feynman diagram for $q\bar{q} \to \gamma\gamma$ via a massive spin-2 KK graviton.

or $-1/\overline{M_P}$) in the corresponding vertices, as used in $\mathcal{L}_{\rm HLZ}$ or $\mathcal{L}_{\rm GRW}$. Now, we want to calculate the factor $[V_1\ \mathcal{G}\ V_2]$ in these two cases, as they are the only source of difference in these two conventions:

$$[V_1\ \mathcal{G}\ V_2]_{\rm HLZ} = \frac{\kappa^2}{4} \times \mathcal{G}_{\rm HLZ} \quad , \tag{D.3}$$

$$
\begin{aligned}
[V_1 \; \mathcal{G} \; V_2]_{\rm GRW} &= \left(\frac{1}{\overline{M}_P}\right)^2 \times \mathcal{G}_{\rm GRW} \\
&= \frac{\kappa^2}{2} \times \frac{1}{2}\mathcal{G}_{\rm HLZ} \quad \text{(using eq. (D.1) \& (D.2))} \\
&= \frac{\kappa^2}{4} \times \mathcal{G}_{\rm HLZ} \qquad .
\end{aligned} \tag{D.4}
$$

So, it is evident from eq. (D.3) and (D.4), that consistent use of any of these formalisms would lead to the same result.

Now, in MadGraph5, the ADD model file is written following the HLZ convention, while the spin-2 HELAS routines use GRW formalism. So, the factor $[V_1 \; \mathcal{G} \; V_2]$ in MadGraph5 gives the following result:

$$
\begin{aligned}
[V_1 \; \mathcal{G} \; V_2]_{\rm MG5} &= [V_1]_{\rm HLZ} \; \mathcal{G}_{\rm GRW} \; [V_2]_{\rm HLZ} \\
&= \frac{\kappa^2}{4} \times \frac{1}{2}\mathcal{G}_{\rm HLZ} \\
&= \frac{1}{2} \times \frac{\kappa^2}{4} \times \mathcal{G}_{\rm HLZ} \qquad .
\end{aligned} \tag{D.5}
$$

Comparing eq. (D.5) with either eq. (D.3) or (D.4), we find that there would be an extra half factor, if one follows the MadGraph5 convention as stated above. Therefore, that extra factor should have to be eliminated properly to get the correct result. Also, while dealing with ADD model, one has to include a proper algorithm which would do the summation over the KK mode propagators under the MadGraph5 environment. All these things are carefully taken care of while presenting all the results in Chapter 4.

D.2 RS Model

On successful completion of the ADD model implementation in MadGraph5, we can readily deal with the RS model also, as the nature of the Lagrangian is very similar in these two cases. A very simple and straight forward modification in the ADD model file would make it work in the RS scenario. To discuss in detail, let us consider the Lagrangian in the RS scenario,

$$\mathcal{L}_{\rm RS} = -\frac{\overline{c_0}}{m_0} \sum_{\vec{n}}^{\infty} T^{\mu\nu}(x)\ h^{(\vec{n})}_{\mu\nu}(x) \qquad , \tag{D.6}$$

where $\overline{c_0} = \frac{\mathcal{K}}{M_P} = c_0\sqrt{8\pi}$ and $m_0 = \mathcal{K}e^{-\pi\mathcal{K}R_c}$. It is obvious from the above discussion of the ADD model that, within MadGraph5 framework, the graviton propagator would naturally follow the GRW formalism. So, this time, the discussed factor $[V_1\ \mathcal{G}\ V_2]$ would take the following form:

$$\begin{aligned} [V_1\ \mathcal{G}\ V_2]_{\rm RS,\ MG5} &= [V_1]_{\rm RS}\ \mathcal{G}_{\rm GRW}\ [V_2]_{\rm RS} \\ &= \frac{\overline{c_0}^2}{m_0^2} \times \frac{1}{2}\mathcal{G}_{\rm HLZ} \qquad . \end{aligned} \tag{D.7}$$

Comparing eq. (D.7) with eq. (D.3) we get,

$$\frac{1}{2}\frac{\overline{c_0}^2}{m_0^2} = \frac{\kappa^2}{4} \qquad , \tag{D.8}$$

$$\Rightarrow \qquad \kappa = \sqrt{16\pi\frac{c_0{}^2}{m_0^2}} \qquad . \tag{D.9}$$

So, we need to modify the ADD model file, where we have maintained the HLZ formalism, in such a way that it obeys the following replacement: $G_N \equiv \frac{c_0{}^2}{m_0^2}$ properly and that's all. Rest of the thing will follow the same course what we have mentioned at the time of discussing ADD model implementation in MadGraph5 environment. However, this time, the algorithm which takes care of the summation of graviton propagators in RS scenario, will be completely different from what is used in ADD case depending on the nature of construction of these two models.

Bibliography

[1] F. Englert and R. Brout, *Broken Symmetry and the Mass of Gauge Vector Mesons*, *Phys.Rev.Lett.* **13** (1964) 321–323.

[2] P. W. Higgs, *Broken symmetries, massless particles and gauge fields*, *Phys.Lett.* **12** (1964) 132–133.

[3] P. W. Higgs, *Broken Symmetries and the Masses of Gauge Bosons*, *Phys.Rev.Lett.* **13** (1964) 508–509.

[4] P. W. Higgs, *Spontaneous Symmetry Breakdown without Massless Bosons*, *Phys.Rev.* **145** (1966) 1156–1163.

[5] G. Guralnik, C. Hagen, and T. Kibble, *Global Conservation Laws and Massless Particles*, *Phys.Rev.Lett.* **13** (1964) 585–587.

[6] T. Kibble, *Symmetry breaking in nonAbelian gauge theories*, *Phys.Rev.* **155** (1967) 1554–1561.

[7] **CMS Collaboration** Collaboration, S. Chatrchyan et al., *Observation of a new boson at a mass of 125 GeV with the CMS experiment at the LHC*, *Phys.Lett.* **B716** (2012) 30–61, [`arXiv:1207.7235`].

[8] **ATLAS Collaboration** Collaboration, G. Aad et al., *Observation of a new*

particle in the search for the Standard Model Higgs boson with the ATLAS detector at the LHC, *Phys.Lett.* **B716** (2012) 1–29, [arXiv:1207.7214].

[9] M. E. Peskin and D. V. Schroeder, *An Introduction To Quantum Field Theory*. Westview Press, 1995.

[10] T. Muta, *Foundations of Quantum Chromodynamics: An Introduction to Perturbative Methods in Gauge Theories*. World Scientific Publishing Co. Pte. Ltd., 1998.

[11] R. K. Ellis, W. J. Stirling, and B. R. Webber, *QCD and Collider Physics*. Cambridge University Press, 1996.

[12] T. Plehn, *Lectures on LHC Physics*, *Lect.Notes Phys.* **844** (2012) 1–193, [arXiv:0910.4182].

[13] G. P. Salam, *Elements of QCD for hadron colliders*, arXiv:1011.5131.

[14] G. 't Hooft and M. Veltman, *Regularization and Renormalization of Gauge Fields*, *Nucl.Phys.* **B44** (1972) 189–213.

[15] G. Corcella, I. Knowles, G. Marchesini, S. Moretti, K. Odagiri, et al., *HERWIG 6.5 release note*, hep-ph/0210213.

[16] G. Corcella, I. Knowles, G. Marchesini, S. Moretti, K. Odagiri, et al., *HERWIG 6: An Event generator for hadron emission reactions with interfering gluons (including supersymmetric processes)*, *JHEP* **0101** (2001) 010, [hep-ph/0011363].

[17] M. Bahr, S. Gieseke, M. Gigg, D. Grellscheid, K. Hamilton, et al., *Herwig++ Physics and Manual*, *Eur.Phys.J.* **C58** (2008) 639–707, [arXiv:0803.0883].

[18] A. Buckley, J. Butterworth, S. Gieseke, D. Grellscheid, S. Hoche, et al., *General-purpose event generators for LHC physics*, *Phys.Rept.* **504** (2011) 145–233, [arXiv:1101.2599].

[19] J. Bellm, S. Gieseke, D. Grellscheid, A. Papaefstathiou, S. Platzer, et al., *Herwig++ 2.7 Release Note*, arXiv:1310.6877.

[20] T. Sjostrand, P. Eden, C. Friberg, L. Lonnblad, G. Miu, et al., *High-energy physics event generation with PYTHIA 6.1*, *Comput.Phys.Commun.* **135** (2001) 238–259, [hep-ph/0010017].

[21] T. Sjostrand, L. Lonnblad, and S. Mrenna, *PYTHIA 6.2: Physics and manual*, hep-ph/0108264.

[22] T. Sjostrand, L. Lonnblad, S. Mrenna, and P. Z. Skands, *Pythia 6.3 physics and manual*, hep-ph/0308153.

[23] T. Sjostrand, S. Mrenna, and P. Z. Skands, *PYTHIA 6.4 Physics and Manual*, *JHEP* **0605** (2006) 026, [hep-ph/0603175].

[24] T. Sjostrand, S. Mrenna, and P. Z. Skands, *A Brief Introduction to PYTHIA 8.1*, *Comput.Phys.Commun.* **178** (2008) 852–867, [arXiv:0710.3820].

[25] S. Catani, F. Krauss, R. Kuhn, and B. Webber, *QCD matrix elements + parton showers*, *JHEP* **0111** (2001) 063, [hep-ph/0109231].

[26] F. Krauss, *Matrix elements and parton showers in hadronic interactions*, *JHEP* **0208** (2002) 015, [hep-ph/0205283].

[27] A. Schalicke and F. Krauss, *Implementing the ME+PS merging algorithm*, *JHEP* **0507** (2005) 018, [hep-ph/0503281].

[28] L. Lonnblad, *Correcting the color dipole cascade model with fixed order matrix elements*, *JHEP* **0205** (2002) 046, [hep-ph/0112284].

[29] K. Hamilton, P. Richardson, and J. Tully, *A Modified CKKW matrix element merging approach to angular-ordered parton showers*, *JHEP* **0911** (2009) 038, [arXiv:0905.3072].

[30] M. L. Mangano, M. Moretti, and R. Pittau, *Multijet matrix elements and shower evolution in hadronic collisions: $Wb\bar{b} + n$ jets as a case study*, *Nucl.Phys.* **B632** (2002) 343–362, [hep-ph/0108069].

[31] M. L. Mangano, M. Moretti, F. Piccinini, and M. Treccani, *Matching matrix elements and shower evolution for top-quark production in hadronic collisions*, *JHEP* **0701** (2007) 013, [hep-ph/0611129].

[32] S. Frixione and B. R. Webber, *Matching NLO QCD computations and parton shower simulations*, *JHEP* **0206** (2002) 029, [hep-ph/0204244].

[33] P. Nason, *A New method for combining NLO QCD with shower Monte Carlo algorithms*, *JHEP* **0411** (2004) 040, [hep-ph/0409146].

[34] S. Frixione, P. Nason, and C. Oleari, *Matching NLO QCD computations with Parton Shower simulations: the POWHEG method*, *JHEP* **0711** (2007) 070, [arXiv:0709.2092].

[35] S. Alioli, P. Nason, C. Oleari, and E. Re, *A general framework for implementing NLO calculations in shower Monte Carlo programs: the POWHEG BOX*, *JHEP* **1006** (2010) 043, [arXiv:1002.2581].

[36] N. Arkani-Hamed, S. Dimopoulos, and G. Dvali, *The Hierarchy problem and

new dimensions at a millimeter, *Phys.Lett.* **B429** (1998) 263–272, [hep-ph/9803315].

[37] I. Antoniadis, N. Arkani-Hamed, S. Dimopoulos, and G. Dvali, *New dimensions at a millimeter to a Fermi and superstrings at a TeV*, *Phys.Lett.* **B436** (1998) 257–263, [hep-ph/9804398].

[38] N. Arkani-Hamed, S. Dimopoulos, and G. Dvali, *Phenomenology, astrophysics and cosmology of theories with submillimeter dimensions and TeV scale quantum gravity*, *Phys.Rev.* **D59** (1999) 086004, [hep-ph/9807344].

[39] D. Kapner, T. Cook, E. Adelberger, J. Gundlach, B. R. Heckel, et al., *Tests of the gravitational inverse-square law below the dark-energy length scale*, *Phys.Rev.Lett.* **98** (2007) 021101, [hep-ph/0611184].

[40] T. Han, J. D. Lykken, and R.-J. Zhang, *On Kaluza-Klein states from large extra dimensions*, *Phys.Rev.* **D59** (1999) 105006, [hep-ph/9811350].

[41] G. F. Giudice, R. Rattazzi, and J. D. Wells, *Quantum gravity and extra dimensions at high-energy colliders*, *Nucl.Phys.* **B544** (1999) 3–38, [hep-ph/9811291].

[42] L. Randall and R. Sundrum, *A Large mass hierarchy from a small extra dimension*, *Phys.Rev.Lett.* **83** (1999) 3370–3373, [hep-ph/9905221].

[43] L. Randall and R. Sundrum, *An Alternative to compactification*, *Phys.Rev.Lett.* **83** (1999) 4690–4693, [hep-th/9906064].

[44] W. D. Goldberger and M. B. Wise, *Modulus stabilization with bulk fields*, *Phys.Rev.Lett.* **83** (1999) 4922–4925, [hep-ph/9907447].

[45] W. D. Goldberger and M. B. Wise, *Phenomenology of a stabilized modulus*, *Phys.Lett.* **B475** (2000) 275–279, [hep-ph/9911457].

[46] C. Csaki, M. Graesser, L. Randall, and J. Terning, *Cosmology of brane models with radion stabilization*, *Phys.Rev.* **D62** (2000) 045015, [hep-ph/9911406].

[47] C. Csaki, M. L. Graesser, and G. D. Kribs, *Radion dynamics and electroweak physics*, *Phys.Rev.* **D63** (2001) 065002, [hep-th/0008151].

[48] H. Davoudiasl, J. Hewett, and T. Rizzo, *Phenomenology of the Randall-Sundrum Gauge Hierarchy Model*, *Phys.Rev.Lett.* **84** (2000) 2080, [hep-ph/9909255].

[49] J. L. Hewett, *Indirect collider signals for extra dimensions*, *Phys.Rev.Lett.* **82** (1999) 4765–4768, [hep-ph/9811356].

[50] P. Mathews, V. Ravindran, K. Sridhar, and W. van Neerven, *Next-to-leading order QCD corrections to the Drell-Yan cross section in models of TeV-scale gravity*, *Nucl.Phys.* **B713** (2005) 333–377, [hep-ph/0411018].

[51] P. Mathews and V. Ravindran, *Angular distribution of Drell-Yan process at hadron colliders to NLO-QCD in models of TeV scale gravity*, *Nucl.Phys.* **B753** (2006) 1–15, [hep-ph/0507250].

[52] M. Kumar, P. Mathews, and V. Ravindran, *PDF and scale uncertainties of various DY distributions in ADD and RS models at hadron colliders*, *Eur.Phys.J.* **C49** (2007) 599–611, [hep-ph/0604135].

[53] K.-m. Cheung and G. L. Landsberg, *Drell-Yan and diphoton production at*

hadron colliders and low scale gravity model, *Phys.Rev.* **D62** (2000) 076003, [hep-ph/9909218].

[54] R. Frederix, M. Mandal, P. Mathews, V. Ravindran, and S. Seth, *Drell-Yan, ZZ, W^+W^- production in SM & ADD model to NLO+PS accuracy at the LHC*, *Eur.Phys.J.* **C74** (2014) 2745, [arXiv:1307.7013].

[55] O. J. Eboli, T. Han, M. Magro, and P. Mercadante, *Diphoton signals for large extra dimensions at the Tevatron and CERN LHC*, *Phys.Rev.* **D61** (2000) 094007, [hep-ph/9908358].

[56] M. Kumar, P. Mathews, V. Ravindran, and A. Tripathi, *Diphoton signals in theories with large extra dimensions to NLO QCD at hadron colliders*, *Phys.Lett.* **B672** (2009) 45–50, [arXiv:0811.1670].

[57] M. Kumar, P. Mathews, V. Ravindran, and A. Tripathi, *Direct photon pair production at the LHC to order α_s in TeV scale gravity models*, *Nucl.Phys.* **B818** (2009) 28–51, [arXiv:0902.4894].

[58] R. Frederix, M. K. Mandal, P. Mathews, V. Ravindran, S. Seth, et al., *Diphoton production in the ADD model to NLO+parton shower accuracy at the LHC*, *JHEP* **1212** (2012) 102, [arXiv:1209.6527].

[59] N. Agarwal, V. Ravindran, V. Tiwari, and A. Tripathi, *Z boson pair production at the LHC to O(alpha(s)) in TeV scale gravity models*, *Nucl.Phys.* **B830** (2010) 248–270, [arXiv:0909.2651].

[60] N. Agarwal, V. Ravindran, V. K. Tiwari, and A. Tripathi, *W^+W^- production in Large extra dimension model at next-to-leading order in QCD at the LHC*, *Phys.Rev.* **D82** (2010) 036001, [arXiv:1003.5450].

[61] P. Mathews, S. Raychaudhuri, and K. Sridhar, *Getting to the top with extra dimensions*, *Phys.Lett.* **B450** (1999) 343–347, [hep-ph/9811501].

[62] P. Mathews, S. Raychaudhuri, and K. Sridhar, *Testing TeV scale quantum gravity using dijet production at the Tevatron*, *JHEP* **0007** (2000) 008, [hep-ph/9904232].

[63] J. M. Campbell, J. Huston, and W. Stirling, *Hard Interactions of Quarks and Gluons: A Primer for LHC Physics*, *Rept.Prog.Phys.* **70** (2007) 89, [hep-ph/0611148].

[64] M. Golden and S. R. Sharpe, *Three Weak Gauge Boson Production at the SSC*, *Nucl.Phys.* **B261** (1985) 217.

[65] V. D. Barger and T. Han, *Triple Gauge Boson Production at* e^+e^- *and pp Supercolliders*, *Phys.Lett.* **B212** (1988) 117.

[66] **SM AND NLO MULTILEG and SM MC Working Groups** Collaboration, J. Alcaraz Maestre et al., *The SM and NLO Multileg and SM MC Working Groups: Summary Report*, arXiv:1203.6803.

[67] T. Binoth, G. Ossola, C. Papadopoulos, and R. Pittau, *NLO QCD corrections to tri-boson production*, *JHEP* **0806** (2008) 082, [arXiv:0804.0350].

[68] A. Lazopoulos, K. Melnikov, and F. Petriello, *QCD corrections to tri-boson production*, *Phys.Rev.* **D76** (2007) 014001, [hep-ph/0703273].

[69] G. Bozzi, F. Campanario, V. Hankele, and D. Zeppenfeld, *NLO QCD corrections to W+W- gamma and Z Z gamma production with leptonic decays*, *Phys.Rev.* **D81** (2010) 094030, [arXiv:0911.0438].

[70] G. Bozzi, F. Campanario, M. Rauch, and D. Zeppenfeld, *$Z\gamma\gamma$ production with leptonic decays and triple photon production at next-to-leading order QCD*, *Phys.Rev.* **D84** (2011) 074028, [arXiv:1107.3149].

[71] T. C. collaboration, *Data-Driven Background Estimates for SUSY diphoton Searches"*, *CMS-PAS-SUS-09-004*.

[72] A. Zerwekh, C. Dib, and R. Rosenfeld, *Triple photon production at the Tevatron in technicolor models*, *Phys.Lett.* **B549** (2002) 154–158, [hep-ph/0207270].

[73] J. Vermaseren, *New features of FORM*, math-ph/0010025.

[74] J. Pumplin, D. Stump, J. Huston, H. Lai, P. M. Nadolsky, et al., *New generation of parton distributions with uncertainties from global QCD analysis*, *JHEP* **0207** (2002) 012, [hep-ph/0201195].

[75] **CMS Collaboration** Collaboration, S. Chatrchyan et al., *Search for signatures of extra dimensions in the diphoton mass spectrum at the Large Hadron Collider*, *Phys.Rev.Lett.* **108** (2012) 111801, [arXiv:1112.0688].

[76] **ATLAS Collaboration** Collaboration, G. Aad et al., *Search for Extra Dimensions using diphoton events in 7 TeV proton-proton collisions with the ATLAS detector*, *Phys.Lett.* **B710** (2012) 538–556, [arXiv:1112.2194].

[77] L. Brown and R. Feynman, *Radiative corrections to Compton scattering*, *Phys.Rev.* **85** (1952) 231–244.

[78] G. 't Hooft and M. Veltman, *Scalar One Loop Integrals*, *Nucl.Phys.* **B153** (1979) 365–401.

[79] G. Passarino and M. Veltman, *One Loop Corrections for e+ e- Annihilation Into mu+ mu- in the Weinberg Model*, *Nucl.Phys.* **B160** (1979) 151.

[80] G. van Oldenborgh and J. Vermaseren, *New Algorithms for One Loop Integrals*, *Z.Phys.* **C46** (1990) 425–438.

[81] T. Binoth, J. Guillet, and G. Heinrich, *Reduction formalism for dimensionally regulated one loop N point integrals*, *Nucl.Phys.* **B572** (2000) 361–386, [`hep-ph/9911342`].

[82] G. Duplancic and B. Nizic, *Reduction method for dimensionally regulated one loop N point Feynman integrals*, *Eur.Phys.J.* **C35** (2004) 105–118, [`hep-ph/0303184`].

[83] A. Denner and S. Dittmaier, *Reduction schemes for one-loop tensor integrals*, *Nucl.Phys.* **B734** (2006) 62–115, [`hep-ph/0509141`].

[84] T. Binoth, J. P. Guillet, G. Heinrich, E. Pilon, and C. Schubert, *An Algebraic/numerical formalism for one-loop multi-leg amplitudes*, *JHEP* **0510** (2005) 015, [`hep-ph/0504267`].

[85] W. Beenakker, *Electroweak Corrections: Techniques and Applications*. PhD thesis, Univ. Leiden, 1989.

[86] E. A. Mirabelli, M. Perelstein, and M. E. Peskin, *Collider signatures of new large space dimensions*, *Phys.Rev.Lett.* **82** (1999) 2236–2239, [`hep-ph/9811337`].

[87] P. Mathews, S. Raychaudhuri, and K. Sridhar, *Large extra dimensions and deep inelastic scattering at HERA*, *Phys.Lett.* **B455** (1999) 115–119, [`hep-ph/9812486`].

[88] X.-G. Wu and Z.-Y. Fang, *Revisiting the Real Graviton Effects at CERN LHC within the Quantum Gravity Theory with Large Extra Dimensions*, *Phys.Rev.* **D78** (2008) 094002, [arXiv:0810.3314].

[89] P. Mathews, V. Ravindran, and K. Sridhar, *NLO-QCD corrections to dilepton production in the Randall-Sundrum model*, *JHEP* **0510** (2005) 031, [hep-ph/0506158].

[90] N. Agarwal, V. Ravindran, V. K. Tiwari, and A. Tripathi, *Next-to-leading order QCD corrections to the Z boson pair production at the LHC in Randall Sundrum model*, *Phys.Lett.* **B686** (2010) 244–248, [arXiv:0910.1551].

[91] N. Agarwal, V. Ravindran, V. K. Tiwari, and A. Tripathi, *Next-to-leading order QCD corrections to W^+W^- production at the LHC in Randall Sundrum model*, *Phys.Lett.* **B690** (2010) 390–395, [arXiv:1003.5445].

[92] S. Karg, M. Kramer, Q. Li, and D. Zeppenfeld, *NLO QCD corrections to graviton production at hadron colliders*, *Phys.Rev.* **D81** (2010) 094036, [arXiv:0911.5095].

[93] X. Gao, C. S. Li, J. Gao, J. Wang, and R. J. Oakes, *Next-to-leading order QCD predictions for graviton and photon associated production in the Large Extra Dimensions model at the LHC*, *Phys.Rev.* **D81** (2010) 036008, [arXiv:0912.0199].

[94] K.-m. Cheung and W.-Y. Keung, *Direct signals of low scale gravity at e+ e- colliders*, *Phys.Rev.* **D60** (1999) 112003, [hep-ph/9903294].

[95] G. F. Giudice, T. Plehn, and A. Strumia, *Graviton collider effects in one and more large extra dimensions*, *Nucl.Phys.* **B706** (2005) 455–483, [hep-ph/0408320].

[96] S. Ask, *Simulation of Z plus Graviton/Unparticle Production at the LHC*, *Eur.Phys.J.* **C60** (2009) 509–516, [arXiv:0809.4750].

[97] S. Ask, I. Akin, L. Benucci, A. De Roeck, M. Goebel, et al., *Real Emission and Virtual Exchange of Gravitons and Unparticles in Pythia8*, *Comput.Phys.Commun.* **181** (2010) 1593–1604, [arXiv:0912.4233].

[98] **ATLAS Collaboration** Collaboration, G. Aad et al., *Expected Performance of the ATLAS Experiment - Detector, Trigger and Physics*, arXiv:0901.0512.

[99] M. S. Chanowitz, M. Furman, and I. Hinchliffe, *The Axial Current in Dimensional Regularization*, *Nucl.Phys.* **B159** (1979) 225.

[100] B. Harris and J. Owens, *The Two cutoff phase space slicing method*, *Phys.Rev.* **D65** (2002) 094032, [hep-ph/0102128].

[101] S. Catani and M. Seymour, *A General algorithm for calculating jet cross-sections in NLO QCD*, *Nucl.Phys.* **B485** (1997) 291–419, [hep-ph/9605323].

[102] G. Duplancic and B. Nizic, *Dimensionally regulated one loop box scalar integrals with massless internal lines*, *Eur.Phys.J.* **C20** (2001) 357–370, [hep-ph/0006249].

[103] T. Hahn, "FormCalc 4 User's Guide." www.feynarts.de/formcalc/FormCalc-4.1.tar.gz.

[104] **Particle Data Group** Collaboration, K. Nakamura et al., *Review of particle physics*, *J.Phys.* **G37** (2010) 075021.

[105] P. M. Nadolsky, H.-L. Lai, Q.-H. Cao, J. Huston, J. Pumplin, et al., *Implications of CTEQ global analysis for collider observables*, *Phys.Rev.* **D78** (2008) 013004, [arXiv:0802.0007].

[106] M. Kumar, P. Mathews, V. Ravindran, and S. Seth, *Graviton plus vector boson production to NLO in QCD at the LHC*, *Nucl.Phys.* **B847** (2011) 54–92, [arXiv:1011.6199].

[107] M. Kumar, P. Mathews, V. Ravindran, and S. Seth, *Vector boson production in association with KK modes of the ADD model to NLO in QCD at LHC*, *J.Phys.* **G38** (2011) 055001, [arXiv:1004.5519].

[108] R. Frederix, S. Frixione, V. Hirschi, F. Maltoni, R. Pittau, et al., *Four-lepton production at hadron colliders: aMC@NLO predictions with theoretical uncertainties*, *JHEP* **1202** (2012) 099, [arXiv:1110.4738].

[109] S. Frixione, *Isolated photons in perturbative QCD*, *Phys.Lett.* **B429** (1998) 369–374, [hep-ph/9801442].

[110] R. Frederix, S. Frixione, V. Hirschi, F. Maltoni, R. Pittau, et al., *Scalar and pseudoscalar Higgs production in association with a top-antitop pair*, *Phys.Lett.* **B701** (2011) 427–433, [arXiv:1104.5613].

[111] R. Frederix, S. Frixione, F. Maltoni, and T. Stelzer, *Automation of next-to-leading order computations in QCD: The FKS subtraction*, *JHEP* **0910** (2009) 003, [arXiv:0908.4272].

[112] S. Frixione, Z. Kunszt, and A. Signer, *Three jet cross-sections to next-to-leading order*, *Nucl.Phys.* **B467** (1996) 399–442, [hep-ph/9512328].

[113] J. Alwall, M. Herquet, F. Maltoni, O. Mattelaer, and T. Stelzer, *MadGraph 5 : Going Beyond*, *JHEP* **1106** (2011) 128, [arXiv:1106.0522].

[114] H. Murayama, I. Watanabe, and K. Hagiwara, *HELAS: HELicity amplitude subroutines for Feynman diagram evaluations*, .

[115] K. Hagiwara, J. Kanzaki, Q. Li, and K. Mawatari, *HELAS and MadGraph/MadEvent with spin-2 particles*, *Eur.Phys.J.* **C56** (2008) 435–447, [arXiv:0805.2554].

[116] P. de Aquino, K. Hagiwara, Q. Li, and F. Maltoni, *Simulating graviton production at hadron colliders*, *JHEP* **1106** (2011) 132, [arXiv:1101.5499].

[117] A. Martin, W. Stirling, R. Thorne, and G. Watt, *Parton distributions for the LHC*, *Eur.Phys.J.* **C63** (2009) 189–285, [arXiv:0901.0002].

[118] P. Torrielli and S. Frixione, *Matching NLO QCD computations with PYTHIA using MC@NLO*, *JHEP* **1004** (2010) 110, [arXiv:1002.4293].